AN EXPERIMENTAL STUDY ON THE POOL FIRE BURNING CHARACTERISTICS OF N-HEPTANE AND ETHANOL IN THE TUNNELS

A THESIS SUBMITTED TO

THE GRADUATE SCHOOL OF NATURAL AND APPLIED SCIENCES

OF

MIDDLE EAST TECHNICAL UNIVERSITY

TEVFİK ULUÇ YAMALI

IN PARTIAL FULFILLMENT OF THE REQUIREMENTS

FOR

THE DEGREE OF MASTER OF SCIENCE

IN

MECHANICAL ENGINEERING

JUNE 2015

Approval of the thesis:

AN EXPERIMENTAL STUDY ON THE POOL FIRE BURNING CHARACTERISTICS OF N-HEPTANE AND ETHANOL IN THE TUNNELS

submitted by **TEVFİK ULUÇ YAMALI** in partial fulfillment of the requirements for the degree of **Master of Science in Mechanical Engineering Department, Middle East Technical University** by,

Prof. Dr. Mevlüde Gülbin Dural Ünver ___________________
Dean, Graduate School of **Natural and Applied Sciences**

Prof. Dr. Raif Tuna Balkan ___________________
Head of Department, **Mechanical Engineering**

Assoc. Prof. Dr. Ahmet Yozgatlıgil ___________________
Supervisor, **Mechanical Engineering Dept., METU**

Examining Committee Members:

Prof. Dr. Kahraman Albayrak
Mechanical Engineering Dept., METU ___________________

Assoc. Prof. Dr. Ahmet Yozgatlıgil
Mechanical Engineering Dept., METU ___________________

Assoc. Prof. Dr. Mehmet Metin Yavuz
Mechanical Engineering Dept., METU ___________________

Asst. Prof. Dr. Feyza Kazanç
Mechanical Engineering Dept., METU ___________________

Assoc. Prof. Dr. Selin Aradağ Çelebioğlu
Mechanical Engineering Dept., TOBB ETU ___________________

Date: 16.06.2015

I hereby declare that all information in this document has been obtained and presented in accordance with academic rules and ethical conduct. I also declare that, as required by these rules and conduct, I have fully cited and referenced all material and results that are not original to this work.

Name, Last Name: T. Uluç YAMALI

Signature :

ABSTRACT

AN EXPERIMENTAL STUDY ON THE POOL FIRE BURNING CHARACTERISTICS OF N-HEPTANE AND ETHANOL IN THE TUNNELS

Yamalı, Tevfik Uluç

M.Sc., Department of Mechanical Engineering

Supervisor: Assoc. Prof. Dr. Ahmet Yozgatlıgil

June 2015, 100 pages

The road and railway tunnel disasters in recent decades drew the attention of fire safety engineers. The effects of mechanical ventilation, tunnel geometry, physical and chemical properties of fuel on fire characteristics such as heat release rate, smoke temperature distributions along the tunnel and burning rate are experimentally examined on full scaled, large scaled and reduced scaled tunnel models. Although there are many studies on the effects of conventional fuels like gasoline and diesel, the blended fuels and radiative effects of fire are barely addressed in tunnel fire scenarios. In this study, heptane pool fires and 10 %, 20 % and 30 % volumetric fractions of ethanol blended heptane pool fires are studied with square and rectangular pan geometries under 0.5 m/s to 2.5 m/s ventilation conditions with 0.5 m/s incremental intervals in a reduced scale tunnel model based on the Froude number scaling. Two separate experimental matrices are prepared with one variable at a time approach. The fuel mass, temperature distribution, O_2, CO_2 and CO gas concentration are measured and are compared to observe the effect of changing parameters. The interior wall surfaces of tunnel are covered with high reflecting material for particular ethanol pool fires. The radiative heat flux of fire, the back radiation of walls and combustion gases are respectively measured through a series of experiments.

Keywords: Fire safety, Mechanical ventilation, Heat release rate, Burning rate, Heptane, Ethanol, Froude number scaling, Radiative heat flux

ÖZ

TÜNELLERDE N-HEPTAN VE ETANOL HAVUZ YANGINLARININ YANMA ÖZELLİKLERİ ÜZERİNE DENEYSEL BİR ÇALIŞMA

Yamalı, Tevfik Uluç
Yüksek Lisans, Makine Mühendisliği Bölümü
Tez Yöneticisi: Doç. Dr. Ahmet Yozgatlıgil

Haziran 2015, 100 sayfa

Son yıllarda karayolu ve demiryolu tünellerinde meydana gelen kazalar yangın güvenliği mühendislerinin dikkatini çekmektedir. Mekanik havalandırma, tünel geometrisi, fiziksel ve kimyasal özellikleri farklı yakıtların ısı salınım hızı, yanma gazı sıcaklık dağılımı ve yanma hızı gibi değerlerin yangın nitelikleri üzerine etkileri, gerçek, büyük ve küçük ölçekli tünel modellerinde deneysel olarak incelenmektedir. Benzin ve dizel gibi konvansiyonel yakıtların etkileri birçok çalışmaya konu olsa da karışım yakıtların ve alevin ışınımsal etkilerini araştırmış çalışmalar oldukça az sayıdadır. Bu çalışmada, dizelin vekil yakıtı olarak kullanılan heptan ve % 10, % 20 ve % 30 hacimsel oranlarda etanol ve heptan ile oluşturulmuş karışım yakıtların havuz yangınları, kare ve dikdörtgen tava kullanılarak 0.5 m/s'den 2.5 m/s'ye 0.5 m/s artış aralıklarıyla oluşturulan havalandırma koşullarında, Froude sayısı ölçeklendirmesi esas alınarak hazırlanmış olan küçük ölçekli tünel modelinde araştırılmıştır. Her seferinde tek değişken değiştirme yaklaşımı ile iki ayrı deney matrisi hazırlanmıştır. Yakıt kütlesi, sıcaklık dağılımı, O_2, CO_2 ve CO gaz derişimleri ölçülmüş ve değişen parametrelerin etkileri gözlemlenmiştir. Belirli etanol havuz yangınları için tünel iç duvarları yüksek ışınımsal yansıtma özelliğine sahip malzeme ile kaplanmıştır. Akışa ters yöndeki ışınımsal ısı akısı ve duvarlardan yansıyan ters ışıma bir dizi deney gerçekleştirilerek ölçülmüştür.

Anahtar Kelimeler: Yangın güvenliği, Mekanik havalandırma, Isı salınım hızı, Yanma hızı, Heptan, Etanol, Froude sayısı ölçeklendirmesi, Işınımsal ısı akısı

To My Family

ACKNOWLEDGEMENTS

First and above all, I would like to express my gratitude to my supervisor, Professor Ahmet Yozgatligil, for his continued encouragement of my research and contributions to my education. I would also like to thank Professor Kahraman Albayrak and Professor Metin Yavuz for their invaluable suggestions and comments on this work.

I would like to extend my sincerest appreciation to my friends Buket Sevcan Akkanat, Sina Shafee, Ilter Imran Bodur and Ramin Barzegar for the assistance. I wish you the best of luck in all of your future endeavors.

I would like to acknowledge the contributions of Hukseflux Thermal Sensors B. V. and Testo Ltd. for this research study. The fast responses of their helpful members have always accelerated the progression of the study.

I sincerely want to thank the administrative and technical staff of Mechanical Engineering Department at Middle East Technical University.

And lastly, I am grateful to my parents who supported and encouraged me to pursue my ambitious goals. I can never truly repay for what they've done to me.

TABLE OF CONTENTS

LIST OF TABLES

LIST OF FIGURES

LIST OF SYMBOLS

Fr	Froude number
$\dot{m}''$	Burning rate, g/m^{2}s
g	Gravitational acceleration, m/s^2
D	Characteristic dimension, m
$\dot{Q}$	Heat release rate, kW
ΔH_c	Heat of combustion, kJ/kg
T	Temperature, K
c_p	Specific heat, kJ/kg K
ΔT_{max}	Max. excess gas temperature, K
$\dot{m}$	Mass flow rate, kg/s
L	Flame height, m
x	Mole fraction
U_c	Critical ventilation velocity, m/s
H	Tunnel height, m
$\overline{H}$	Hydraulic tunnel height, m
$\dot{V}$	Volumetric flow rate, m^3/s
V	Ventilation velocity, m/s
V'	Dimensionless vent. velocity
P	Perimeter
b_{fo}	Radius of the fire source, m
H_{ef}	Vertical distance, m
St	Stanton number

Subscripts

∞	Ambient conditions
eff	Effective
o	Standard conditions

Abbreviations

HRR	Heat release rate
HGV	Heavy good vehicle
OCC	Oxygen consumption calorimetry
CDG	Carbon dioxide generation
THR	Total heat release
PDE	Partial differential equation
EU	European Union
HC	Hydrocarbon

Greek symbols

ρ	Density
μ	Viscosity
ϕ	Oxygen depletion factor
σ	Stefan-Boltzmann constant (5.67×10^{-8} W/m^{2}K^4)
ε	Emissivity

CHAPTER 1 INTRODUCTION

1.1 Motivation

The casualties of recent accidents in tunnels concentrated the studies on tunnel fire issues. The enclosure fire characteristics and smoke control have been investigated to understand the behavior of fire and secure the area inside the tunnel. It has been proved that there might be various parameters that affect the burning nature of the fire such as ventilation velocity, tunnel geometry (cross-sectional area, vertical shafts, inclination angle etc.), fuel type, pool depth (for liquid fuels), fuel surface area, blockage ratio and back radiation. Although the effects of numerous parameters were previously studied, the studies on pool fire demonstrations in tunnel models are substantially limited. Besides, the contribution of radiative heat transfer and back radiation have always been challenging to estimate due to the experimental difficulties and costly equipment. The heat release rate (HRR) of the fire is conjectured based on the oxygen consumption, O_2/CO generation rates and mass balance. However, the radiative heat emitted by the fire cannot be measured using these techniques. A common way of measuring radiative heat flux relies on the principle of thermoelectric effect which explains that the temperature difference creates electric voltage between two different conducting materials in contact. The studies related with thermal radiation measure the irradiance of the flame and collaborate with the simplified theoretical models for large pool fires in open atmosphere and for compartment fires. This study concentrates on the effects of ventilation velocity, fuel content and pan geometry on the combustion characteristics of fire in a scaled model tunnel. It also investigates the effects of back-radiation from the walls with high reflectivity.

1.2 Introduction

The effort of understanding the fire phenomena has been a primary objective of humankind throughout the history. People possibly gained their first experience with fire in Paleolithic Era which occupied the time period between 2.5 million years ago to 10,000 BP (McClellan & Dorn, 2006). The invention of fire might have been a necessity due to the inhospitable environmental conditions or just by coincidence. The first measurements of temperature and heat flux were taken in nineteenth century with the discovery of thermoelectric effects by famous scientists T. J. Seebeck and J. C. A. Peltier. Further developments on fire safety measures and computer aided analysis occurred in twentieth century (Lawson, 2009). The preventions were taken and the standards were set after the tunnel fire disasters in the beginning of twentieth century.

The tunnel fires showed that the fires in enclosure systems such as roadway/railway tunnels, buildings and mines exhibit different behaviors of burning than outdoor fires. The studies point out that radiation plays a prominent role in enclosure fires (Karlsson & Quintiere, 2000). The radiation exchange between walls and fuel surface in a participating gas medium may alter the characteristic properties of combustion. The descriptive properties such as heat release rate, burning rate, concentrations of gas species and the gas temperatures in the vicinity of the fire may differ for various fire scenarios.

The different behaviors of fire may have pose a threat for human life. The toxic gases may spread to any distance in any direction. The acceptable and tenable limit of evacuation for tunnel fire situations was stated to be 6,000 to 8,000 ppm of carbon monoxide concentration for 5 minutes of exposure (Miclea, et al., 2007). On the other hand, the intensive heat energy emitted from the fire may also cause severe burns, injuries and fatalities. The effects of heat on human health were defined as hyperthermia, body surface burns and respiratory tract burns in a previous study (NFPA, 2009). The threshold water saturated temperature for burning of respiratory tract and radiative heat flux with maximum 30 minutes exposure for skin burns were found as 60°C and 2.5 kW/m^2 in the same study. Yet another study more comprehensively reports the maximum, acceptable level of thermal radiation for human in open spaces as 1.42 kW/m^2 at 55°C of skin temperature (U.S Department of Housing and Urban Development, 2011). The report of U.S. Department of Housing and Urban Development also represents the maximum thermal radiant heat flux exposure to buildings as 31.5 kW/m^2 for a maximum duration of 15 minutes before the response of fire department and the breakout of spontaneous ignition.

The last statement displays that the enclosure fires are not only deathly but also destructive. The heat power of the fire may reach up to a certain value that starts ignition of combustible materials and even melts down the hardly combustibles. The intense fire leads to structural damage and collapse. A study performed in Cergy Pontoise University investigated the combustion characteristics of asphalt and concrete. It was found that asphalt surface starts to burn at around 500°C after 8 minutes of heating with emission of suffocating and carcinogenic gases. In comparison, non-flammable concrete exhibits stable mechanical characteristics and does not emit hazardous gases.

The hot, toxic gases driven by buoyancy forces rises due to the temperature differences. In a confined space, the gases propagate towards the inlets and exits of the structure. If the smoke generation rate of fire is high (e.g. sooty fires), the smoke accumulates under the ceiling and the gas stratum thickens. In order to drive out the hazardous gases rapidly, *the mechanical ventilation* is utilized. The longitudinally blown air suppresses the smoke but if the ventilation speed is sufficiently high, the air may interact with the fire as well. This case is undesirable because of *the oxygen supply effect* of air. The enclosure fires generally suffer *oxygen starvation* due to *the low oxygen availability* in the vicinity of the fire. However, the high ventilation conditions supply abundant amount of oxygen. The high amount of oxygen interacting with fuel affects the product concentrations in the reaction mechanism.

The preferential goal of mechanical ventilation is related with physical interference rather than chemistry. The movement of smoke is independent of direction. To establish a secured evacuation path, the hot gases must be fully discharged by means of ventilation. In tunnel fire scenarios, the minimum ventilation velocity that prevents the smoke propagation in opposite direction of air flow (i.e. *the backlayering*) is called as *the critical ventilation velocity*. P. H. Thomas is probably the first researcher who describes the critical ventilation velocity using the ratio of buoyancy and inertial forces (Thomas, 1968).

1.3 Aim of the Thesis

The aim of this thesis is to determine the effects of ventilation velocity, fuel content, pan geometry and radiation on combustion characteristics such as heat release rate, burning rate and ceiling gas temperature distribution.

The longitudinally controlled mechanical ventilation is used to direct the movement of smoke. The aim is to detect the critical ventilation velocity which is the minimum ventilation velocity to prevent the smoke flow in upstream direction from a fire in the tunnel. However, the quantity of ventilation velocity may cause significant changes in combustion characteristics as well.

Since the source of fire is fuel, the combustion characteristics are strongly dependent on the fuel properties. The entire reaction mechanism is based on the chemical formula of the fuel. Along with the chemical properties, the physical interactions between the fuel and its environment are also important. The properties such as pool surface area, pool depth and pool diameter affect the burning rate, heat release rate and duration of the fire.

The properties such as pool diameter (for circular pool fires) and aspect ratio (for tetragonal pool fires) cause the fire volume, flame length and fire luminosity to change. The enclosure fires with enhanced radiative energy are known to have different effects on pool fire burning characteristics compared to free burning fire characteristics. Especially for large pool fires with highly luminous flames, the heating effects of radiation inside the structure increases up to a level of consideration.

The objective of the study is to investigate the effects of ventilation velocity, fuel content, pan geometry and radiative emissions on heat release rate, burning rate and ceiling gas temperature distribution in a reduce scaled tunnel model.

CHAPTER 2 BACKGROUND AND LITERATURE REVIEW

2.1 Introduction

According to ancient beliefs, fire was considered to be the one of four basic elements of universe. It was believed that fire was brought to humans by gods, legendary heroes and animals in various cultures. Regardless of how, the symbols, altars, rituals and beliefs showed that the creative and destructive power of fire was highly esteemed by human being.

However, in modern world, it is known that fire is a chemical chain reaction of combustible materials with oxidizer at required activation energy. Once the activation energy is reached, the *ignition* occurs and reaction spreads out over the contact surface between reactants and oxidizer. This process is commonly known as *combustion.* A common knowledge is that, the combustion materials in solid and liquid forms do not burn. The strong intermolecular forces in solids and liquids keep the material together and prevent the infiltration of oxidizer. The material at the surface encountering with oxidizer turns into gaseous form exceeding the melting and boiling points. This process occurs in different ways for liquid and solid fuels. Liquid fuels evaporate directly into the gaseous fuel. The *gasification* of solids happens through *pyrolysis* in which the solid particles are thermally decomposed.

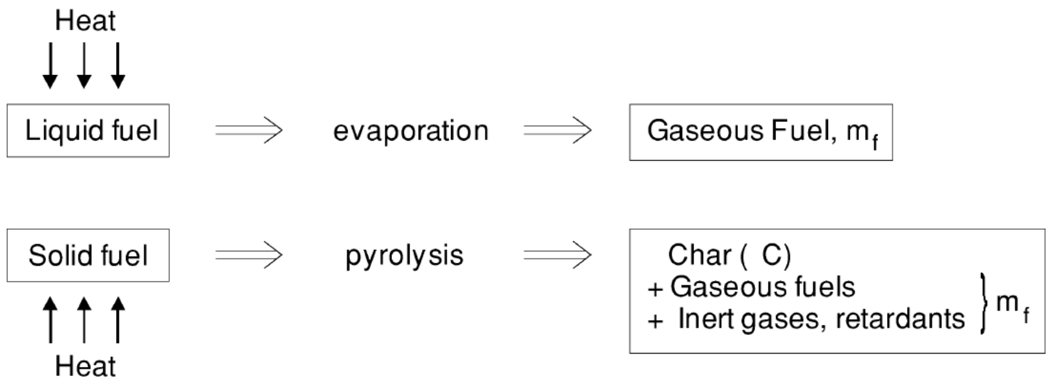

Figure 2.1 Fuel gasification process in liquids and solids. (Karlsson & Quintiere, 2000)

2.1.1 Compartment Fire Stages

The compartment fires, known as the fires in confined spaces, show similar trends for variations of temperature and heat release rate. From break out to extinction, 5 stages (ignition, growth, flashover, fully developed fire and decay) occur before the completion of combustion process. The ignition is the stage which the fire starts. The fire grows if the fuel and oxygen supply is adequate, otherwise the fire become extinct before reaching the flashover stage. The oxygen supply in growth period is generally sufficient because the gas emissions of immature fires are low. At this stage, the fire is said to be *fuel-controlled* because the only limiting factor is fuel. The flashover occupies the shortest time period of combustion process but the thermal variations during flashover are the highest among other stages. In this period, the radiation comes from the accumulated hot gases is considerably high and the ignition of unburnt combustible materials starts. The maximum heat release rate and burning rate reach to a steady state only in fully developed stage. Since the hot product gas concentrations are too high, available oxygen concentration in the environment decreases. In this case, the fire is controlled by the oxidizer and is called as *ventilation-controlled fire*.

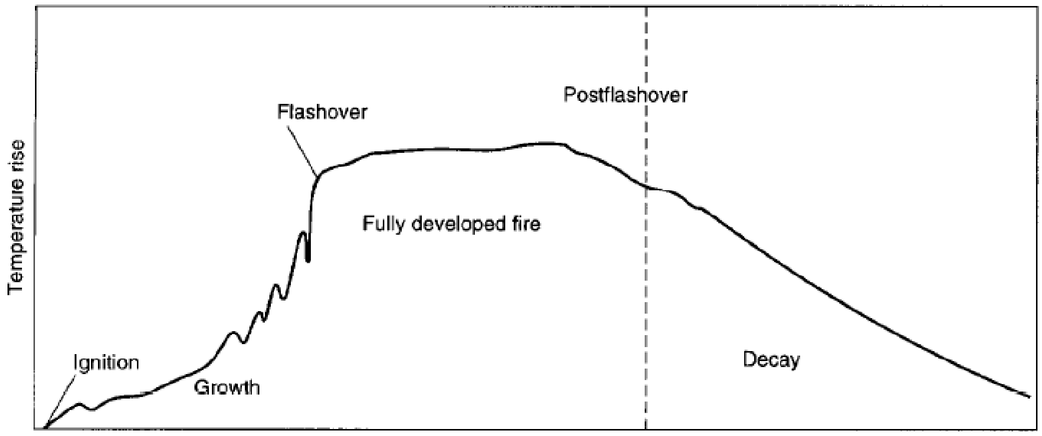

Figure 2.2 Stages of compartment fire. (Walton & Thomas, 1995)

2.1.2 Flame Types

In combustion of liquid fuels, different flame types may form according to the oxygen/fuel content in the combustion zone and the dominant driving force of the fluids. The flame is described as *the diffusion flame (non-premixed flame),* if the fuel and oxidizer initially encounter in the zone where combustion occurs. A candle flame or a camp fire may be shown as an example of diffusion flame. In diffusion flames, the fuel does not interact with enough oxidizer due to low rate of diffusion. A sooty, yellow flame is formed as the result of ineffective combustion. If the fuel and oxidizer are mixed before reaching the area of combustion, the fuel particles react with abundant supply of oxidizer and an improved combustion occurs. This type of flames are known as *the pre-mixed flames.* The pre-mixed flames have higher temperatures in comparison with diffusion flames as is also understood from the blue, low soot producing flame structure (e.g. stove fires). Other than the concepts of diffusion and pre-mixed flames, another flame type is defined based on the mechanism of driving force involved. If the fuel is forced into the combustion zone with a high momentum rather than the naturally occurring diffusion speed, the driving force will not be the buoyancy anymore. The flames of pressurized fuel are called as *the jet flames*. The jet flames have high burning rate and heat release rate. The high temperatures of jet flames are utilized in heavy industry works such as welding.

The relative importance of inertia and buoyancy is stated as a measure used to determine the type of fire (Drysdale, 1998). The Froude number is used as a tool to classify the fire.

$$Fr = U^2/gD \tag{2.1}$$

In the equation, *U* is the initial velocity of the fuel vapor and it is derived by the heat release rate ($\dot{Q}$) of an assumed circular fuel bed with diameter *D*.

$$U = \frac{\dot{Q}}{\Delta H_c \rho (\pi D^2/4)} \tag{2.2}$$

The relation between $\sqrt{Fr}$ and $\dot{Q}$ has also been determined in the study of (Zukoski & Kubota, 1975). The scaling parameter of dimensionless heat release rate ($\dot{Q}^*$) is defined in the study and the effect of $\dot{Q}^*$ and *D* on flame height is discussed.

$$\dot{Q}^* = \frac{\dot{Q}}{\rho_\infty c_p T_\infty \sqrt{gD} D^2} \tag{2.3}$$

The flame height, as a parameter of flame size, may provide valuable information about the interaction of fire with its surroundings. In one of the first studies that measures the flame height of a particular fuel, the functional relationship is presented as, (Thomas, Webster, & Raftery, 1960)

$$\frac{L}{D} = f\left(\frac{\dot{m}^2}{\rho^2 g D^5 \Delta T}\right) \tag{2.4}$$

Yet another study that investigates the relationship between normalized flame height (*L/D*) and dimensionless heat release rate ($\dot{Q}'$), puts forth the different regimes of pool fires (diffusion flames) and jet flames that are shown in Figure 2.3.

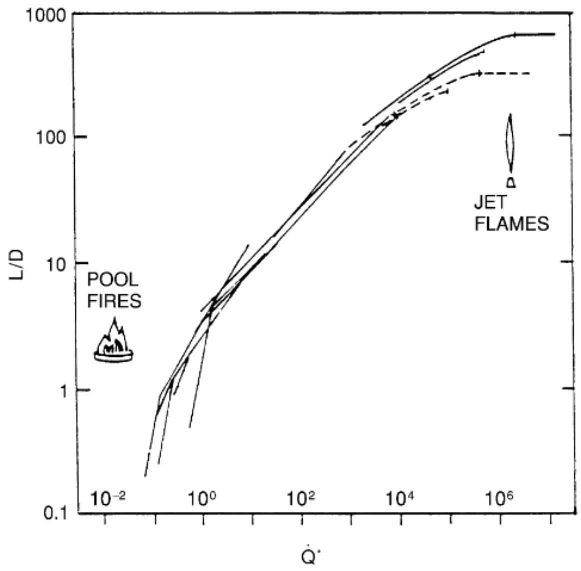

Figure 2.3 Normalized flame height vs. dimensionless heat release rate. Adapted from (McCaffrey, 1995)

The studies on flame height show that the behavior of fire in confined spaces may exhibit significant changes due to restrictions in air entrained in the enclosed space. According to the experimental results, the temperature variations of flame with height may differ in bounded case and the flame heights may increase up to 20 % depending on the dimensionless heat release rate interval of the fire (Hasemi & Takunaga, 1984). In 1980, Babrauskas claims that the 'cut-off height, h_c' of the flame may be related with the horizontal propagation distance, h_r, under the ceiling.

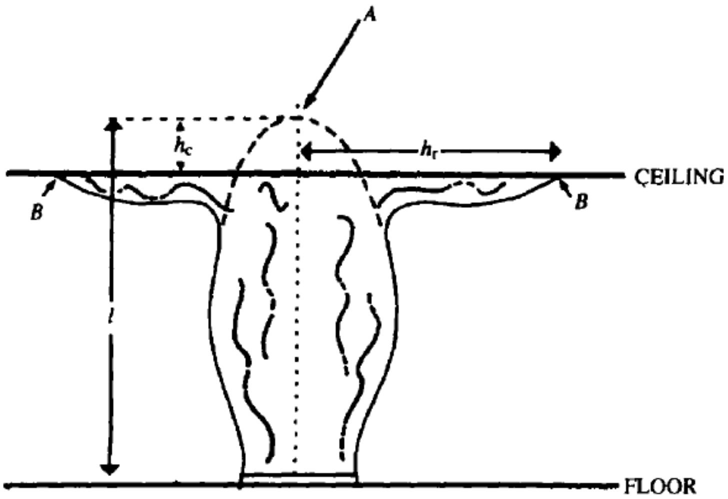

Figure 2.4 Flame deflection under a ceiling, showing 'cut-off height' and horizontal propagation of flame. Adapted from (Babrauskas, 1980)

2.2 Tunnel Fires

In late 19th century, the tunnel fire catastrophes drew the attention of fire safety authorities. The fires in Mont-Blanc (1999), Tauern (1999) and Gotthard (2001) road tunnels showed that the tunnel fire safety issues must be addressed considering the increasing transport activity growth. In 2007 European Energy and Transport report of European Commission, the transport activity growth is projected to increase at a rate of 1.4 % per year (for the volume of transportation of passengers) and 1.7 % per year (for the volume of freight transport) in between 2005 to 2030 (Capros, Mantzos, Papandreou, & Tasios, 2007). Considering the statistical inferences, the major tunnel accidents in the last thirty years were tabulated by a recent study (Vianello, Fabiano, Palazzi, & Maschio, 2012).

Table 2.1 Major tunnel accident in the last thirty years. Adapted from (Vianello, Fabiano, Palazzi, & Maschio, 2012)

Year	***Tunnel***	***Country***	***Length [m]***	***Fatalities***	***Injured***	***Vehicle***
1980	Sakai	Japan	459	5	5	10
1982	Caldecott	USA	1028	7	2	8
1983	Pecrile	Italy	600	8	22	10
1986	L'Armé	France	1105	3	5	5
1987	Gumefens	Switzerland	340	2		3
1993	Serra Ripoli	Italy	442	4	4	16
1994	Hugouenot	South Africa	6111	31	28	1
1995	Pfaender	Austria	6719	53	4	4
1996	I. Femmine	Italy	148	5	10	20
1999	M. Bianco	Italy	11600	39		26
1999	Tauren	Austria	6400	12		40
2001	Gothard	Switzerland	17000	11	10	8
2003	Vicenza	Italy	600	6	50	
2006	Viamala	Switzerland	750	9	6	3
2007	Ehrentalerberg	Austria	3345	-	12	39
2007	Burnley	Australia	3400	3	-	7
2007	Santa Clarita	USA	165	3	23	33
2007	San Martino	Italy	4800	2	10	1
2008	Ofenauer	Austria	1390	-	17	18
2009	Eiksund	Norway	7765	5		2
2009	Gubrist	Switzerland	3200	-	4	2
2009	Arlberg	Austria	13976	1	2	2
2010	Trojane	Slovenia	885		5	6
2010	Wuxi Lihu	China	10950	24	19	
2010	Seelisberg	Switzerland	9000	-	5	2

*This table is a reduced form of the master copy. The original one can be attained from the reference.

Unlike the unconfined fires, the tunnel fires may pose many hazards. Alongside with severe burn injuries, gas intoxication, low visibility, anoxia and injuries by falling debris or spalling concrete are possible life threatening factors.

2.3 Scale Modelling

The full scaled and reduced-scale experimentations are the only way of testing a fire scenario in a laboratory environment. Although it is getting harder to keep up pace with the technology, the available software support still requires upgrades to provide analogous results with experimental data. The complex geometries, fuel types and heat losses obligate researchers to make theoretical assumptions. An accurate and time-saving mesh system of a tunnel ceiling must be sophisticated and simple at the same time. On the other hand, the combustion chemistry of fuels and inflammables in varying ambient conditions definitely changes for even a simplest hydrocarbon with known chemical formula. Therefore, the most accurate, reliable and cost-effective way of verification is to conduct reduce-scale experiments. The concept of scaling is based upon the similitude of a physical phenomenon by obeying the laws of physics via the dimensionless variables. Three basic methods are known to derive the dimensionless variables;

- The Buckingham pi method
- The partial differential equation (PDE) method
- Dimensional analysis

The Buckingham pi theorem offers the determination of four dimensionless parameters (Π_{1-4}) by eliminating the three repeating variables (u_{∞}, l, μ) of velocity function. The PDE method uses two governing equations of steady, two-dimensional momentum equation and conservation of mass. Lastly, the dimensional analysis relates the control volume approach with Newton’s law of viscosity and derives the same dimensionless variables from the dimensionless form of the equation. The other dimensionless groups for fire phenomena are derived in the study of J. Quintiere (2006) and a detailed list of dimensionless variables is presented.

2.4 Heat Release Rate

The heat release rate is the rate at which heat energy is generated by burning and is also known as *firepower*. Since, the priori mechanism for combustion is the vaporization of fuel, the multiplication of mass flow rate of fuel vapor,$\dot{m}_F$ with the complete heat of combustion, Δh_c, describes the HRR as,

$$\dot{Q} = \dot{m}_F \Delta h_c \tag{2.5}$$

Obviously, the Equation 2.5 is a theoretical approach for complete combustion. A more realistic expression requires the determination of *combustion efficiency*,χ which is defined as,

$$\chi = \frac{\Delta H_{eff}}{\Delta H_c} \tag{2.6}$$

In a tunnel fire scenario, *the effective heat of combustion*, ΔH_{eff}, is hard to find because of the effects of varying parameters (such as oxygen concentration or temperature in the vicinity of the fire) on reaction mechanism of combustion process. However, a practical solution for calculation of HRR is suggested by W. J. Parker in 1982. The idea is to use the constant heat of 13.1 MJ per kilogram of oxygen consumed which is the same for most of the organic materials as found in a previous study (Thornton, 1917). A subsequent study found the average value for larger series of solids, liquids and gases as 12.8 MJ/kg of oxygen with variation of ±7 % (Tewarson, 1995). By measuring the concentrations of species in the exhaust duct, the oxygen consumption can be calculated as a product of volumetric flow rate in the exhaust duct and the decrease in the oxygen concentration (Parker, 1977).

$$\dot{Q} = \left(\phi - \left(\frac{E'' - E'}{E'}\right)\left(\frac{1-\phi}{2}\right)\frac{x_{CO}^{A}}{x_{O_2}^{A}}\right) E' x_{O_2}^{o} \dot{V}_A \tag{2.7}$$

In the Equation 2.7, E' and E'' are constants, x symbolizes the concentrations of species in standard atmosphere designated with superscript, o and the ones measured by the analyzer (with superscript A), $\dot{V}_A$ is the inflow of air and ϕ is the oxygen depletion factor as shown in Equation 2.8.

$$\phi = \frac{x_{O_2}^{o} - x_{O_2}^{A}\left(1 - x_{CO_2}^{o} - x_{H_2O}^{o}\right)/\left(1 - x_{CO_2}^{A} - x_{CO}^{A}\right)}{x_{O_2}^{o}\left(1 - x_{O_2}^{A}/\left(1 - x_{CO_2}^{A} - x_{CO}^{A}\right)\right)} \tag{2.8}$$

The oxygen consumption calorimetry (OCC) is considered in different aspects by previous studies. In the work of Brohez and co-workers (1999), the HRR is calculated based on the carbon dioxide generation (CDG) calorimetry. The formulation of HRR is established by introducing a soot generation correction factor. The chemicals with different soot tendencies are tested in the INERIS bench scale calorimeter. It is concluded that the soot generation factor may be important for accurate HRR calculations depending on the chemical structure of the material and degree of the ventilation condition (Brohez, Delvosalle, Marlair G., & Tewarson, 1999). The following study of Brohez and others includes the oxygen consumption method as well. The significance of soot generation, incompleteness of combustion and water generation factor are also discussed and a similar HRR formulation for OCC is derived for applications. The HRR results of CDG calorimetry and OCC are compared with soot generation and without soot generation. It is found that neglecting of soot generation may give significant errors in HRR calculation (Brohez, Delvosalle, Marlair, & Tewarson, 2000).

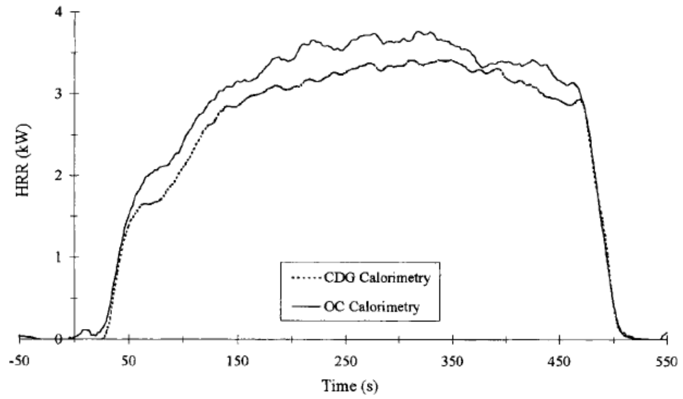

Figure 2.5 Heat release rate from OCC and CDG calorimetry without correction of soot generation for 1,2,4-trimethlybenzene (Brohez, Delvosalle, Marlair, & Tewarson, 2000)

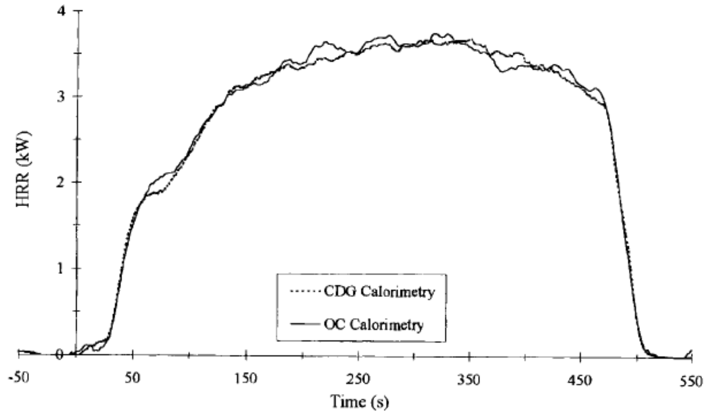

Figure 2.6 Heat release rate from OCC and CDG calorimetry corrected for soot generation for 1,2,4-trimethlybenzene (Brohez, Delvosalle, Marlair, & Tewarson, 2000)

Another study on OCC and CDG calorimetry is performed by H. Pretrel, W. Le Saux and L. Audouin in 2013. The incomplete combustion of hydrocarbon (eq. 2.9) is expressed as the reaction for complete combustion minus two reactions for the oxidation reaction of carbon monoxide and soot produced (eq. 2.10).

$$C_nH_m + \left(n + \frac{m}{4} - \frac{x}{2} - y\right)\ O_2$$
$$\rightarrow\ (n - x - y)\ CO_2 + x\ CO + y\ C + \frac{m}{2}\ H_2O \tag{2.9}$$

$$C_nH_m + \left(n + \frac{m}{4}\right)\ O_2$$
$$\rightarrow n\ CO_2 + \frac{m}{2}\ H_2O - x\left\{CO + \frac{1}{2}O_2 \rightarrow CO_2\right\} - y\{C + O_2 \rightarrow CO_2\} \tag{2.10}$$

From the Equation 2.10, the expressions for energy released per unit of mass of CO and CDG are proposed. The HRR calculations for propane combustion are performed for two different fire scenarios (single room and multi-room fires) and the results are compared. As a result of experiments, the CDG method is found as the most accurate method with accuracy within 10 % for determining the HRR (Pretrel, Le Saux, & Audouin, 2013).

In tunnel fire tests, the HRR is measured to observe the effects of various parameters (e.g. ventilation velocity, fuel properties or radiation) on fire behavior. The study of H. Ingason and A. Lönnermark in 2005 presents valuable information about the effects of HRR on fire behaviors. Four large-scale tests are carried out with initial ventilation velocities in the range 2.8-3.2 m/s. The fire source is a heavy goods vehicle (HGV) trailer mock-up with specified cargo of wood and polyethylene pallets (for test T1), wood pallets and polyurethane mattresses (for test T2), furniture and rubber tyres (for T3), paper cartons and polystyrene cups (for test T4). The total mass flow rate, gas velocity, concentration of species and HRR are measured in different heights of the tunnel cross-section.

Figure 2.7 Photos of the test commodity used in the large-scale tests (Ingason & Lönnermark, 2005)

Table 2.2 Peak HRR and fire growth from the Runehamar tests (Ingason & Lönnermark, 2005)

Test no.	Time from ignition to peak HRR (min)	Linear fire growth rate from 5 MW up to 100 MW (R = linear regression coefficient) (MW/min)	Peak HRR (MW)
T1	18.5	20.1 (0.996)	201.9
T2	14.1	26.3 (0.992)	156.6
T3	10.0	16.4 (0.998)	118.6
T4	7.4	16.9[a] (0.996)	66.4

[a] 5–66.4 MW.

The model scale fire experiments are conducted by R. Hansen and H. Ingason in 2012. In the study, the overall HRR results of longitudinally ventilated model tunnel (1:15 scaled) and model scale fire experiments (1:4 scaled) are calculated. Multiple wooden pile sources with constant and varying distances are burnt using two different ignition criteria (critical heat flux and ignition temperature). The ignition source is the heptane soaked strip of insulations and their HRR is found as 30 kW from the experimental data. The overall HRR is calculated based on a single exponential function as a method of estimating the total HRR in the system. Then, the results of calculated and measured HRR are compared and good agreements are received. Figure 2.8 shows the measured and calculated HRR for test 3P(4) in which 4 rows of 112 wooden pallets with total mass of 39.7 kg are used as the fire source and 983 kW of maximum total HRR with 535 MJ of total energy is released (Hansen & Ingason, 2012).

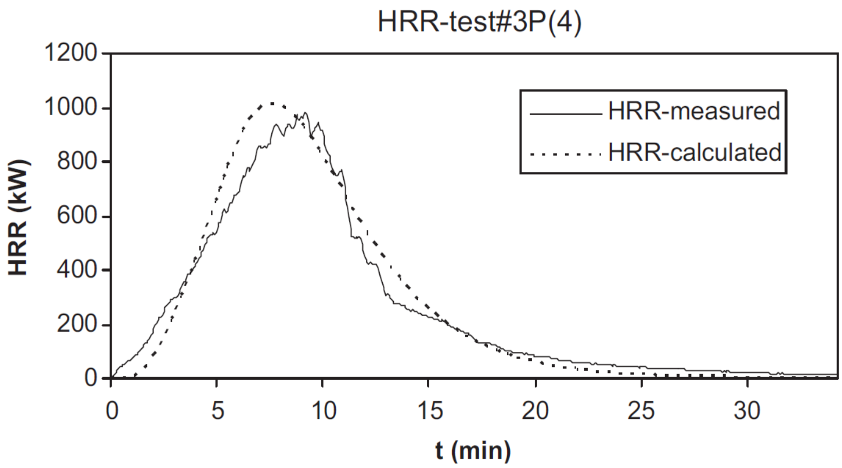

Figure 2.8 Measured HRR vs. calculated HRR for test 3P(4) (Hansen & Ingason, 2012)

2.5 Longitudinal Ventilation Velocity

The longitudinal ventilation systems are extensively utilized in tunnels. The purpose of ventilation is to dispatch the smoke out of the tunnel and to create a smoke free region. The control of smoke movement is supplied by mechanical ventilation but the natural ventilation is also studied to investigate the effects of insufficient ventilation conditions. The 'sufficiency' of ventilation condition is currently researched in many studies on tunnel fire safety issues. The primary design parameter, *the critical ventilation velocity*, was probably first discoursed by P. H. Thomas in 1968. The critical ventilation velocity is described as a function of the ratio of buoyancy and inertial forces. The derived equation gives the critical ventilation velocity as one-third power of the HRR (Thomas, 1968).

$$U_c = \left(\frac{gH\dot{Q}}{\rho_o T_o c_p A}\right)^{1/3} \quad (2.11)$$

In the succeeding studies, new formulations of critical ventilation velocity are produced paying regard to different HRR ranges, dimensionless critical ventilation velocity and dimensionless HRR with tunnel height and hydraulic tunnel height. A brief list of most recently derived equations is presented by Brahim and workmates (2011) in Table 2.3.

Table 2.3 Models derived to calculate the critical ventilation velocity (Brahim, Mourad, Afif, & Ali, 2011)

Formulae	***Remark***	***Source***
$U_c = \left(\frac{gH\dot{Q}}{\rho_o T_o c_p A}\right)^{1/3}$		(Thomas, 1968)
$U_c = \left(\frac{gH\dot{Q}}{\rho_o T_o c_p A R_{;,c}}\right)^{1/3}$	$R_{;,c} = 4.5$	(Danziger & Kennedy, 1982)
$U_c{}^* = 0.35\left(\frac{\dot{Q}^*}{0.124}\right)^{1/3} \quad for\ \dot{Q}^* < 0.124$ $U_c{}^* = 0.35 \quad for\ \dot{Q}^* > 0.124$	$U_c{}^* = \frac{U}{\sqrt{gH}}$ $\dot{Q}^* = \frac{\dot{Q}}{\rho_o T_o c_p g^{1/2} H^{5/2}}$	(Oka & Atkinson, 1995)
$U_c{}' = 0.4\left(\frac{\dot{Q}'}{0.20}\right)^{1/3} \quad for\ \dot{Q}' < 0.20$ $U_c{}' = 0.30 \quad for\ \dot{Q}' \geq 0.20$	$U_c{}^* = \frac{U_c}{\sqrt{gH}}$ $Q' = \frac{Q}{\rho_o T_o c_p g^{1/2} \overline{H}^{5/2}}$ $\overline{H} = 4A/P$	(Wu & Bakar, 2000)
$U_a{}^* = c_1 \frac{\sqrt{1 + c_2 Q_o^{*\,2/3}}}{1 + 6.13\, Q_o^{*\,2/3}} Q_o^{*\,1/3}$ $(H/w) = 1, \quad c_1 = 1.44, \quad c_2 = 3.57$ $(H/w) = 0.5, c_1 = 1.48, \quad c_2 = 3.11$	$U_a{}^* = \frac{U_a}{\sqrt{gH}}$ $Q_o^* = \frac{Q}{\frac{\gamma}{\gamma - 1} p \sqrt{g} H^{5/2}}$	(Kunsch, 2002)

Although the ventilation velocity has significant effect on smoke flow control, its effects on fire should also be studied. The high ventilation velocities may provide efficient convective heat transfer and smoke discharge. However, the oxygen content near the fire also increases. The interaction of fuel with sufficient amount of oxygen means that the ratio of available fuel to oxygen mass will significantly change. The product of this ratio with the ratio of oxygen mass to fuel mass for complete combustion, known as *the stoichiometric ratio (r)*, yields *the equivalence ratio* (ϕ) (Quintiere, 2006).

$$\phi = \left(\frac{mass\ of\ available\ fuel}{mass \text{ of available oxygen}}\right) r \tag{2.12}$$

In diffusion flames, the concentrations of species depend on the fuel mixture fraction (the ratio of mass of atoms that are originally fuel to mass of the gaseous mixture) and equivalence ratio. Thus, the concentrations may be theoretically estimated. The application of equivalence ratio is difficult because it requires the exact formulation for the chemical reaction (Karlsson & Quintiere, 2000).

2.6 Burning Rate

The energy release rate of fire depends on the mass flow rate of vaporized fuel as shown in Equation 2.5. However, the vaporization rate of volatiles is related with the heat transfer from the flame to the fuel. The burning rate, $\dot{m}''$, is stated as the ratio of the difference of heat flux supplied by the flame, $\dot{Q}_F''$, and the heat losses, $\dot{Q}_L''$, to the heat required to produce the volatiles, L_v (Drysdale, 1998).

$$\dot{m}'' = \frac{\dot{Q}_F'' - \dot{Q}_L''}{L_v} \tag{2.13}$$

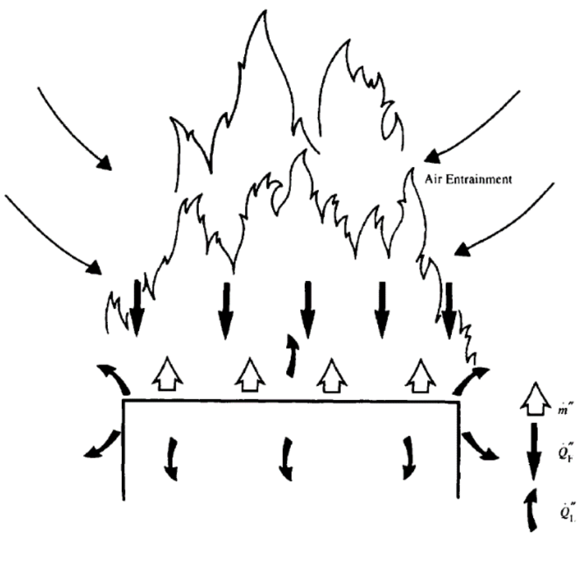

Figure 2.9 Heat and mass transfer on a burning surface (Drysdale, 1998)

Equation 2.13 with previous discussions show that the burning rate is related not only the fuel properties but also the properties of combustion. The studies investigate the effects of different fuels and environmental conditions on burning rate. Different ventilation conditions and pool sizes are proved to have considerable effects on combustion duration and burning rate. Associated with tunnel fires, the effects of cross air flow speed on burning rate is studied for various pool lengths. The square (5 cm to 25 cm) and rectangular (10 cm×20 cm and 10 cm×40 cm) pools with gasoline fuel source are used to measure the burning rates for 0 m/s to 3.1 m/s cross air flow speeds. The results shows that increasing pool size in quiescent condition cause burning rate to increase but under a cross air flow, the trend of burning rate is reversed (Hu, Liu, & Li, 2011).

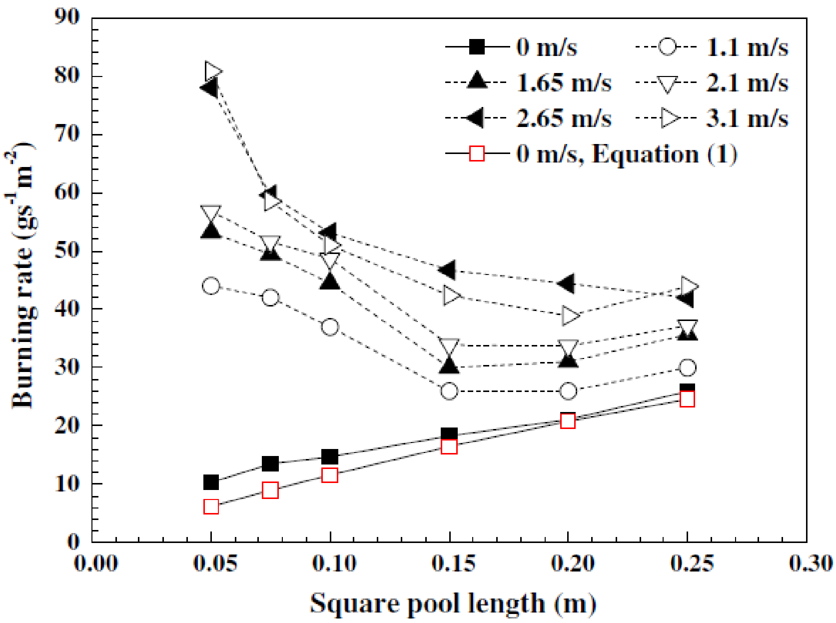

Figure 2.10 Variation of burning rate with square pool length (Hu L. , Liu, Xu, & Li, 2011)

Similarly, another experimental research was performed to reveal the effects of transverse air flow on burning rate. Square (ranged from 7.5 cm to 30 cm) and rectangular (the same area with 15 cm square pool but with aspect ratio 4:1) methanol pool fires are ventilated with air flows ranged in speed from quiescent to 5.5 m/s. The results implies that the burning rate for quiescent air is constant at 12.1 g/m^{2}s and the burning rates up to 5.5 m/s air flow shows a monotonic, 2.5 times increase (Woods, Fleck, & Kostiuk, 2006). The mass burning rate and flame tilt of acetone pool fire is studied in a more recent work. The wind tunnel with 1.2 m height and 0.8 m width is ventilated with air flow speed ranged from 0 m/s to 3 m/s at two reduced ambient pressures (100 kPa and 64 kPa). The radiation-controlled (pool diameter is over 20 cm) rectangular pool fires are tested for various aspect ratios (n). The experimental results shows that there is a linear relationship between the mass burning rate and pool aspect ratio in quiescent condition. The results also shows the increasing tendency of burning rate at low altitude with greater ambient pressure as in Figure 2.11 (Tang, Hu, Zhang, Zhang, & Dong, 2015).

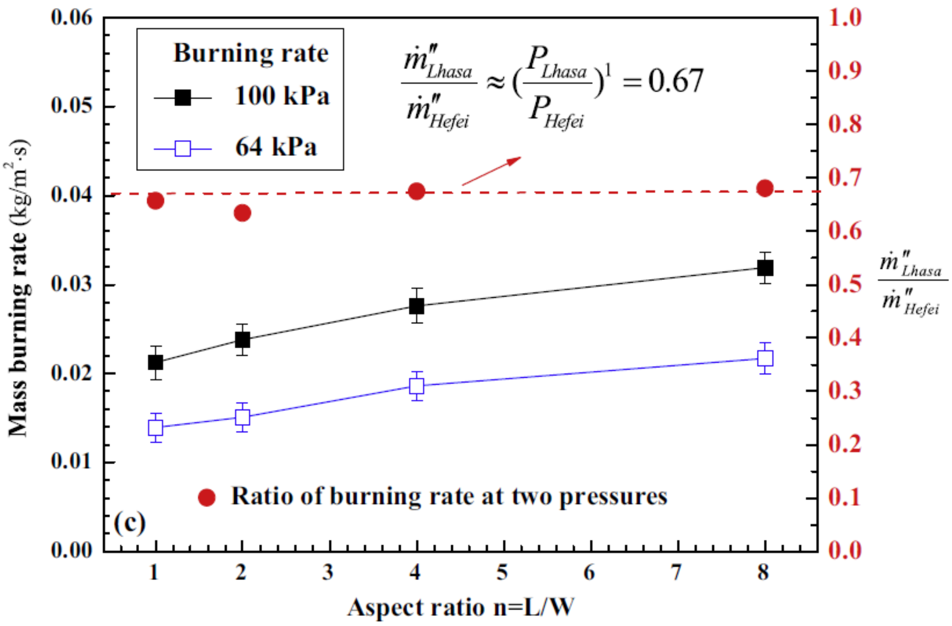

Figure 2.11 Burning rates of rectangular pool fires with different aspect ratios at two atmospheric pressures with no cross air flow (Tang, Hu, Zhang, Zhang, & Dong, 2015)

2.7 Temperature Distribution

The stability calculation of tunnel structure is an important design step against high thermal exposure of the fire. The heat exposed in tunnel fires is calculated through the standardized time-temperature curves such as ISO 834, the Hydrocarbon Curve (HC) or the RWS (Rijkswaterstaat) curve. These curves are based on small/large scale empirical data. The curves are used to calculate the temperature distribution as a function of the distance.

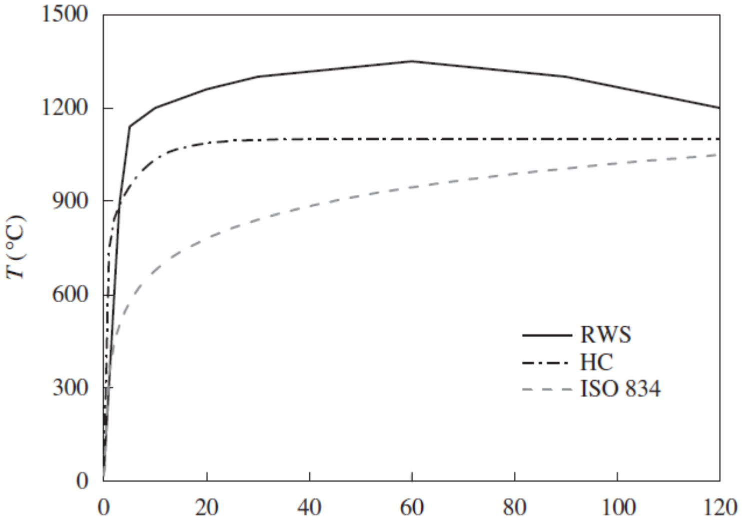

Figure 2.12 Standardized time-temperature curves for road tunnel applications (Li & Ingason, 2012)

An equation for maximum excess gas temperature beneath the ceiling is formulated by Li et al. (2011) as in eqn. 2.14. In the study, it is emphasized that the maximum gas temperature is independent of the tunnel width (Li, Lei, & Ingason, 2011).

$$\Delta T_{max} = \begin{Bmatrix} 17.5\dfrac{Q^{2/3}}{H_{ef}^{5/3}}, & V' \leq 0.19 \\ \dfrac{Q}{Vb_{fo}^{1/3}H_{ef}^{5/3}}, & V' > 0.19 \end{Bmatrix} \tag{2.14}$$

The effects of ventilation velocity, HRR, tunnel geometry and fire source on the maximum excess gas temperature beneath the ceiling in large tunnel fires are studied applying this equation to compare the experimental results of worldwide large-scaled tunnel tests. The temperature data show that two different regions are formed based on the dimensionless ventilation velocity, fire size and effective tunnel height (Li & Ingason, 2012).

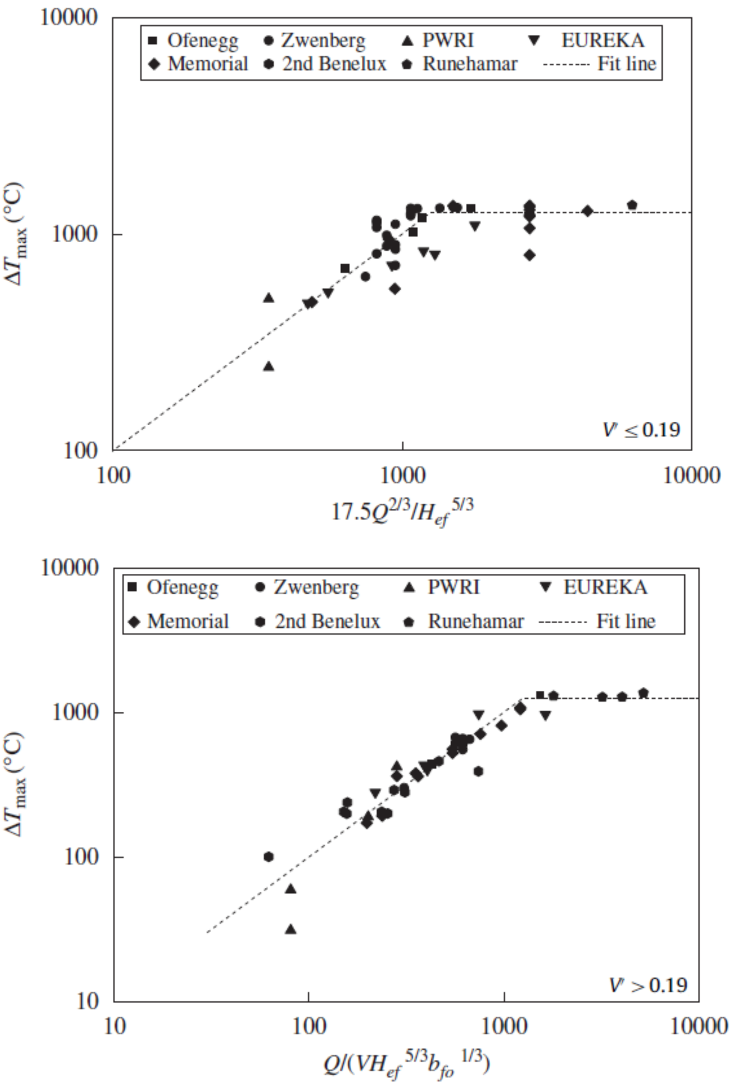

Figure 2.13 Maximum excess temperature beneath the tunnel ceiling in large scale tests (Li & Ingason, 2012)

Another experimental study about temperature distribution is carried out by Hu et al. (2007). Twelve diesel and gasoline fire test are conducted with varying fire size, tunnel section geometry and ventilation velocity in a vehicular tunnel with 96 m to 1032 m length, 1.09 % to 2.1 % slope, 0.1 m to 1.7 m flame height, 0.5 m/s to 2.5 m/s longitudinal ventilation velocity and 0.6 m^2 to 2 m^2 pool size. The temperature results show that the smoke temperature below the ceiling increases with larger fire sizes but it also decays faster through the tunnel (Hu, Huo, Wang, Li, & Yang, 2007).

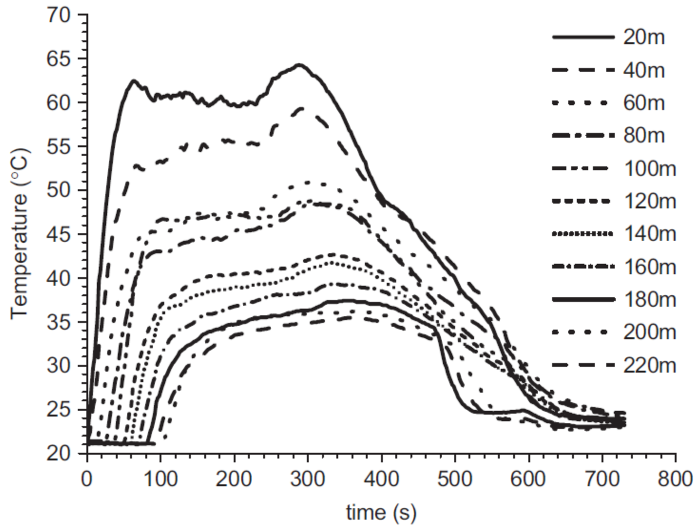

Figure 2.14 Typical temperature curves measured in the tests (Hu, Huo, Wang, Li, & Yang, 2007)

A simplified correlation for temperature distribution is numerically studied by Li et al. (2011). Based on the one-dimensional continuity and energy equations, the following expression in eqn. 2.15 is derived using a characteristic tunnel hydraulic diameter. The numerical models with tunnel cross sectional aspect ratios from 0.5 to 2.0 are used with HRR of fire from 4.4 MW to 22 MW under naturally ventilated condition. The numerical results of this study indicate that the correlation is applicable for all tunnels with different fitting constants for certain aspect ratio criteria (Li, Cheng, Wang, & Zhang, 2011).

$$\frac{\Delta T}{\Delta T_{ref}} = exp\left\{-St \cdot \frac{x - x_{ref}}{d}\right\} \tag{2.15}$$

2.8 Thermal Radiation

If the ventilation inside the tunnel is sufficient, the hot product gases are easily discharged. However, if the control of smoke flow is not maintained, the hot gases start to accumulate and cause the inside temperature to increase. The contribution of radiation mechanism becomes important in such under-ventilated tunnel fire scenarios. It is stated that a body with temperatures smaller than 150-200˚C is mostly under the influence of convection heat transfer but the radiation starts to be significant for temperatures higher than 400˚C and the visible light appears when the body temperature reaches 550˚C due to sufficient radiation in optical region of the spectrum (Drysdale, 1998). The Stefan-Boltzmann equation shows that the total energy emitted by a body is proportional to T^4 and the total emissive power is expressed as

$$E = \varepsilon\sigma T^4 \tag{2.16}$$

Although it is possible to calculate the total emissive power of a surface with given temperature and emissivity, the prediction of radiative power of fire is highly sophisticated due to the obscuring and scattering effects of participating medium. According to sources, the gas molecules which have dipole moment interact with electromagnetic radiation in thermal region (0.4-100 μm) of the wavelength spectrum. Therefore, the diatomic molecules like N_2, O_2 and H_2 do not absorb, emit or reflect electromagnetic wave but heteronuclear molecules such as CO, CO_2 and H_2O have these effects in some wavelength intervals (Drysdale, 1998).

Most of studies on flame radiation of open hydrocarbon pool fires use a theoretical model to estimate the effects of radiation and emissive power. A preferable model for liquid fuel fires is stated as *'solid flame'* radiation model in the study of McGrattan (2000). In the report, three different thermal radiation model are presented and the methodology of solid flame radiation model is explained. This model idealizes the fire as a solid vertical cylinder with diameter and height equal to flame diameter and height which has 20 % luminous zone at the base of the fire and 80 % flame obscuring smoky zone. The radiative fraction of fire is expressed as in eqn. 2.17 (McGrattan, Baum, & Hamins, 2000).

$$\chi_r = \chi_{r_{max}} e^{-kD} \tag{2.17}$$

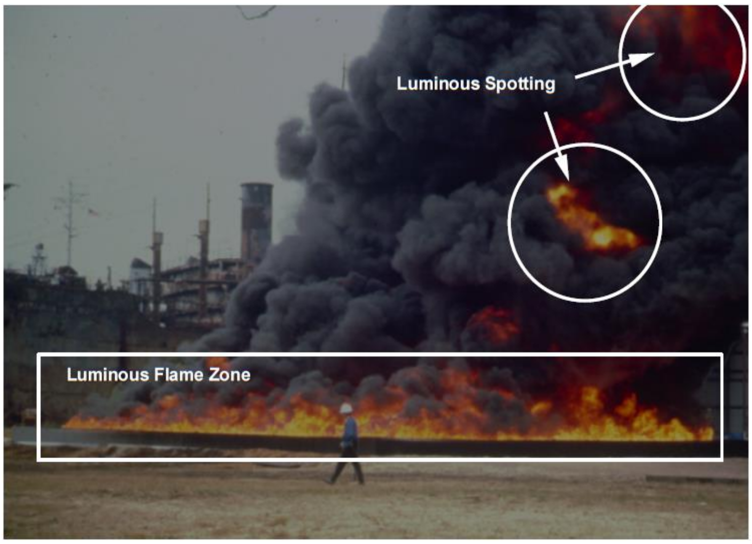

Figure 2.15 Photograph of a 15 m square fire of diesel fuel on water (McGrattan, Baum, & Hamins, 2000)

One of the limited number of experimental works on radiative effects of tunnel fires demonstrates the ethanol and heptane square pool fires dimensions from 10 cm to 25 cm under cross air flow speed ranged in 0-2.5 m/s. The radiation feedback towards the fuel surface is measured using water-cooled radiometer gauges. A fuel-feeding system is established to keep the pool depth constant while the combustion occurs. The radiation flux and fuel mass loss are obtained and the results show that increasing air flow speed decreases the radiation feedback due to the deflection of flame. The reduction is found as more effective for heptane pool fire than that of ethanol pool fire (Hu, Liu, & Wu, 2013).

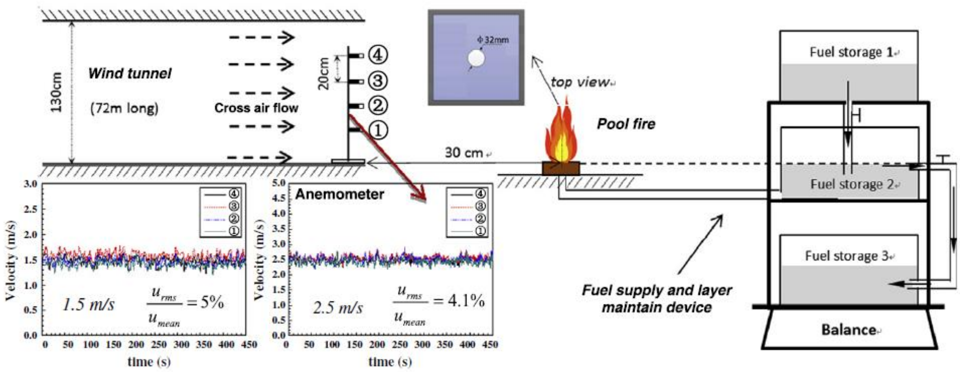

Figure 2.16 Schematic of experimental setup (Hu, Liu, & Wu, 2013)

CHAPTER 3 EXPERIMENTATION

3.1 *Experimental Rig*

In this section, the experimental setup is presented in three parts. The tunnel structure is composed of a steel skeleton covered by an insulation material. The fire sources include the liquid fuels in steel containers (the pans). The instruments measure the O_2, CO_2, CO gas concentrations, weight of the fuel, ceiling temperatures of designated locations and radiative heat coming from the fire and surroundings.

3.1.1 *Tunnel structure*

The structure is made of steel and is insulated on the outside using rock wool material of 5 cm thickness to minimize the heat losses. The cross-section of model is composed of a rectangular base with a semi-circular ceiling. The tunnel height from the apex of the roof is 36.4 cm and the width is 40 cm. The tunnel is comprised of 4 separate compartment modules with 150 cm in length each. There is an opening on the side of combustion compartment which provides access to the inside of tunnel for placement of fuel pan. The air flow is supplied by an axial compressor which takes in the air from a temperature-controlled environment. The entrance of the tunnel is connected to a plenum that is used to regulate the pressure necessary for required ventilation velocity. The incoming air passes through the flow straightener in the entrance of the tunnel. Figure 3.2 shows the experimental setup and pan geometries with dimensions.

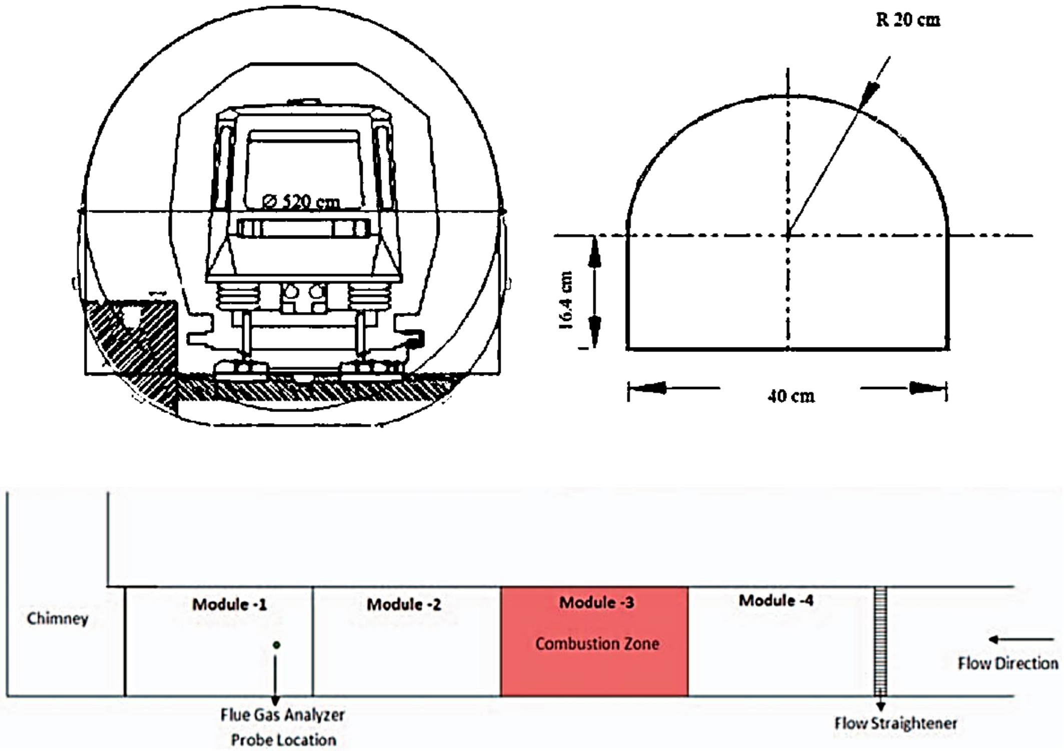

Figure 3.1 Schematics of the prototype and model tunnel cross section (Kayili, Yozgatligil, & Eralp, 2011)

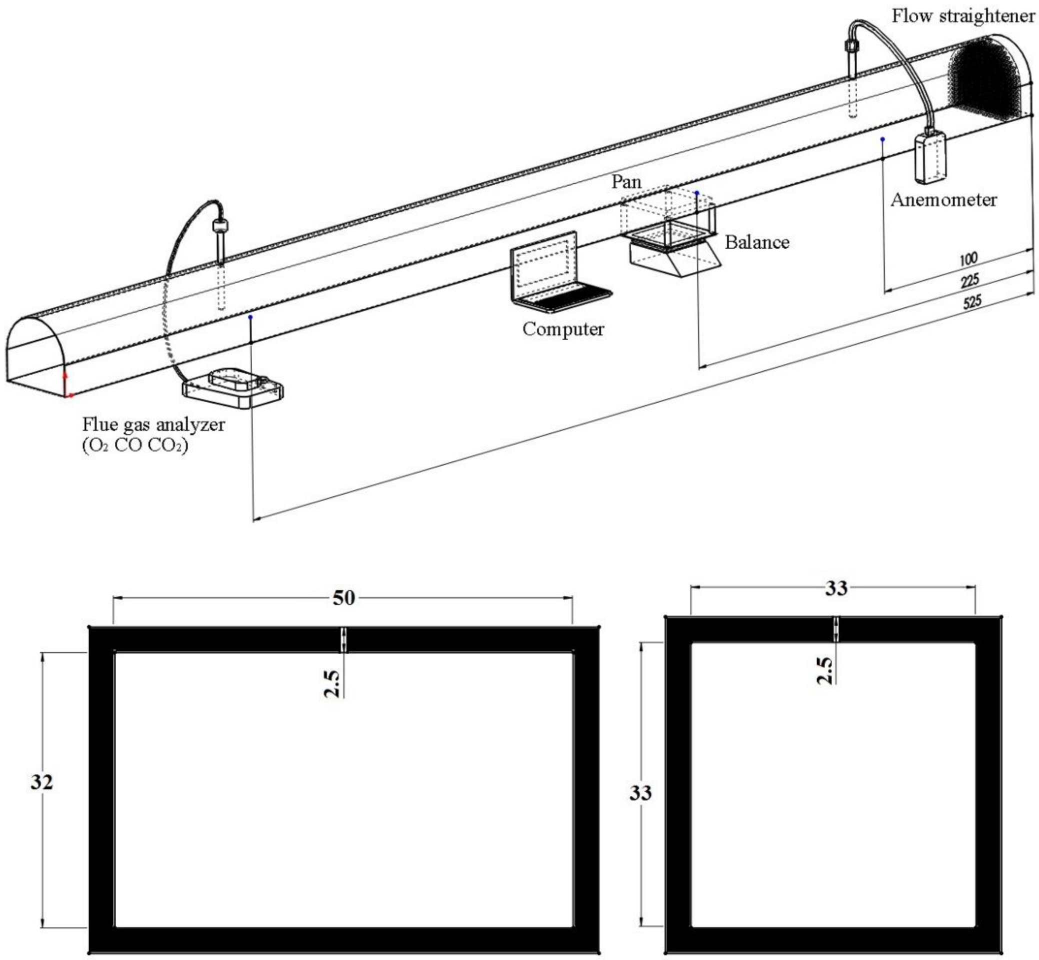

Figure 3.2 Experimental setup and pan geometries (dimension in cm)

3.1.2 Fire Sources

The burning materials are n-heptane and ethanol (in liquid phase under standard conditions) with chemical properties as shown in Table 3.1. Square and rectangular steel pans are used as fuel tray with surface areas of 0.1089 m^2 and 0.1600 m^2, respectively. The fire takes place at the center of the combustion zone (Figure 3.1).

Table 3.1 Chemical properties of n-heptane and ethanol

Chemical Formula	C_7H_{16}	C_2H_6O
Molecular Weight	100.20 kg/kmol	46.1 kg/kmol
Melting Point	-91 °C	-114 °C
Boiling Point	98 °C	78.4 °C
Water Solubility	Miscible	Practically insoluble
Higher Calorific Value	48506 kJ/kg	29700 kJ/kg
Net Calorific Value	44566 kJ/kg at 25 °C	28865 kJ/ kg at 25 °C
Density	684 kg/m^3 at 25 °C	789 kg/m^3 at 25 °C
Vapor Pressure	40 mmHg at 20 °C	43.7 mmHg at 20 °C
Stability	Highly Flammable	Highly Flammable
CAS Database Ref.	64-17-5	142-82-5
NIST Chemistry Ref.	64-17-5	142-82-5

3.1.3 Instruments

The HRR can be calculated based on the OCC method (Parker, 1977). Product species concentrations are measured by TESTO 350-S flexible flue gas analyzer. The device is designed for applications of industrial combustion plants, emission checking of burners/boilers in the industrial sector and measurements of gas turbines/engines of all kinds. The gas analyzer is capable of measuring O_2, CO and CO_2 concentration. The device can be loaded with upgrade modules up to six module including any of the NO, NO_2, H_2S, HC, SO_2, C_xH_y compounds. The recalibration is applied by initiating a phase called ‘zeroing phase’. The declaration of conformity, measuring ranges and accuracies and the lists of CO_2 and other gas recalibrations are presented in the appendices. The scan rate of gas analyzer is set as default (1 scan per second) so that the O_2 (%), CO (ppm) and CO_2 (%) concentrations are obtained for every second of combustion duration.

Figure 3.3 Testo 350-S portable measuring system for professional flue gas analysis

A total of 27 K-type thermocouples are placed in the upstream, combustion and downstream regions as seen in Figure 3.4. The configuration of thermocouple tree between combustion and downstream sections is also seen on the figure. It should be noted that the rest of the thermocouples are fixed 20 mm below the ceiling to measure the smoke layer temperature.

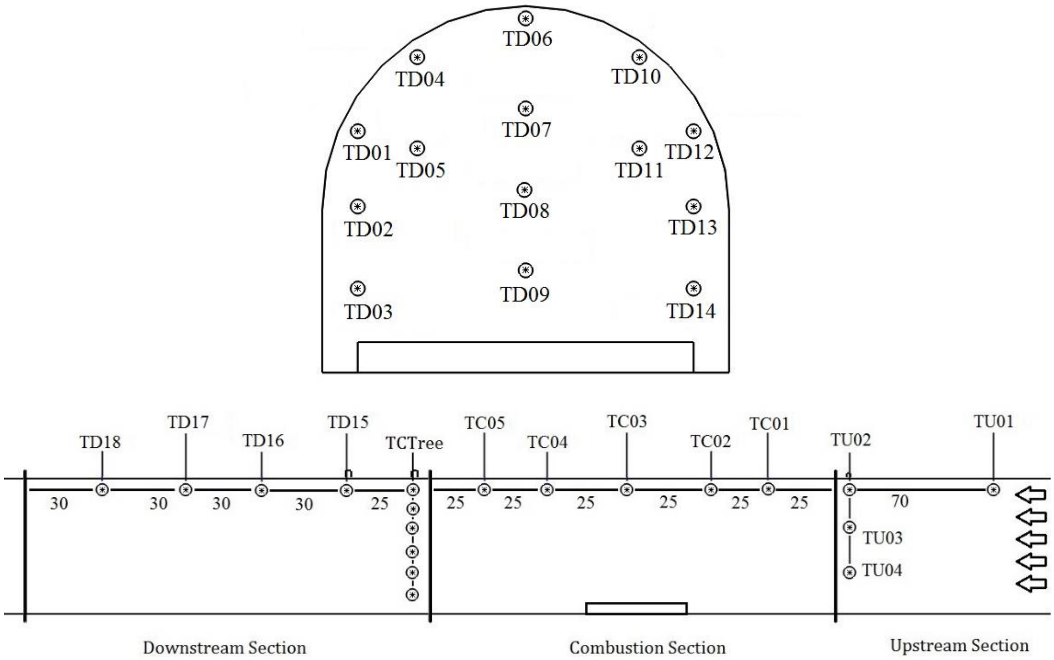

Figure 3.4 Thermocouple tree configuration and thermocouple distribution along the tunnel

The fiberglass reinforced, mineral isolated, K-type thermocouples are composed of NiCr-Ni alloy and can be operated between -200°C and 1200°C with a tolerance of ±0.75 % (or ±2.2°C). Thermocouples are connected to the Omega OMB-DAQ-3005 data acquisition system and the temperature data are simultaneously obtained. The OMB-DAQ-3005 1-Mhz, 16-Bit USB data acquisition system involves the main module and the OMB-PDQ30 expansion module in direct connection with the primary unit. Each module contains six terminals and each terminal has four channels on itself. Three analog and three digital terminals are placed on the main module. The expansion module involves only six analog terminals. The pinout schematics of the modules are presented in appendices. The differential method is used to connect the voltage signals to the terminals.

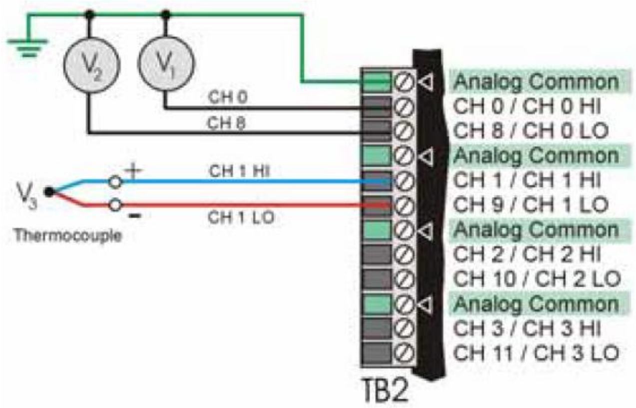

Figure 3.5 Single-Ended (V1 and V2) and differential (V3) connections to analog input channels

DaqView software program is used to gather the synchronized temperature information from the K-type thermocouples. The program converts the voltage data into temperature and records at preset scan rate (1 scan/sec) while displaying on the screen.

For calculation of mass loss rate, the fuel mass is constantly recorded using an A&D GX-K Series Precision balance. The pan is carefully placed onto the balance without any contact with the surroundings for each test. The inclination of pan surface is set to 0° and is measured with an inclinometer. USB connected balance is operated via RsCom v.4.01 software program. The scan rate is set to 1 scan/sec. The program displays the weight for each second on the screen.

Figure 3.6 A&D GX-K series precision balance

The water cooled heat flux sensor (according to Schmidt Boelter) is mounted into the system for specified experiments. The sensor directly measures the radiative and convective heat flux coming from a semispherical field of view to the black coated heat sensitive surface of the device. A water cooling subsystem is established to minimize the errors related with conductive heat transfer on the sensor. The sensor is vertically oriented in the upstream sector of combustion compartment. Considering the flame heights, the sensor is avoided to measure the radiation directly coming from the fire for specific fire scenarios. However the radiation directly coming from the fire and its surroundings is also measured in separate experiments.

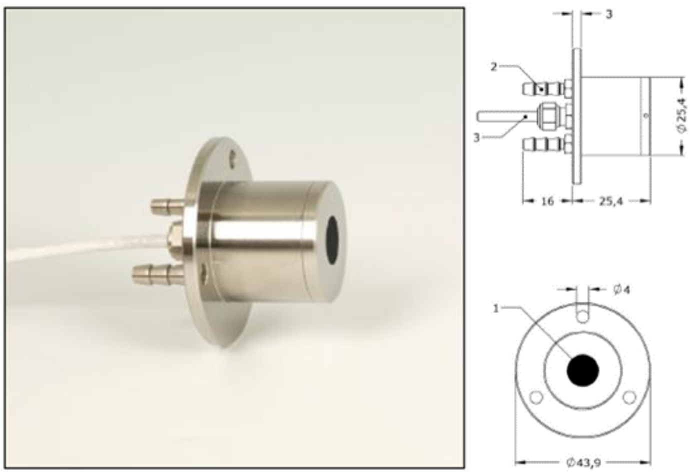

Figure 3.7 SBG01 Water cooled heat flux sensor

3.2 Experimentation

Before performing n-heptane and ethanol pool fire experiments, a series of sample test are conducted. While conducting the experiments, a procedure is formed and the same procedure is applied for each experiment. Since the air flow control is usually difficult to maintain in most of the experimental studies, the flow characterization is a prerequisite to specify the characteristics of the air flow. The next subsections provide information about the previous studies performed on the same experimental setup, the experimental matrices and how the experiments are implemented.

3.2.1 Previous Studies in Tunnel Setup

In 2009, a comprehensive doctoral study was conducted to investigate the effects of different blockage ratios on HRR (Kayili, 2009). Based on a theory, the wood cribs with different configurations are prepared as fire source. The wood sticks with different dimensions are burned under 1, 2 and 3 m/s ventilation conditions.

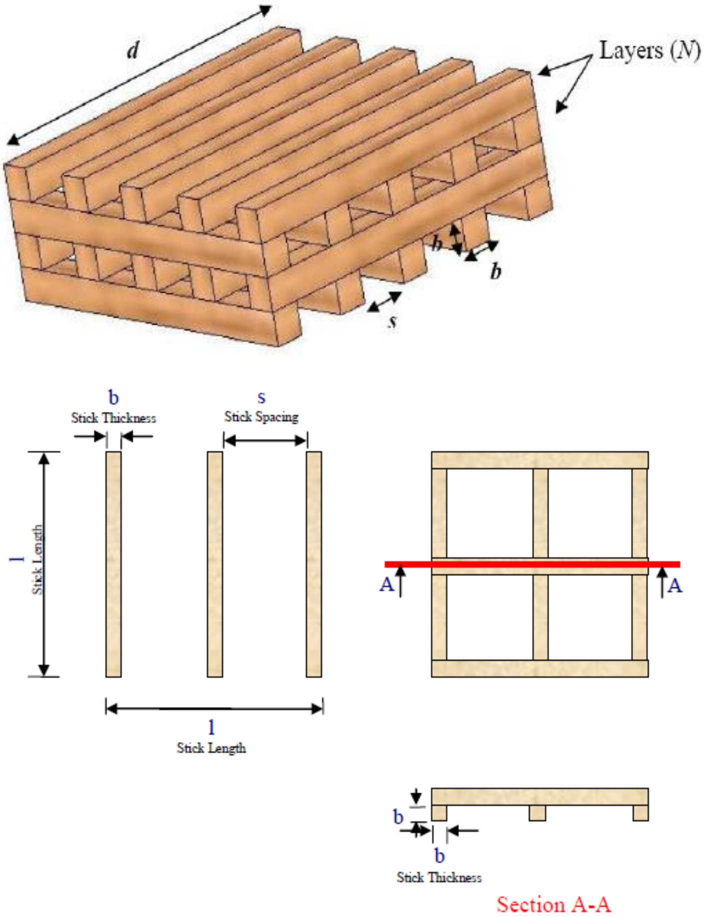

Figure 3.8 Wood crib structure (Kayili, 2009)

HRR, ceiling temperature and mass loss rate measurements are obtained. The analysis of variance statistical technique is employed to generalize the experimental results. The analysis results shows that the effect of blockage ratio is around 80 % on HRR as shown in Figure 3.9.

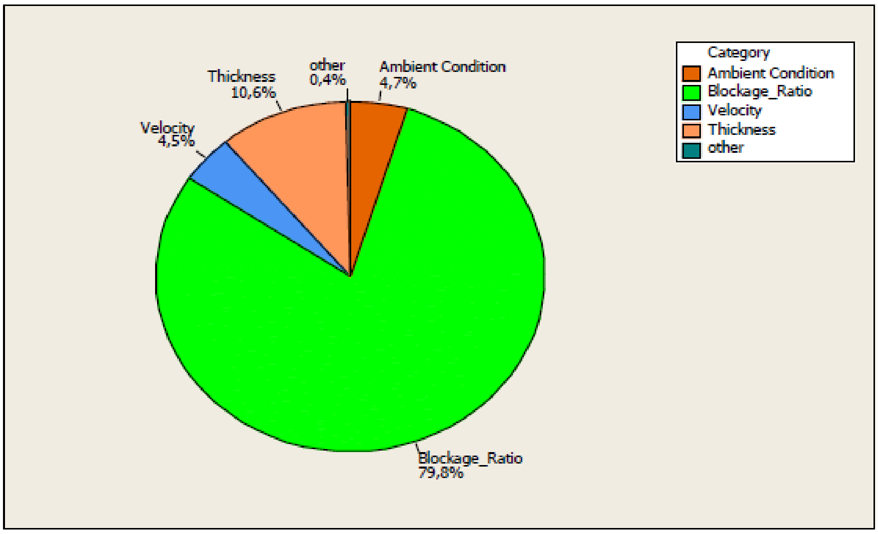

Figure 3.9 Pie chart for a cause of variation in HRR (L=W) (Kayili, 2009)

In another work, Celik (2011) investigates the behavior of ethanol, gasoline and blend pool fires in tunnels with different ventilation conditions. 100 ml, 200 ml and 300 ml ethanol, gasoline and mixture fuels are tested for 0 m/s, 0.5 m/s, 1.5 m/s and 2.5 m/s ventilation velocities with square and rectangular pans. The experimental and numerical results are matched. The experimental results show that the mass loss rate behaviors for 100 ml and 200 ml has consistency with other studies in literature. It is found that mass loss rate increases with increasing fuel amount. It is stated that the peak HRR values remain steady at 1.5 m/s and 2.5 m/s. The decrease in peak HRR of gasoline and mixture pool fires are explained as the reason of flame deflection between 0.5 m/s and 1.5 m/s ventilation conditions. The deflection effect is found as ineffective for non-luminous ethanol fires (Celik, 2011).

3.2.2 Air Flow Characterization

The velocity and temperature measurements are obtained in upstream and combustion sections of the model tunnel using hot-wire anemometer and inclined manometer without combustion occurs.

3.2.2.1 Independent Variable

The independent variables (the inputs) are changed to observe the effect of changing parameters such as ventilation velocity, pan geometry, fuel content or pool depth. However the flow characterization is only applied to visualize the flow profile and to determine the ventilation velocity requirements. The only independent variable is the ventilation velocity by the way of an adjustable-speed compressor.

3.2.2.2 Controlled Variables

- The atmospheric temperature, T_{out} (Air temperature of the area at which the model tunnel is located)
- The room temperature, T_{in} (Air temperature inside laboratory which is intake to the compressor)
- The gravity of acceleration, g = 9.81 m/s
- The atmospheric pressure, P_{atm} = 683 mmHg (91 kPa)
- The density of air at room temperature, ρ_{air} = 1.15 kg/m^3
- The density of ethyl alcohol, $\rho_{eth.alc}$ = 789 kg/m^3

3.2.2.3 Test Procedure

- All the measurement devices are prepared for operation.
- The inside and outside temperatures are recorded according to the readings of anemometer and a thermometer.
- The atmospheric pressure is checked and recorded.
- The compressor is initiated at its maximum speed until the temperature inside the tunnel reaches a stable value between the outside and inside temperatures.
- After reaching a stable temperature inside the tunnel, the compressor speed is decreased to the desired value (463 rpm).
- The compressor speed is altered and the stabilization is ensured again.
- The velocity and temperature values are recorded at the upstream section with intervals of 5 cm.
- The velocity and temperature values are then measured at the combustion section using a pitot tube and an anemometer.

The schematic of the model tunnel and location of measurement points are indicated in Figure 3.10.

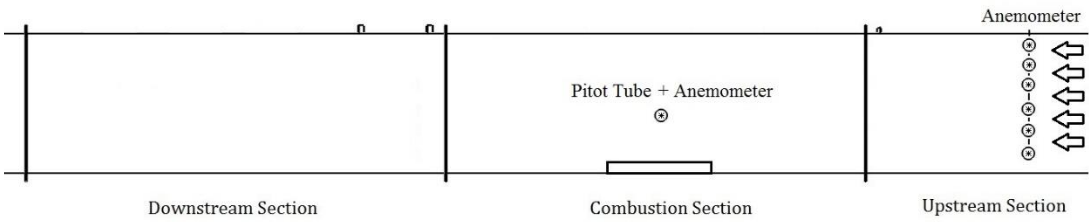

Figure 3.10 Reading locations of ventilation velocity

3.2.2.4 Results of Air Flow Characterization

Figure 3.11 shows the velocity profiles at different vertical heights at upstream section. In case of 0.5 m/s, it is observed that the velocity has a smoother profile compared to higher ventilation velocities.

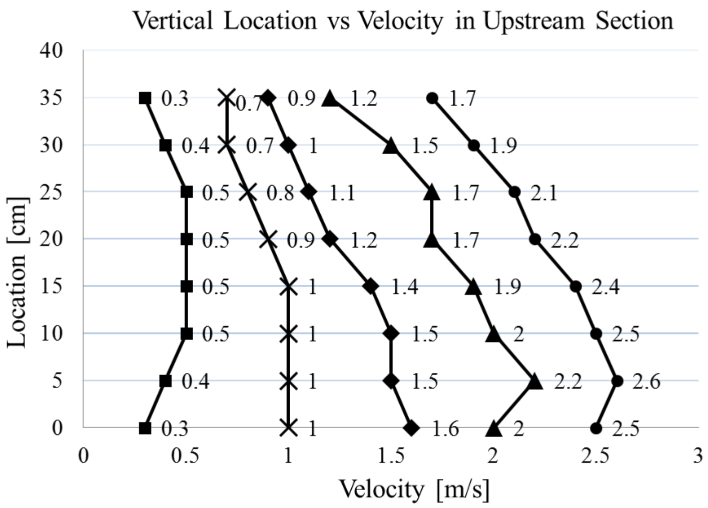

Figure 3.11 Location vs. measured velocities in upstream section of tunnel

The velocity measurements in combustion section are taken from a point 15 cm above the center of pan. Figure 3.12 shows comparison of the measured velocities by anemometer and Pitot tube in the combustion section. The manometer reading for 0.5 m/s was not possible due to device tolerance issue.

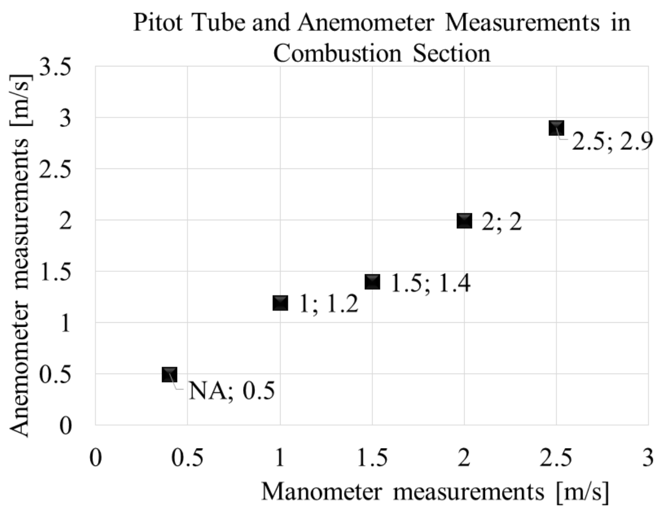

Figure 3.12 Comparison of the measured velocities by anemometer and manometer in combustion section

3.2.3 Experimental Matrices

The whole of experiments are composed of three different groups depending on the fuel type. Pure n-heptane, pure ethanol and volumetric mixing ratios of 10 %, 20 % and 30 % ethanol blended n-heptane fuels are used in experiments.

Pure n-heptane cannot be considered as a fuel source but fuel-oils such as gasoline or diesel involve n-heptane hydrocarbon. Since the crude oil based gasoline and diesel fuels are complex mixtures of vast amount of hydrocarbons, the exact fluid composition is almost impossible to determine. Certain specification based on a set of measurable parameters like the cetane number, provides the proper combustion conditions to internal combustion engines to run up to hundred-thousands of kilometers without any malfunctioning (Meijer, 2010).

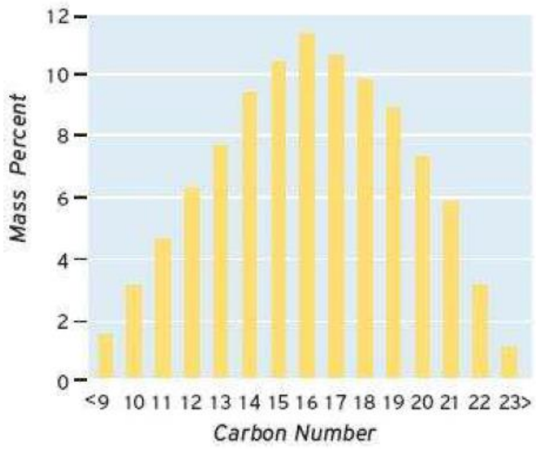

Figure 3.13 Carbon number distribution of typical diesel fuel (Chevron, 2007)

It is commonly known that n-heptane is an unsophisticated compound that satisfies the property targets of commercial diesel fuel. The property targets are stated as the fundamental physical and chemical fuel properties and they are listed by Meijer (2010).

Table 3.2 Properties of diesel and n-heptane (Meijer, 2010)

Variable	***Diesel***	***N-Heptane***	***Units***
Cetane number	56	56	[-]
Boiling Point	483-634	372	[K]
Lover Heating Value	41.54	44.6	[MJ/kg]
AF Stoichiometric	14.7	15.4	[-]
C Ratio	86.2	30.4	[molar%]
H Ratio	13.3	69.6	[molar%]
O Ratio	0.5	0	[molar%]
C/H Ratio	1.85	2286	[-]
Molar Mass	170	100	[kg/kmol]
Latent Heat of Evaporation	250	316	[kJ/kg]

In this study, n-heptane is used as a single component surrogate fuel of diesel fuel and it is one of the controlled variables of experiments performed. The independent variables for experiments of n-heptane pool fires are listed below.

Table 3.3 Experimental matrix of n-heptane pool fires

Exp. Code	***Fuel Type***	***Pan Geometry***	***Pool Depth [mm]***	***Vent. Vel. [m/s]***
HP01-S-05	n-Heptane	Square	0.92	0.5
HP01-S-10	n-Heptane	Square	0.92	1
HP01-S-15	n-Heptane	Square	0.92	1.5
HP01-S-25	n-Heptane	Square	0.92	2.5
HP02-S-05	n-Heptane	Square	1.84	0.5
HP02-S-10	n-Heptane	Square	1.84	1
HP02-S-15	n-Heptane	Square	1.84	1.5
HP02-S-25	n-Heptane	Square	1.84	2.5
HP03-S-05	n-Heptane	Square	2.76	0.5
HP03-S-15	n-Heptane	Square	2.76	1
HP03-S-10	n-Heptane	Square	2.76	1.5
HP03-S-25	n-Heptane	Square	2.76	2.5
HP01-S-05	n-Heptane	Rectangular	0.62	0.5
HP01-R-10	n-Heptane	Rectangular	0.62	1
HP01-R-15	n-Heptane	Rectangular	0.62	1.5
HP01-R-25	n-Heptane	Rectangular	0.62	2.5
HP02-R-05	n-Heptane	Rectangular	1.24	0.5
HP02-R-10	n-Heptane	Rectangular	1.24	1
HP02-R-15	n-Heptane	Rectangular	1.24	1.5
HP02-R-25	n-Heptane	Rectangular	1.24	2.5
HP03-R-05	n-Heptane	Rectangular	1.86	0.5
HP03-R-10	n-Heptane	Rectangular	1.86	1
HP03-R-15	n-Heptane	Rectangular	1.86	1.5
HP03-R-25	n-Heptane	Rectangular	1.86	2.5

The experiment codes described on Table 3.3 briefly give information about the fuel type, fuel amount, pan size and ventilation velocity. The abbreviation HP in the beginning of the codes stand for n-heptane and the following letters and numbers indicate fuel amount, pan size (S for square and R for rectangle pan) and ventilation velocity (i.e. HP02-R-25 is the experiment with 200 ml of n-heptane burning in rectangular pan under 2.5 m/s ventilation velocity). The corresponding pool depths of 100, 200 and 300 ml n-heptane for square pan are 0.92 mm, 1.84 mm and 2.76 mm, respectively. These values for rectangle pan are 0.62 mm, 1.24 mm and 1.86 mm respectively.

The increasing fuel demand and traffic congestion is already mentioned in previous discussions. The policies to regulate the amount of carbon that is put into the atmosphere is the main concern of most governments. The EU set a target of 8 % reduction in annual greenhouse gas emissions by 2010 respect to emissions of 1990 under the agreement of Kyoto Protocol on greenhouse gas emissions. 32 % of EU's total energy is consumed in transport and the energy consumption and road traffic is projected to increase considerably in future. 28 % of CO_2 produced by transport in Europe is thought to be decreased by increasing the usage of substitute fuels (European Commission, 2004). In the report, a detailed information about biofuels is presented. The product of fermented sugar/starch rich grains, the bioethanol, is used in modern spark-ignition engines as an additive of 5 %. In vehicles with modified engines known as 'flexible fuel vehicles' can be used with 85-100 % of ethanol biofuel.

To investigate the effects of ethanol blended fuel fire in tunnels, a series of experiments with varying ethanol fractions are also conducted. In the experimental matrix, the varying parameters are shown. Similar to ones of Table 3.3, the experiment codes briefly show the varying parameters. MX02-S10-05 gives the fuel volume, pan geometry, volumetric content of ethanol in n-heptane and ventilation velocity. For this case, 200 ml ethanol/n-heptane mixture with 10 % ethanol pool fire is tested with square pan under 0.5 m/s ventilation condition.

Table 3.4 Experimental matrix of blended fuel pool fires

Experiment Code	***Fuel Type***	***Pan Geometry***	***Pool Depth [mm]***	***Vol. % of Ethanol***	***Vent. Vel. [m/s]***
MX02-S10-05	Ethanol/n-Heptane	Square	1.84	10	0.5
MX02-S10-10	Ethanol/n-Heptane	Square	1.84	10	1
MX02-S10-15	Ethanol/n-Heptane	Square	1.84	10	1.5
MX02-S10-25	Ethanol/n-Heptane	Square	1.84	10	2.5
MX02-S20-05	Ethanol/n-Heptane	Square	1.84	20	0.5
MX02-S20-10	Ethanol/n-Heptane	Square	1.84	20	1
MX02-S20-15	Ethanol/n-Heptane	Square	1.84	20	1.5
MX02-S20-25	Ethanol/n-Heptane	Square	1.84	20	2.5
MX02-S30-05	Ethanol/n-Heptane	Square	1.84	30	0.5
MX02-S30-10	Ethanol/n-Heptane	Square	1.84	30	1
MX02-S30-15	Ethanol/n-Heptane	Square	1.84	30	1.5
MX02-S30-25	Ethanol/n-Heptane	Square	1.84	30	2.5
MX02-R10-05	Ethanol/n-Heptane	Rectangular	1.24	10	0.5
MX02-R10-10	Ethanol/n-Heptane	Rectangular	1.24	10	1
MX02-R10-15	Ethanol/n-Heptane	Rectangular	1.24	10	1.5
MX02-R10-25	Ethanol/n-Heptane	Rectangular	1.24	10	2.5
MX02-R20-05	Ethanol/n-Heptane	Rectangular	1.24	20	0.5
MX02-R20-10	Ethanol/n-Heptane	Rectangular	1.24	20	1
MX02-R20-15	Ethanol/n-Heptane	Rectangular	1.24	20	1.5
MX02-R20-25	Ethanol/n-Heptane	Rectangular	1.24	20	2.5
MX02-R30-05	Ethanol/n-Heptane	Rectangular	1.24	30	0.5
MX02-R30-10	Ethanol/n-Heptane	Rectangular	1.24	30	1
MX02-R30-15	Ethanol/n-Heptane	Rectangular	1.24	30	1.5
MX02-R30-25	Ethanol/n-Heptane	Rectangular	1.24	30	2.5

CHAPTER 4 EXPERIMENTAL RESULTS AND DISCUSSIONS

In this section, the burning rate, HRR, maximum ceiling temperatures and radiative heat flux results are represented and the effects of ventilation velocity, pool depth, mixing ratio and radiative properties of enclosure surfaces on HRR, burning rate and ceiling temperature distribution are discussed. The complementary figures and graphs are presented in appendices.

4.1 Results of n-Heptane Pool Fire Experiments

4.1.1 Effects of Ventilation Velocity, Pool Depth and Pool Geometry on the Ceiling Temperature Distribution

The results of different ventilation conditions (0.5 m/s to 2.5 m/s) prove that the ventilation velocity plays a fundamental role on HRR, burning rate and ceiling gas temperatures. Because of the competing effects of oxygenation and cooling, the combustion characteristics may exhibit different behaviors.

The ventilation controls the movement of hot product gases. The gas movement is tracked through ceiling temperature variations and the critical ventilation velocity is estimated accordingly. Equation 2.11 also estimates the critical ventilation velocity as proportional to one-third power of convective heat release rate. The convective HRR is considered to be 70 % of the total heat release (Li, Lei, & Ingason, 2010). As can be seen on Figure 4.1, high gas temperatures in the upstream section show that the smoke moves in not only downstream direction but also in the opposite direction of ventilation air flow. The formation of backlayering flow is evident from ceiling temperature results of 0.5 m/s ventilated case. At 1 m/s and above, the maximum ceiling temperatures in upstream and combustion sections continue to decrease. The lower ceiling temperatures show that the smoke stratification in upstream section disappears and around 1 m/s, the critical ventilation is reached. This is in well agreement with corresponding data in the literature which estimate critical ventilation velocity between 0.96 m/s and 1.3 m/s depending on the values of convective HRR and gas temperature in the formula of Thomas (1968).

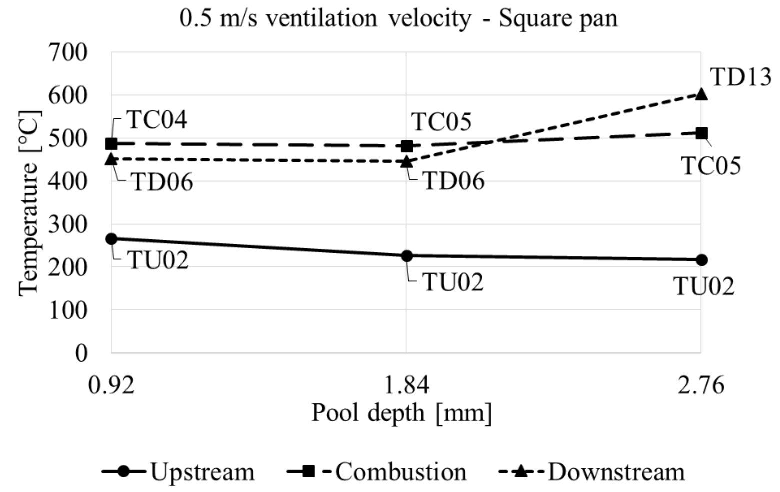

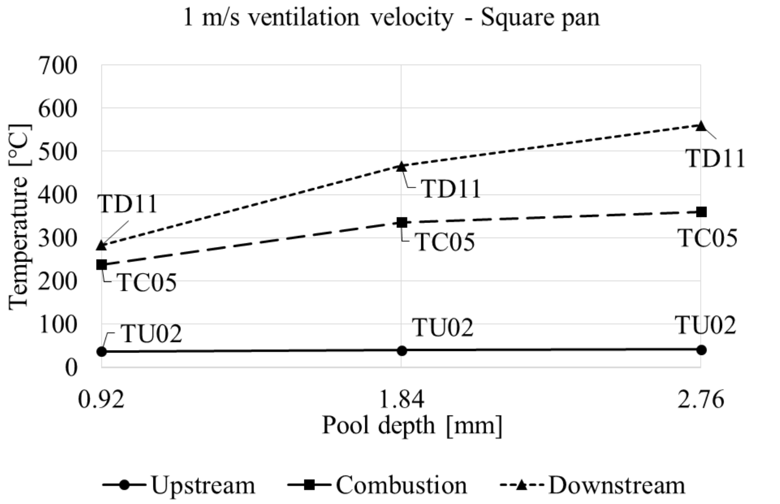

Figure 4.1 Maximum ceiling temperature data of heptane pool fires under 0.5 m/s and 1 m/s ventilation velocities with square pan

The graphs in Figure 4.1 and Figure 4.3 also shows the decrease in maximum ceiling temperatures in upstream and combustion sections for enhancing ventilation conditions up to 2.5 m/s. The influence of cooling in downstream section is limited. The temperatures of downstream section barely decrease to 500˚C at 1.5 m/s ventilation condition. After this point, the slight decrease in downstream temperatures stops due to the deflection of fire and the predominant oxygenation effects of fire on cooling effects of ventilation in downstream region. This phenomena is further investigated by examining the O_2, CO gas concentrations and HRR graphs in Figure 4.2. The graphs show that the oxygen concentrations inside the tunnel increase with increasing ventilation velocity. CO and CO_2 concentrations decrease due to enhanced ventilation. Therefore the lower HRR are calculated for these cases but the maximum ceiling temperatures inside the combustion section for 2.76 mm pool depth cases do not decrease further under 1.5 m/s and 2.5 m/s ventilation conditions. This can be interpreted as the deflection of fire towards the downstream side of the combustion section and enhanced oxygenation effects due to the excess air supplied with 2.5 m/s ventilation velocity. Thus, these effects cause the ceiling temperatures in combustion region to increase even though the HRR declines.

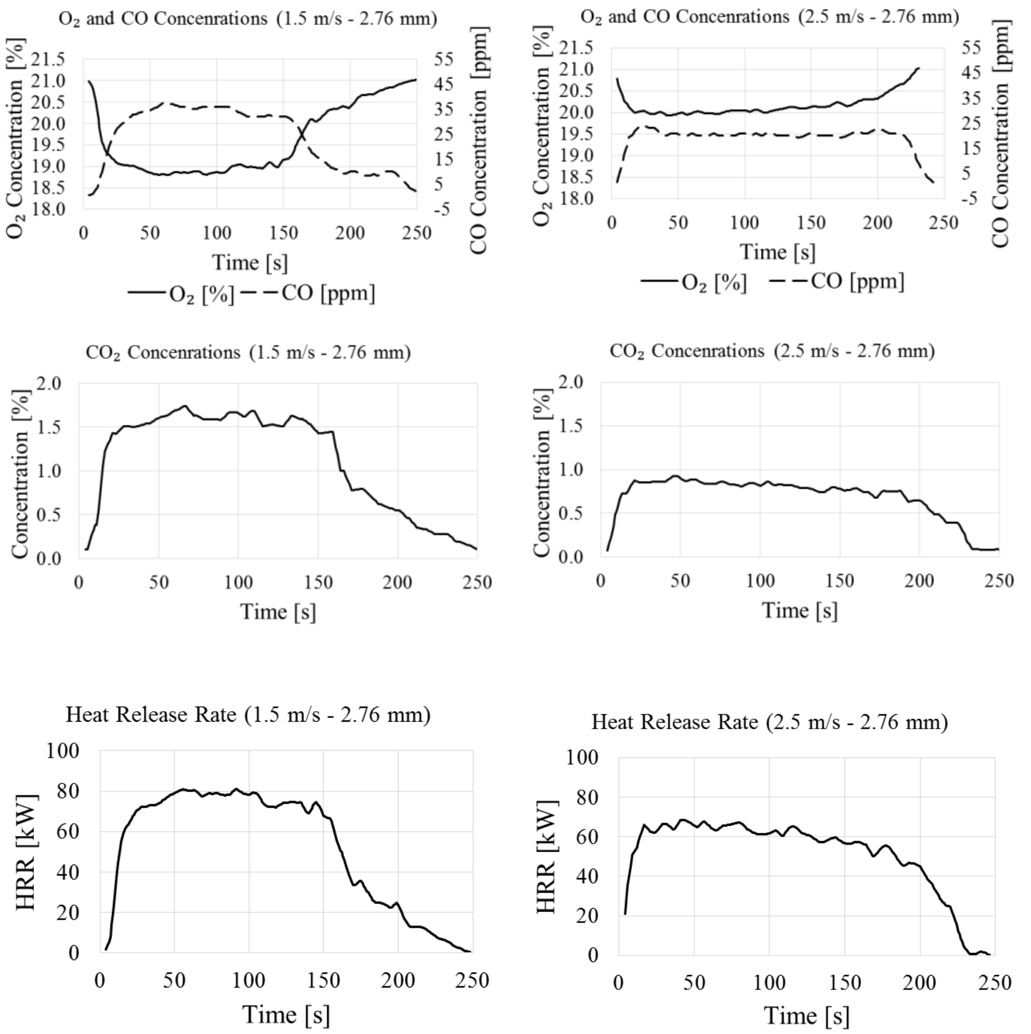

Figure 4.2 O_2, CO_2, CO gas concentrations and HRR history of square pool fires 2.76 mm pool depth under 1.5 m/s and 2.5 m/s ventilation conditions

The ceiling temperature in combustion and downstream sections increases with increasing pool depths. This is an obvious result of increasing HRR for higher pool depths as illustrated in Figure 4.7. The condensed phase under the burning surface is heated by the convective and radiative heat transferred to the surface and the condensed phase reaches the boiling point faster. The rapid combustion of gas phased fuel occurs for pool fires with higher depths. Hence, the temperature and HRR increase.

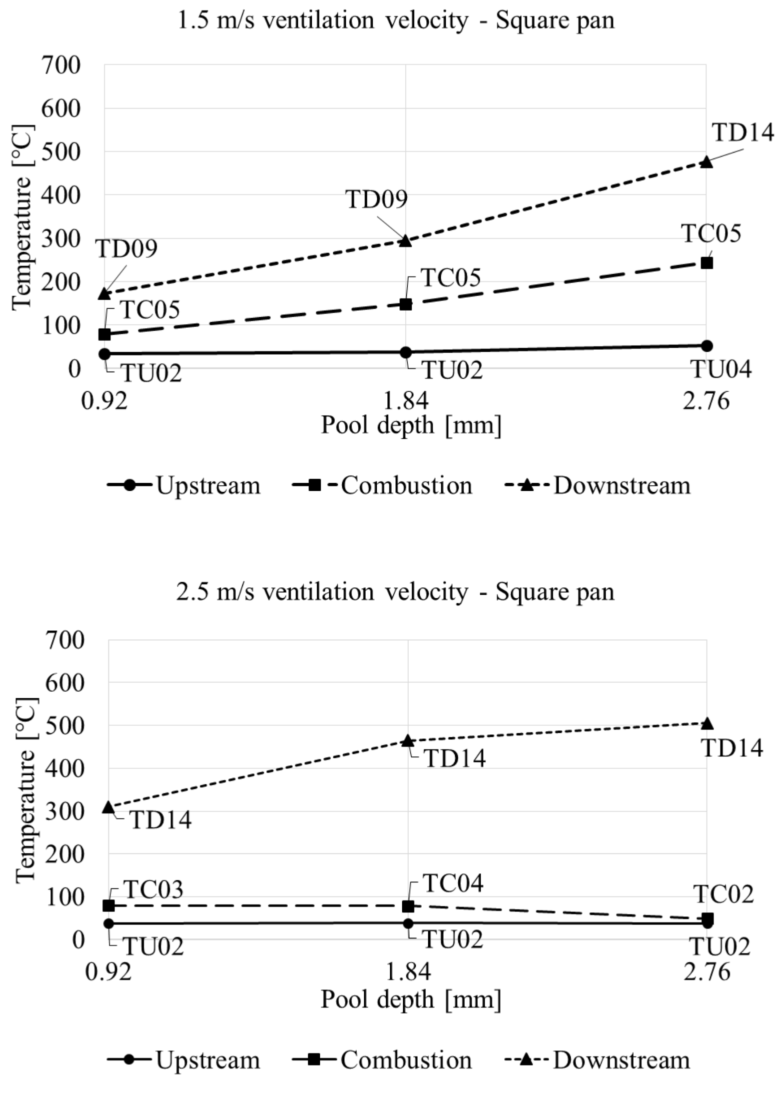

Figure 4.3 Maximum ceiling temperature data of heptane pool fires under 1.5 m/s and 2.5 m/s ventilation velocities with square pan

The experiments with rectangular pan geometry are also performed under same conditions. The ceiling temperature results of rectangular pan are higher than square pan cases due to increasing fire size and radiative effects (Figure 4.4 and Figure 4.5). The critical ventilation condition is again reached under 1 m/s ventilation condition.

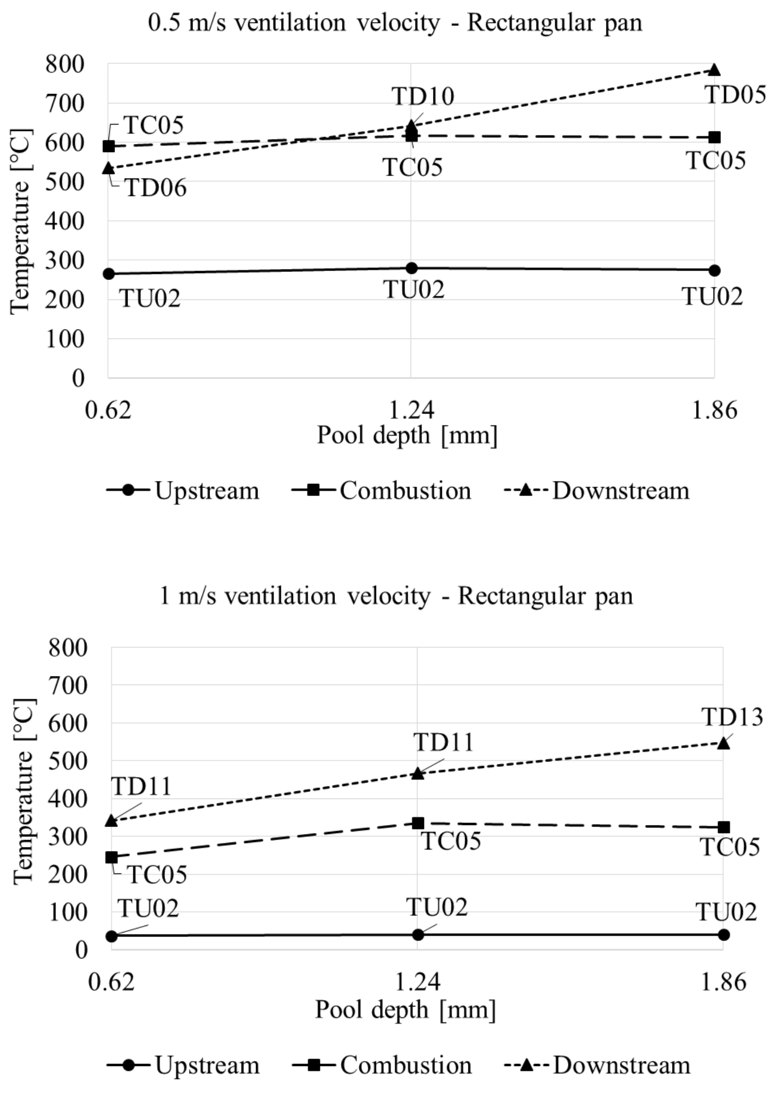

Figure 4.4 Maximum ceiling temperature data of heptane pool fires under 0.5 m/s and 1 m/s ventilation velocities with rectangular pan

Figure 4.5 show that the cooling effects are significant up to 1.5 m/s ventilation condition. Therefore, the temperatures in all regions continuously decrease. The fire is deflected in 2.5 m/s ventilation case of rectangular pool fires with 1.24 mm and 1.86 mm pool depth. As a result the temperatures in downstream section increase.

The effect of deflection decrease for lower pool depths. The ceiling temperatures of rectangular pool fires with 1.24 mm and 1.86 mm pool depths change between 400-500˚C and 500-700˚C however the variation is between 320-350˚C for 0.62 mm pool depth case. From 1.5 m/s to 2.5 m/s ventilation condition, the temperatures of square pan cases change in the range of 180-310˚C, 300-480˚C and 480-500˚C for 0.92 mm, 1.84 mm and 2.76 mm pool depths respectively.

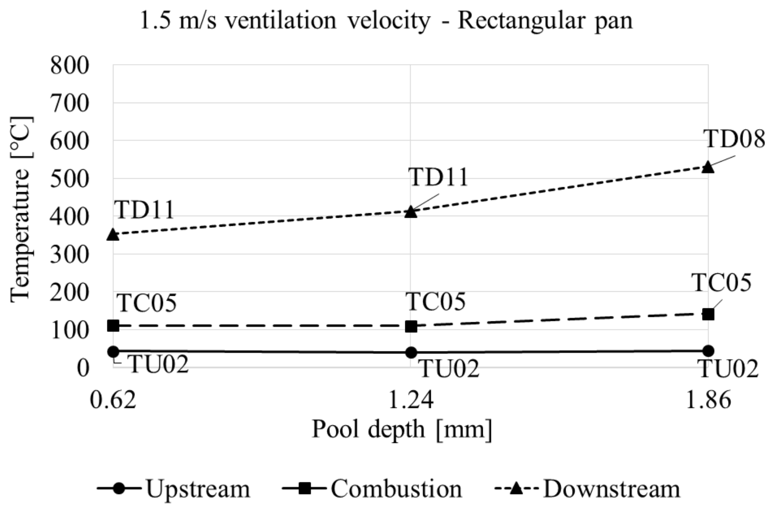

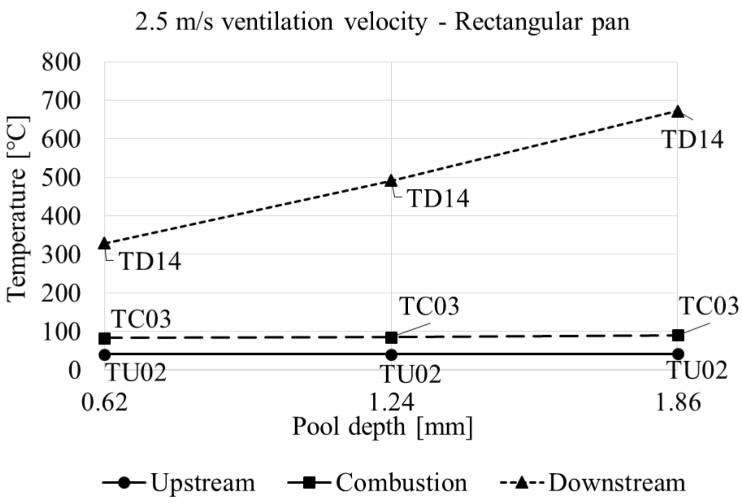

Figure 4.5 Maximum ceiling temperature data of heptane pool fire under 1.5 m/s and 2.5 m/s ventilation velocities with rectangular pan

Although the similar temperature trends for enhancing ventilation velocities are observed in rectangular pan cases, the decrease in downstream section from 1 m/s to 1.5 m/s ventilation condition is reversed at 2.5 m/s ventilation velocity. The downstream ceiling temperatures reached to 700˚C for 2.5 m/s ventilation case. The result of similar conditions with square pan case barely escalates to 500˚C even with a higher pool depth (2.76 mm). The related HRR and burning rate values in Figure 4.7 and Figure 4.12 are almost constant for 1.5 m/s and 2.5 m/s ventilation cases of rectangular pool fires. To understand the reason of the increment in temperature, the HRR and gas concentration plots are particularly inspected. The graphs in Figure 4.6 indicate that increasing ventilation velocity increases the oxygen availability in the vicinity of fire. The oxygen concentrations at 2.5 m/s ventilation velocity reach 19 % while the minimum oxygen concentrations under 1.5 m/s ventilation condition are around 18 %. The product gas concentrations (i.e. CO_2 and CO) are diluted with enhanced ventilation. The HRR values for 2.5 m/s ventilation case are slightly higher than the ones of 1.5 m/s ventilation condition. These may cause the ceiling temperature in downstream section to increase but the major effects are the oxygenation and deflection of fire again. The high ventilation velocity deflects the fire towards the downstream as it happens in similar cases of square pool fires but this time the size of the fire is also greater. Therefore, the main reason of bounce in ceiling temperature of combustion section is the deflection of fire and enhanced oxygen supply.

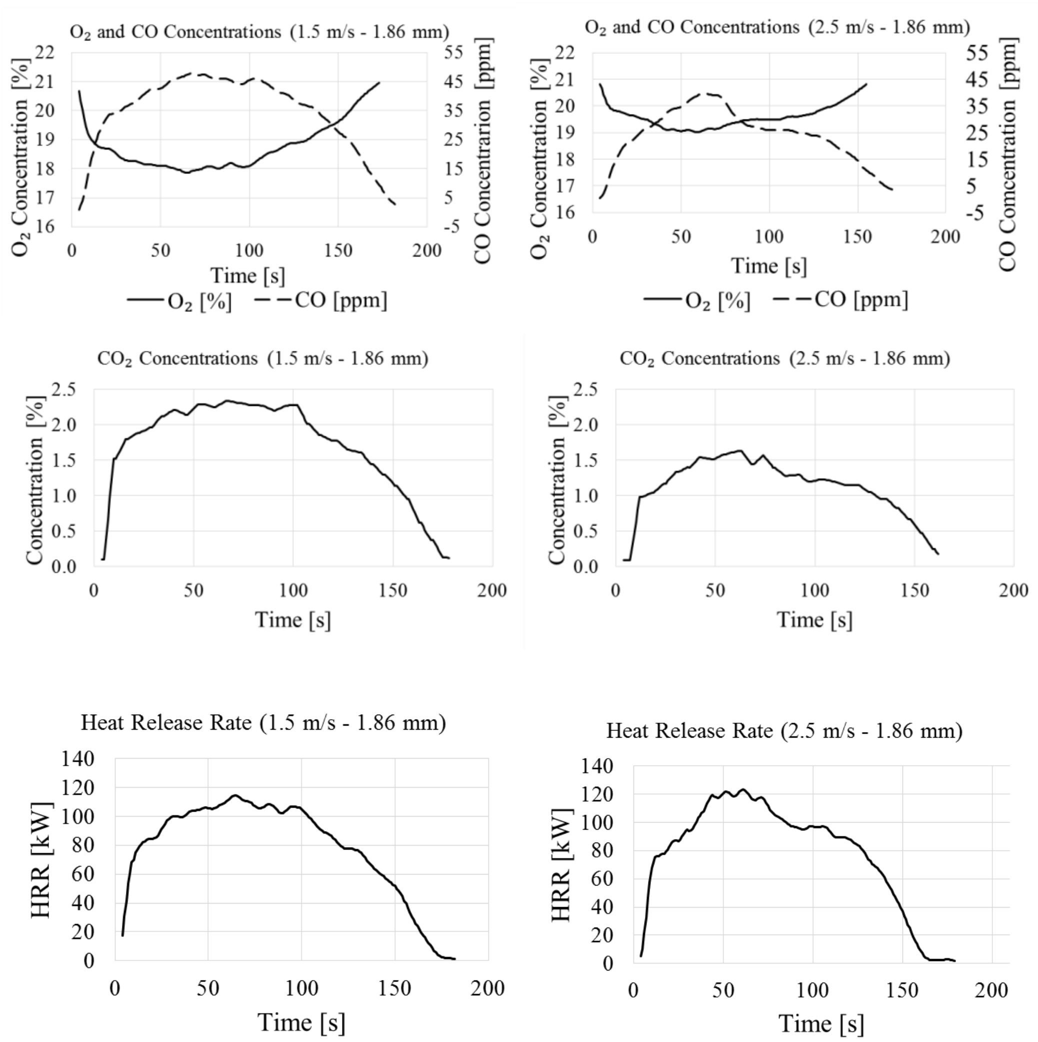

Figure 4.6 O_2, CO_2, CO gas concntrations and HRR history of rectangular pool fires with 1.86 mm pool depth under 1.5 m/s and 2.5 m/s ventilation conditions

4.1.2 Effects of Ventilation Velocity, Pool Depth and Pool Geometry on HRR and THR

The HRR and NTHR calculated based on oxygen consumption calorimetry method are plotted on Figure 4.7 and Figure 4.8. HRR values on Figure 4.7 are obtained by time-averaging HRR history over the range of quasi-steady combustion as it is applied in a previous study (Roh, Ryou, Kim, Jung, & Jang, 2007). Except for rectangle pan cases with 1.86 mm pool depth, HRR and NTHR have a peak value at 1 m/s after which point, they tend to decrease at 1.5 and 2.5 m/s ventilation velocities. One of the important point is that the combustion durations are lower for 1.84 mm and 2.76 mm square pan pool fires at 1 m/s ventilation velocity. However the lowest HRR are obtained in 0.5 m/s ventilation condition due to low oxygen availability.

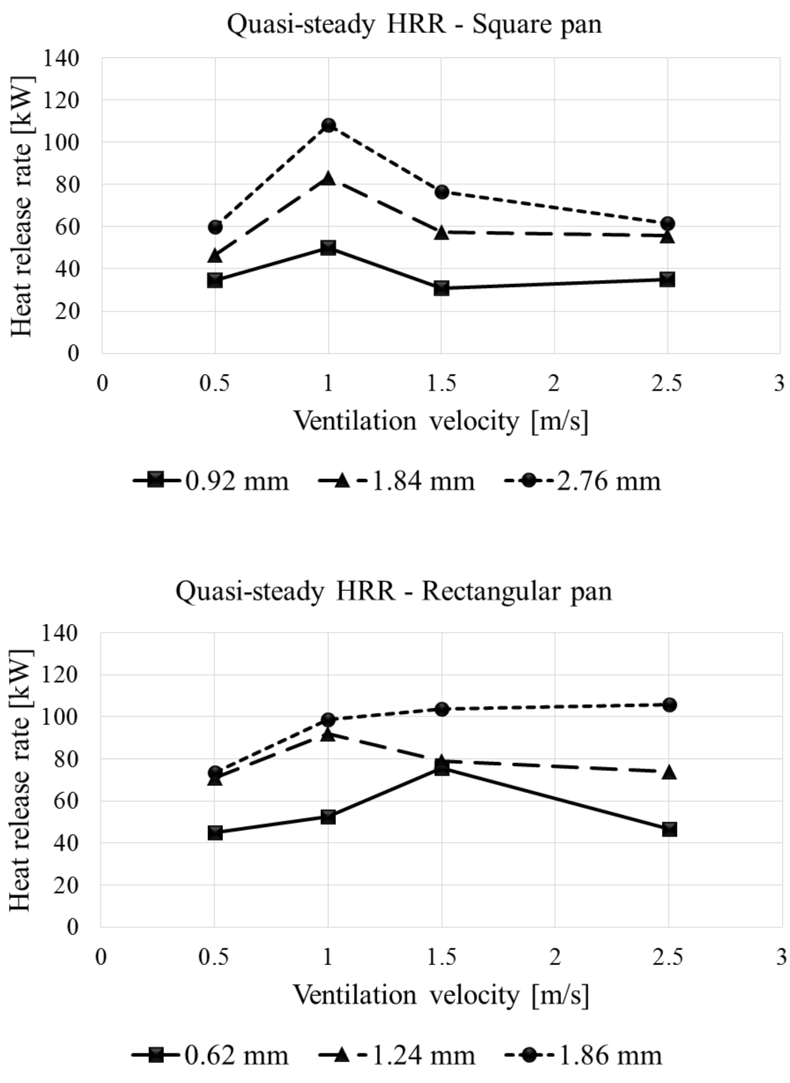

Figure 4.7 Quasi-steady HRR results of heptane pool fires

The NTHR can be described as the total energy release per unit volume of fuel. It has the lowest values at 0.5 m/s ventilation condition. It is known that significant amount of unburnt pyrolysis product gases may be produced due to underventilation condition (Karlsson & Quintiere, 2000). This statement supports that the combustion inefficiently occurs under 0.5 m/s ventilation condition. At 1 m/s ventilation velocity, NTHR has the peak values for the majority of the cases.

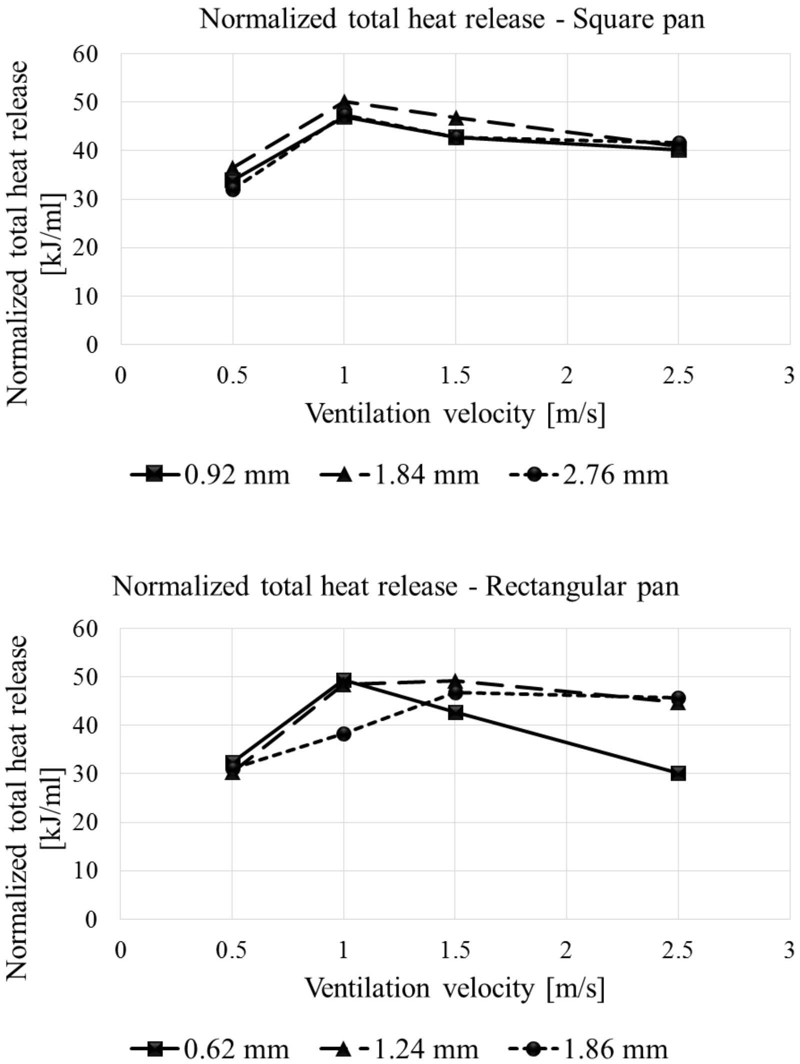

Figure 4.8 Normalized total heat releases of heptane pool fires

4.1.3 Effects of Ventilation Velocity, Pool Depth and Pool Geometry on Product Gas Concentrations

The measuring point of product gases is illustrated in Figure 3.1 and Figure 3.2. O_2, CO_2 and CO concentrations are the variables measured in the tunnel outlet during the combustion. The other variables are O_2, CO_2 and H_2O concentrations of incoming air as shown in Equation 2.8. A time history of the product gas concentrations are formed for each experiment to calculate the HRR as a function of time as shown in Figure 4.9.

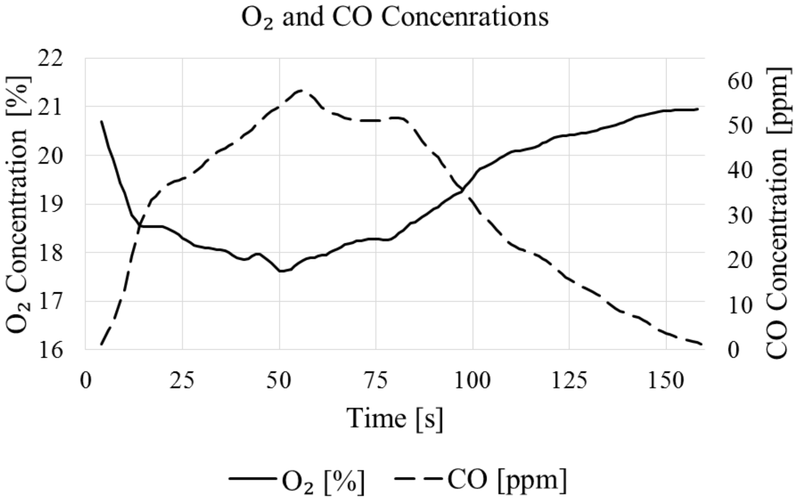

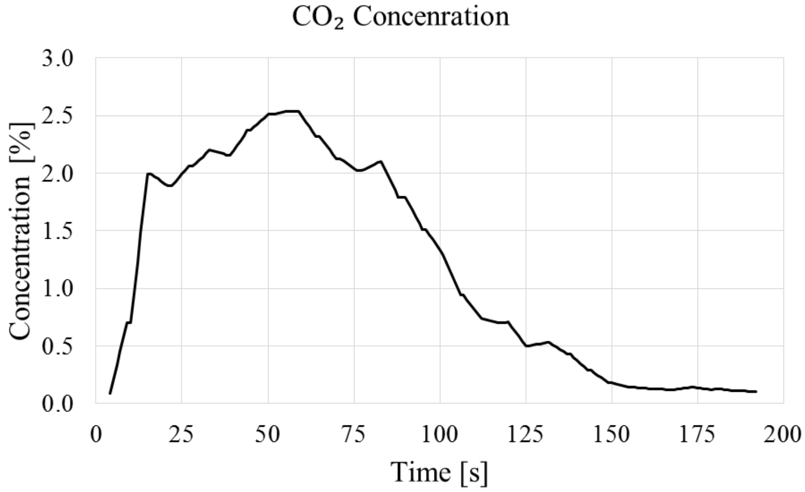

Figure 4.9 Time history of O_2, CO_2 and CO concentrations for HP01-S00-05

While comparing the concentration results of different conditions, the peak values are evaluated. The minimum O_2 concentrations are reached in underventilated (0.5 m/s) conditions. The CO_2 and CO concentrations of rectangular pan cases are higher than the square pool fires. The total of O_2, CO_2 and CO concentrations for 0.5 m/s ventilation case is always lower than the ones with 1 m/s, 1.5 m/s and 2.5 m/s ventilation conditions. These values are measured as 20.1 %, 20.6 %, 20.8 % and 20.1 % for square pool fires with 0.92 mm pool depth under 0.5 m/s, 1 m/s, 1,5 m/s and 2.5 m/s ventilation conditions, respectively.

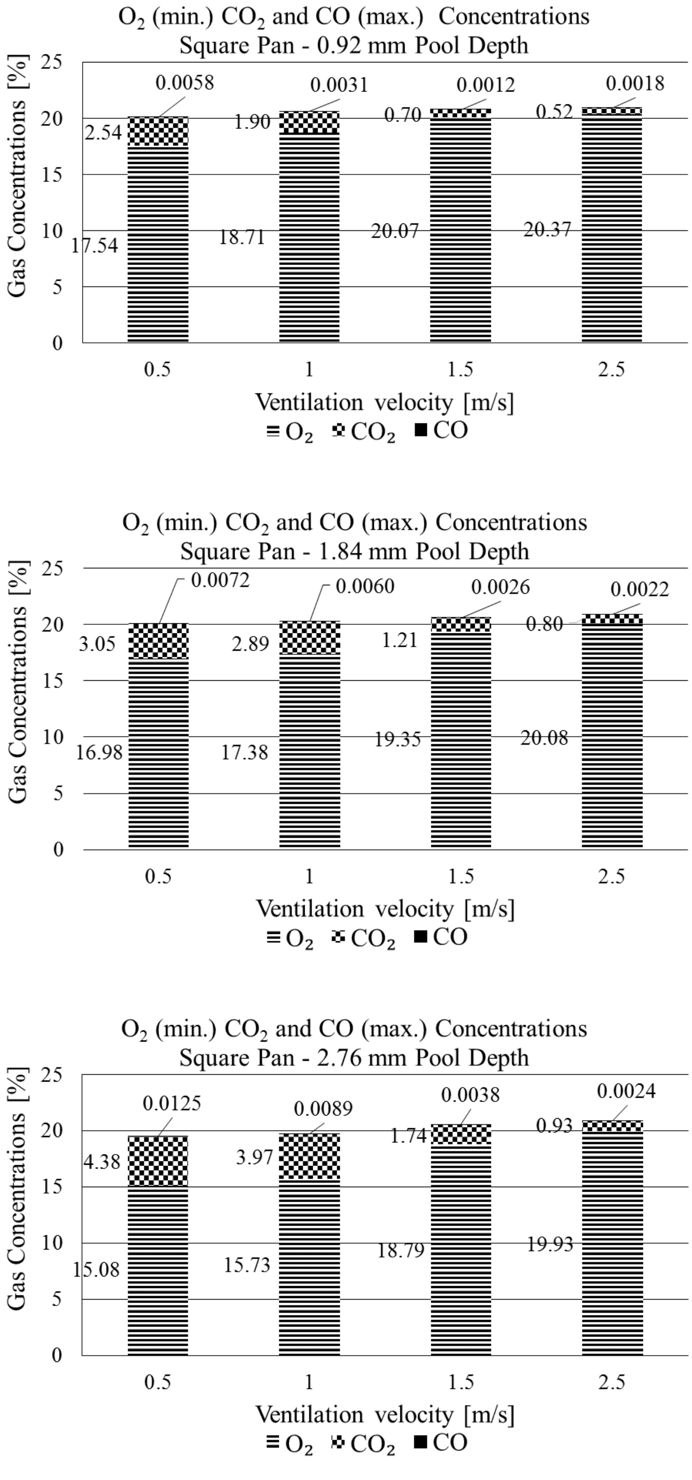

Figure 4.10 O_2, CO_2 and CO concentrations of heptane pool fires with square pan

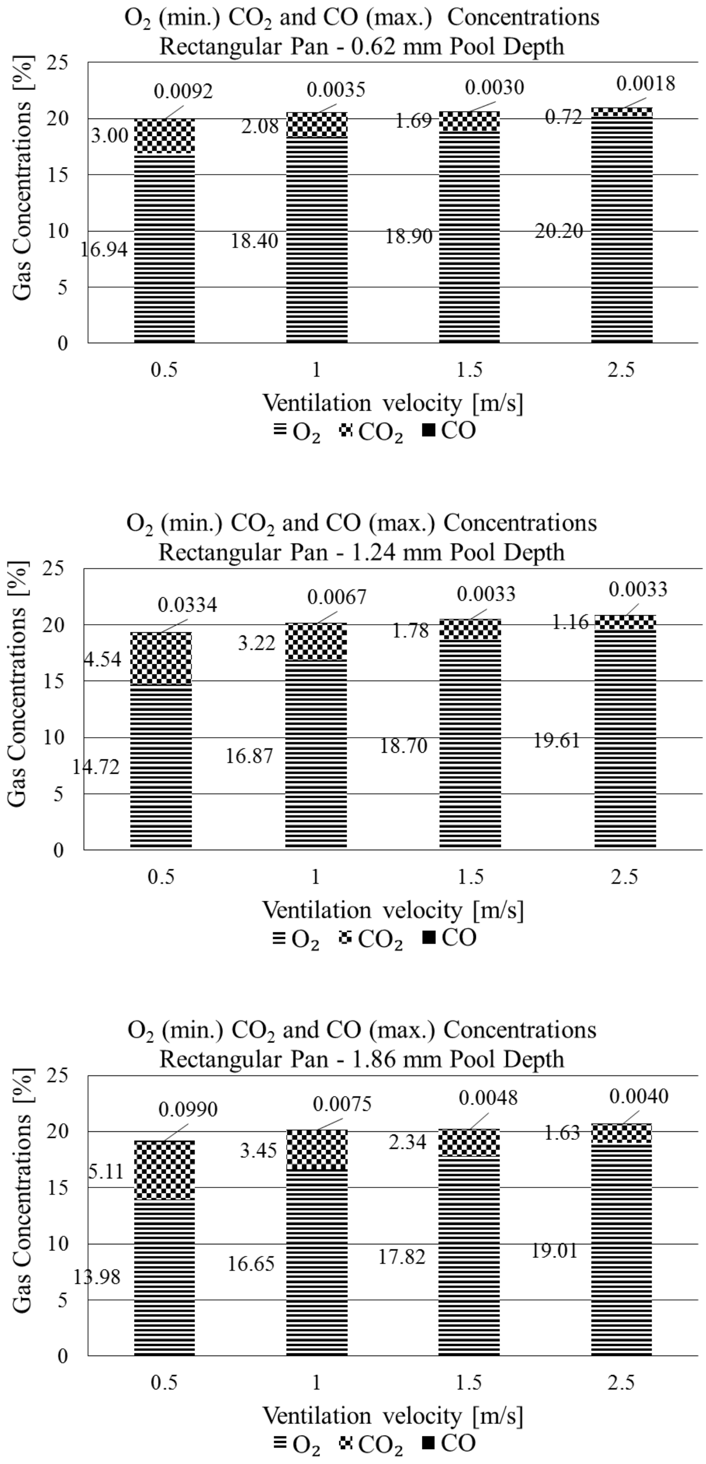

Figure 4.11 O_2, CO_2 and CO concentrations of heptane pool fires with rectangular pan

4.1.4 Effects of Ventilation Velocity, Pool Depth and Pool Geometry on Burning Rate and Combustion Duration

The steady burning rates have stable regimes that have the highest values for 2.76 mm (for square pan fires) and 1.86 mm (for rectangular pool fires) as shown in Figure 4.12. The variations of burning rates show that the pool depth is highly influential. The fuel in condensed phase under the burning surface is heated by the fire. Higher temperatures in the vicinity of pool accelerate the evaporation of fuel. The heating effects of fire on burning rate has been studied and empirical formulations have been derived in previous studies (Hu L. , Liu, Xu, & Li, 2011), (Woods, Fleck, & Kostiuk, 2006), (Chen, Lu, Li, Kang, & Lecoustre, 2011) and (Hu L. H., Liu, Peng, & Huo, 2009). Hu et al. (2009) have studied on square/rectangular gasoline and methanol pool fires with 0 to 3 m/s longitudinal air flows in a wind tunnel with 1.8 m in height and 6 m in test section length. It is found that both gasoline and methanol burning rates increase with increasing longitudinal air flow. It is stated that increasing air flow enhanced the deflection of fire towards the pool rim and more heat is supplied to the fuel. The similar situation may be discussed between 0.5 m/s and 1 m/s ventilation velocities. However, it should be noted that the ceiling temperatures of combustion section at 1.5 m/s and 2.5 m/s ventilation conditions are around 100˚C (in Figure 4.3 and Figure 4.5), so that the cooling effects of ventilation are dominant in this region. The decrease of burning rates for 1.5 m/s and 2.5 m/s ventilation conditions may be the results of the cooling effect.

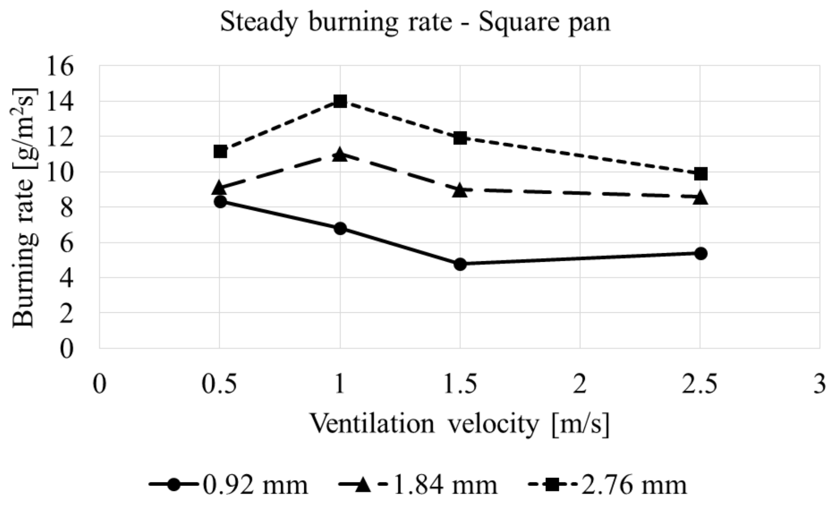

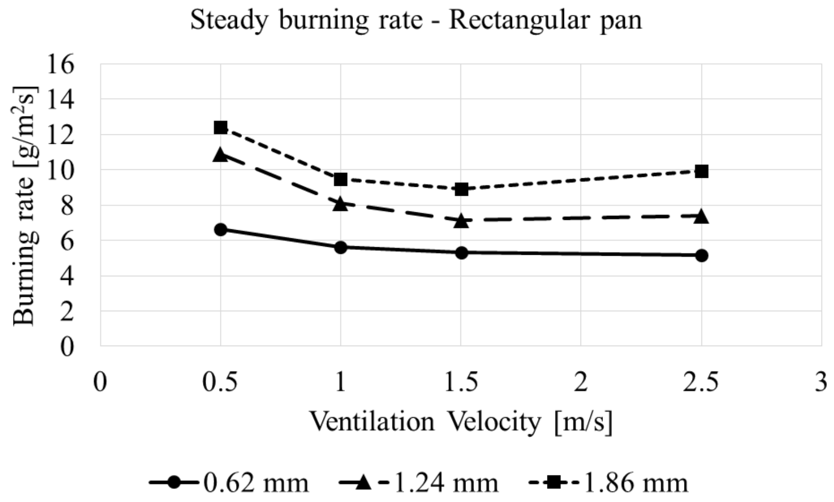

Figure 4.12 Steady burning rates of heptane pool fires

The following figures show the time histories of mass and burning rates for 0.5 m/s ventilation condition. It is apparent that the slope of mass vs. time graphs increase with increasing fuel amount for 65 g, 132 g and 186 g (corresponding pool depths are 0.92 mm, 1.84 mm and 2.76 mm) of heptane fuels with square pan. 186 g heptane pool fire could have burnt out in 300 seconds in parallel with increasing fuel quantities if the heating and cooling effects have insignificant influence on the fuel. However the combustion durations of fuels with 1.84 mm and 2.76 mm are almost the same (225 seconds) due to the heating effects on condensed phase fuel under 0.5 m/s ventilation conditions.

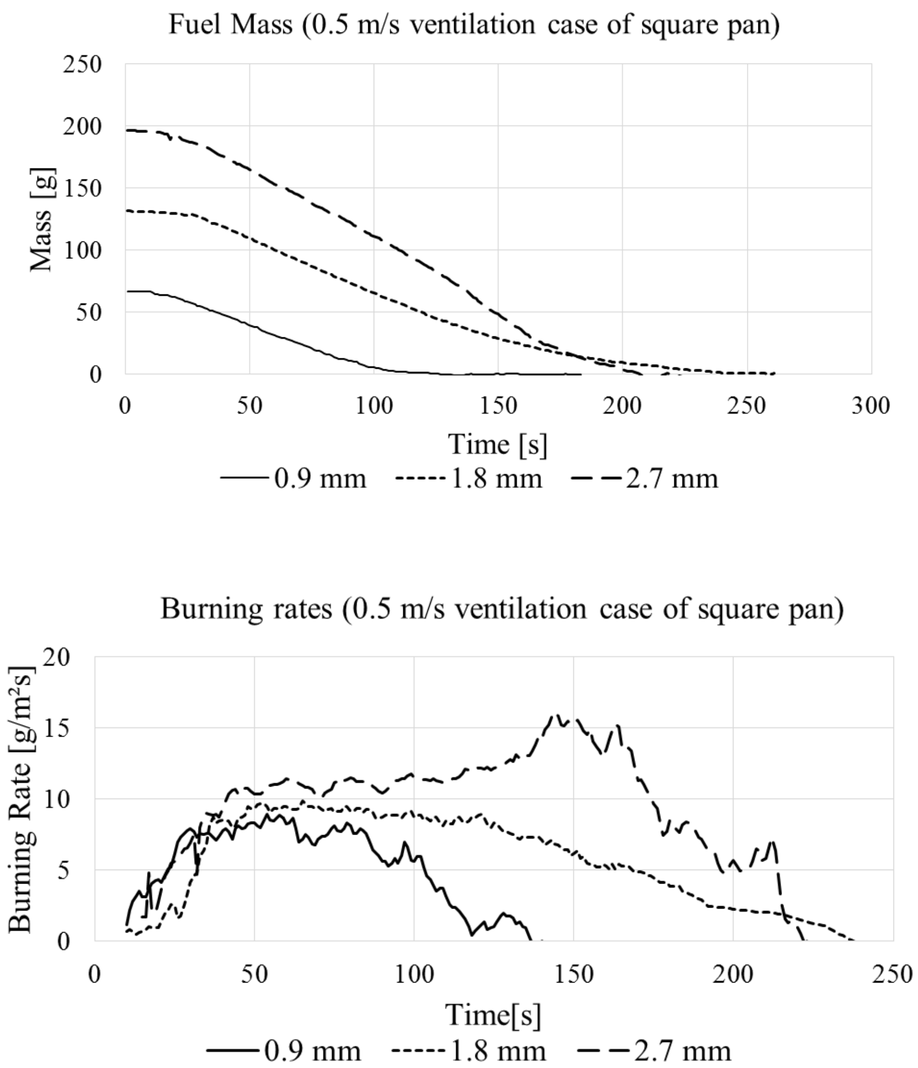

Figure 4.13 Mass loss and burning rates of heptane pool fires for different pool depths with 0.5 m/s ventilation velocity for square pan case

In rectangular pan cases with 0.5 m/s ventilation velocity, the slopes of 132 g and 186 g of heptane fuels are almost equal. Their burning rates reached up to 12 g/m^{2}s. It shows that heating of pan rims has minimal effects on rectangular pan with 1.8 mm pool depth and the combustion duration of this case extends to 200 seconds but theoretically speaking, the combustion duration of 1.8 mm rectangular pool fire should have been 225 seconds regardless of any heating effects.

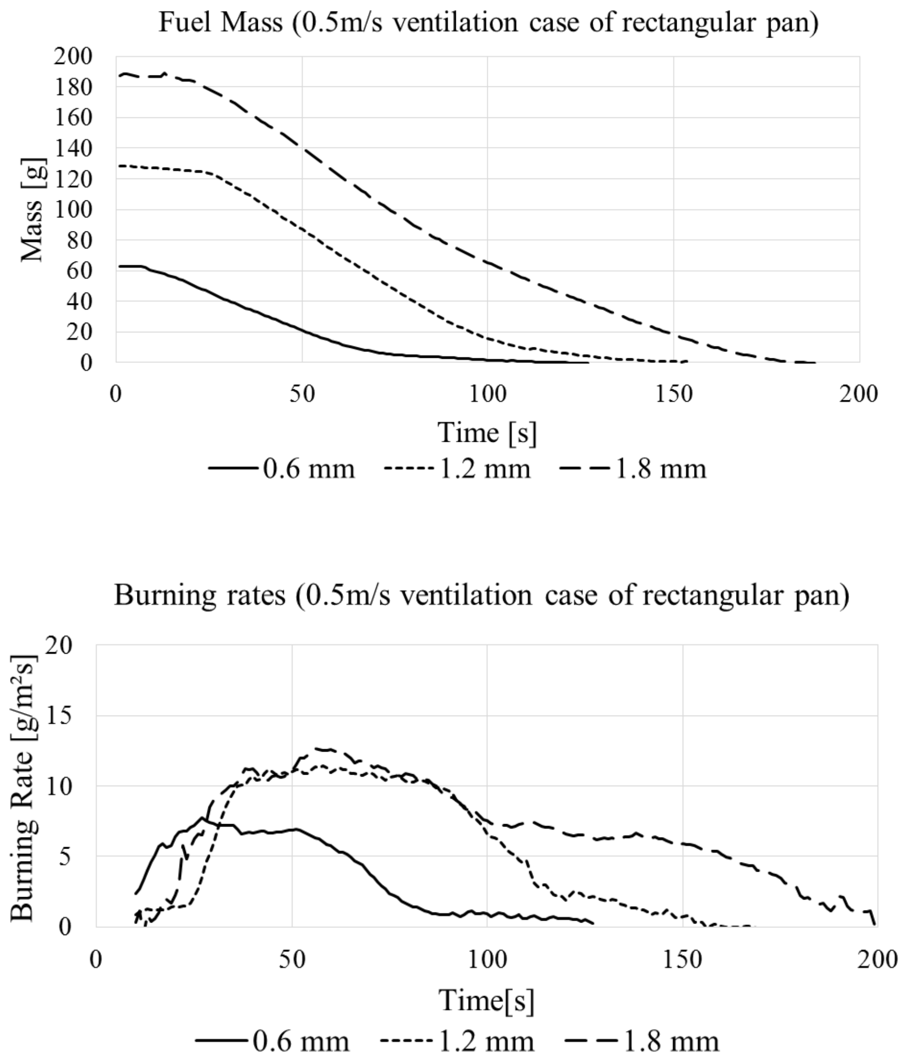

Figure 4.14 Mass loss rates and burning rates of heptane pool fires for different pool depth cases with 0.5 m/s ventilation velocity for rectangular pan case

The overall effects of ventilation and pan geometry on combustion durations are reviewed in Figure 4.15. In the graphs, the general trend of combustion duration can be interpreted as the decremented increase with increasing pool depths. The majority of rectangular pool fire durations are lower than the square pan cases. This means that the burning rates of rectangular pool fires are generally high.

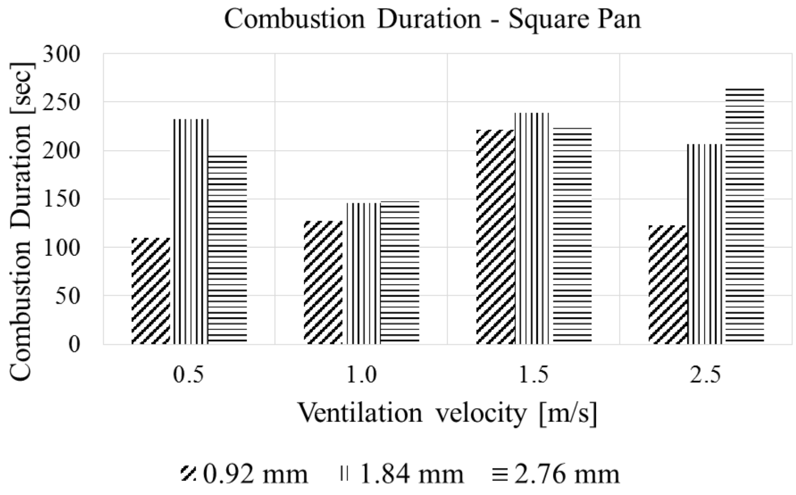

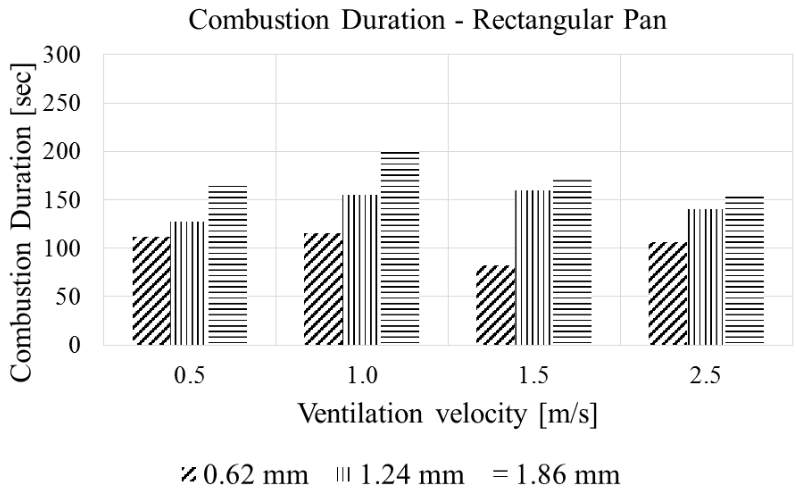

Figure 4.15 Combustion durations of heptane pool fires

4.2 Results of Ethanol/ n-Heptane Pool Fire Experiments

4.2.1 Effects of Ventilation Velocity, Pool Geometry and Ethanol Content on the Ceiling Temperature Distribution

Results indicate that the critical ventilation velocity is achieved between 0.5 m/s and 1 m/s which is in agreement with correlations of previous studies in the literature (Thomas, 1968) and (Wu & Bakar, 2000). The maximum ceiling temperature figures show that increasing ethanol fractions cause downstream ceiling temperatures to increase for square pan cases with 0.5 m/s ventilation velocity. For enhanced ventilation conditions, the ceiling temperatures in downstream section reaches up to 450˚C. This shows that the cooling effect starts to dominate the fire for velocities higher than 0.5 m/s. However the maximum ceiling temperature results of rectangular pan cases are significantly higher than square pan results. The downstream temperatures of 30 % ethanol blended heptane pool fire with rectangular pan under 0.5 m/s ventilation condition are 800˚C and they barely decreased to 500˚C for other ventilation conditions. The only difference between 1 m/s, 1.5 m/s and 2.5 m/s ventilation velocities is the maximum ceiling temperatures of combustion section. The ceiling temperatures in combustion section are around 300-450˚C for rectangular and square pool fires at 1 m/s ventilation velocity, however they decrease to 100-200˚C and 50-100˚C for 1.5 m/s and 2.5 m/s as illustrated in Figure 4.17 and Figure 4.19.

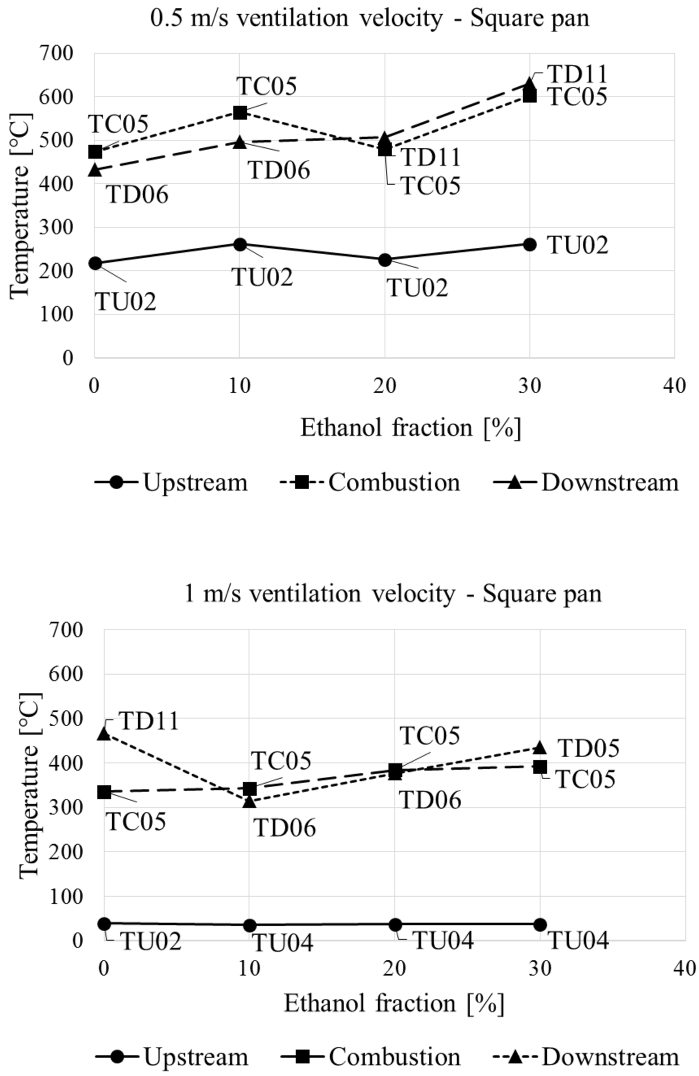

Figure 4.16 Maximum ceiling temperatures of ethanol/heptane pool fires under 0.5 m/s and 1 m/s ventilation conditions with square pan

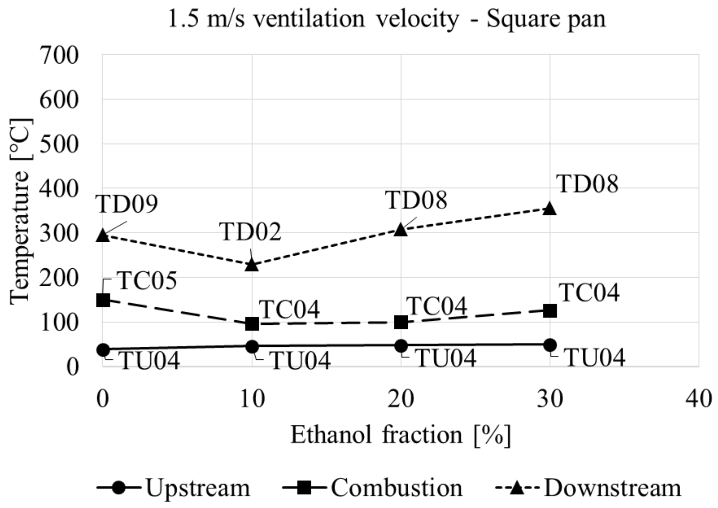

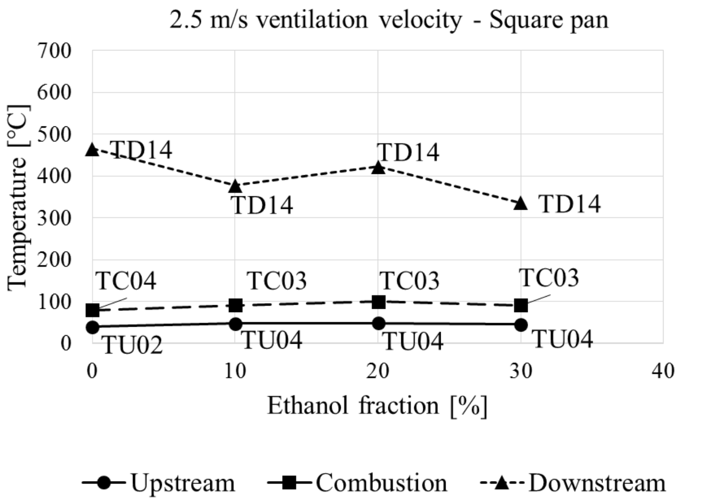

Figure 4.17 Maximum ceiling temperatures of ethanol/heptane pool fires under 1.5 m/s and 2.5 m/s ventilation velocities with square pan

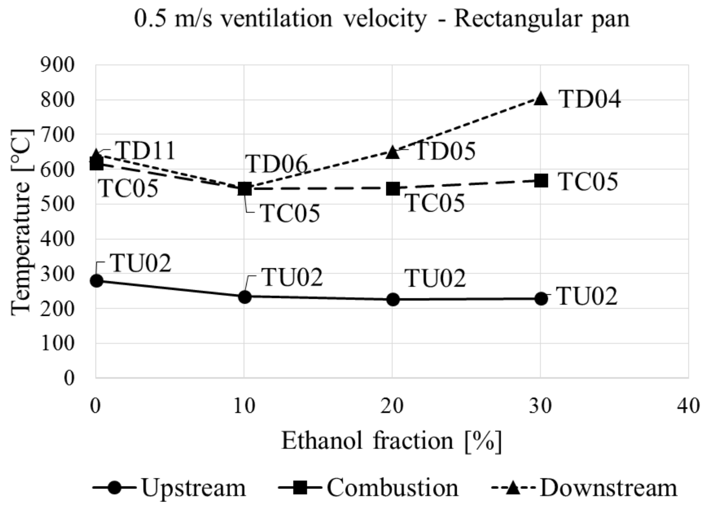

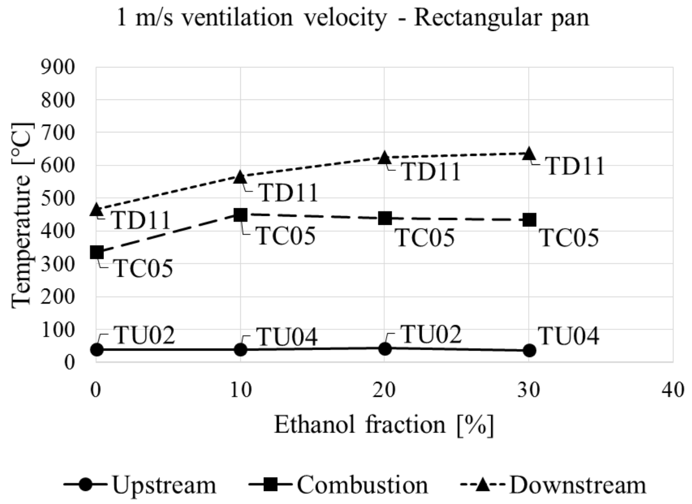

Figure 4.18 Maximum ceiling temperatures of ethanol/heptane pool fires under 0.5 m/s and 1 m/s ventilation conditions with rectangular pan

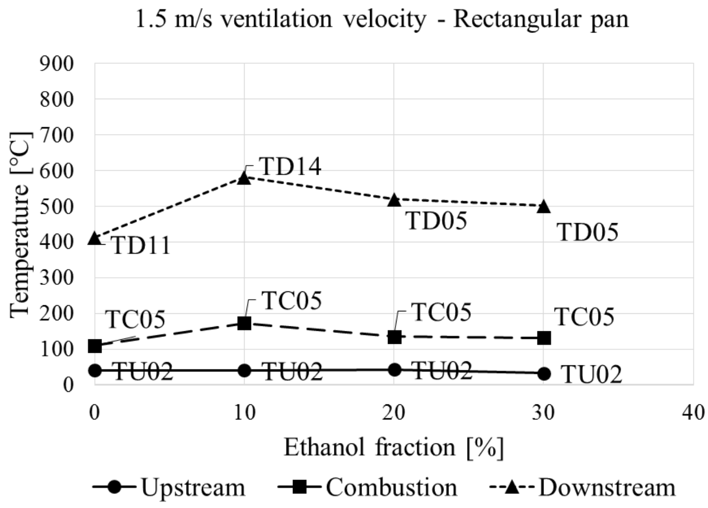

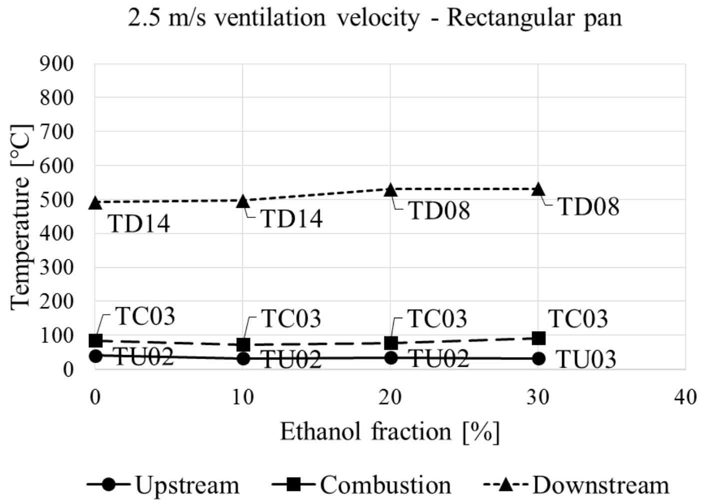

Figure 4.19 Maximum ceiling temperatures of ethanol/heptane pool fires under 1.5 m/s and 2.5 m/s ventilation conditions with rectangular pan

4.2.2 Effects of Ventilation Velocity, Pool Geometry and Ethanol Content on HRR and THR

The general trend of quasi-steady HRR results show that HRR increases with increasing ethanol fraction. The experiments are conducted for same amount of fuel with different ethanol contents. The quasi-steady HRR of rectangular pool fires have peak values at 1 m/s critical ventilation condition for 20 % and 30 % ethanol fractions.

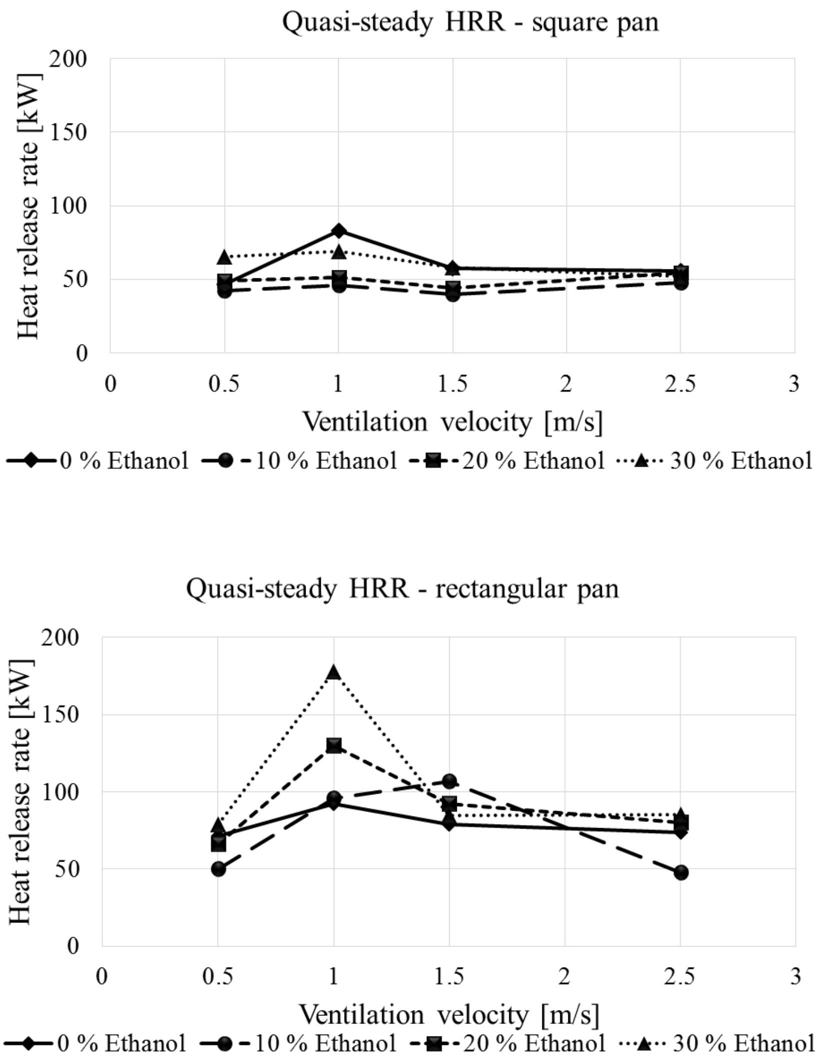

Figure 4.20 Quasi-steady HRR results of ethanol/heptane pool fires

The NTHR of mixture pool fires show that all results have peak total energy emissions at 1 m/s ventilation velocity. The enhanced O_2 concentrations in figures of gas concentrations indicate that the fires with higher O_2 concentrations generally have higher NTHR up to 1 m/s ventilation condition. After this point, the cooling effect of mechanical ventilation overcomes the heating and the NTHR decrease with even higher O_2 concentrations. The NTHR with 0.5 m/s ventilation condition has the lowest values as it happens in heptane pool fire scenarios. It can also be deduced that increasing ethanol fraction leads to lower NTHR. This may be the consequence of decreasing ratio of heptane in the ethanol/heptane mixture fuel.

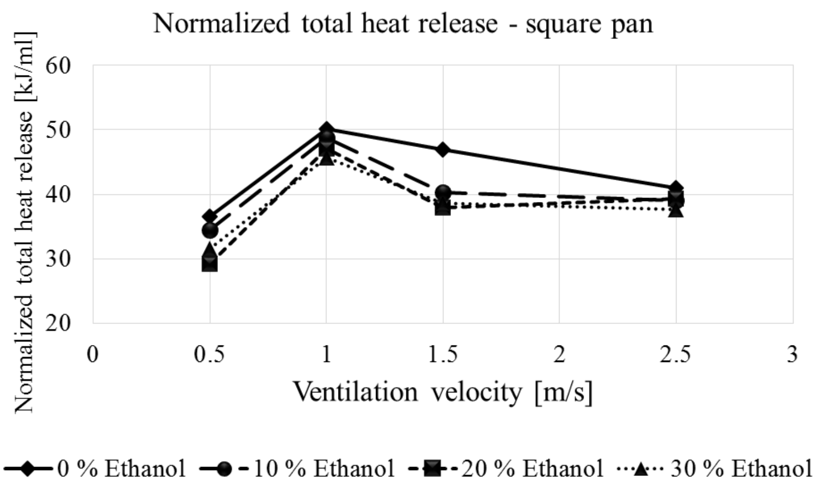

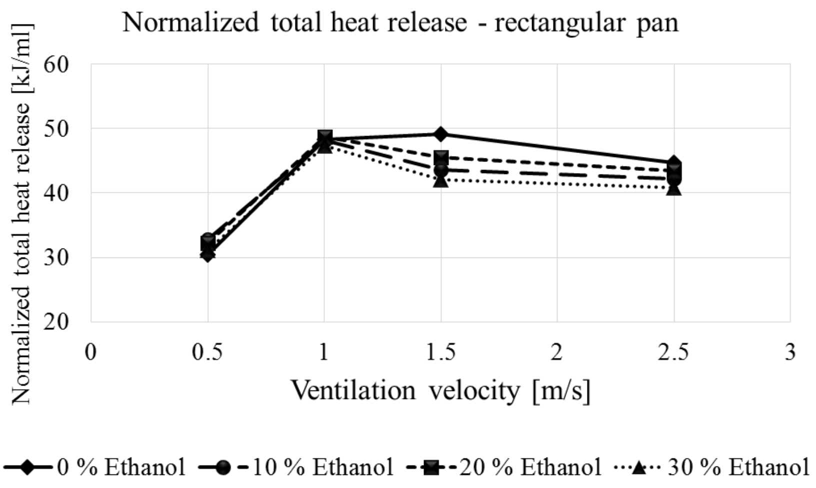

Figure 4.21 Normalized total heat releases of ethanol/heptane pool fires

4.2.3 Effects of Ventilation Velocity, Pool Geometry and Ethanol Content on Product Gas Concentrations

The O_2, CO_2 and CO concentrations are measured for 0 %, 10 %, 20 % and 30 % volumetric fractions of ethanol with n-heptane. 0 % and 30 % ethanol cases of square pool fires show that the product concentrations increase with increasing ethanol fractions. However the fresh air supplied with enhanced ventilation conditions dilutes the smoke and decreases the concentrations of CO_2 and CO. These regimes are hard to catch for some of the cases (e.g. square pool fires with 10 % and 20 % ethanol fractions) due to the turbulent characteristics of air flow and the heterogeneity of smoke-air mixture but the effect of ventilation on concentration are more perceptible for all rectangular pool fires and square pool fires with 0 % and 30 % ethanol fractions. The increasing regimes of total O_2, CO_2 and CO concentrations are also seen in these cases. The total of O_2, CO_2 and CO concentrations decrease when the CO_2 and CO percentages increase.

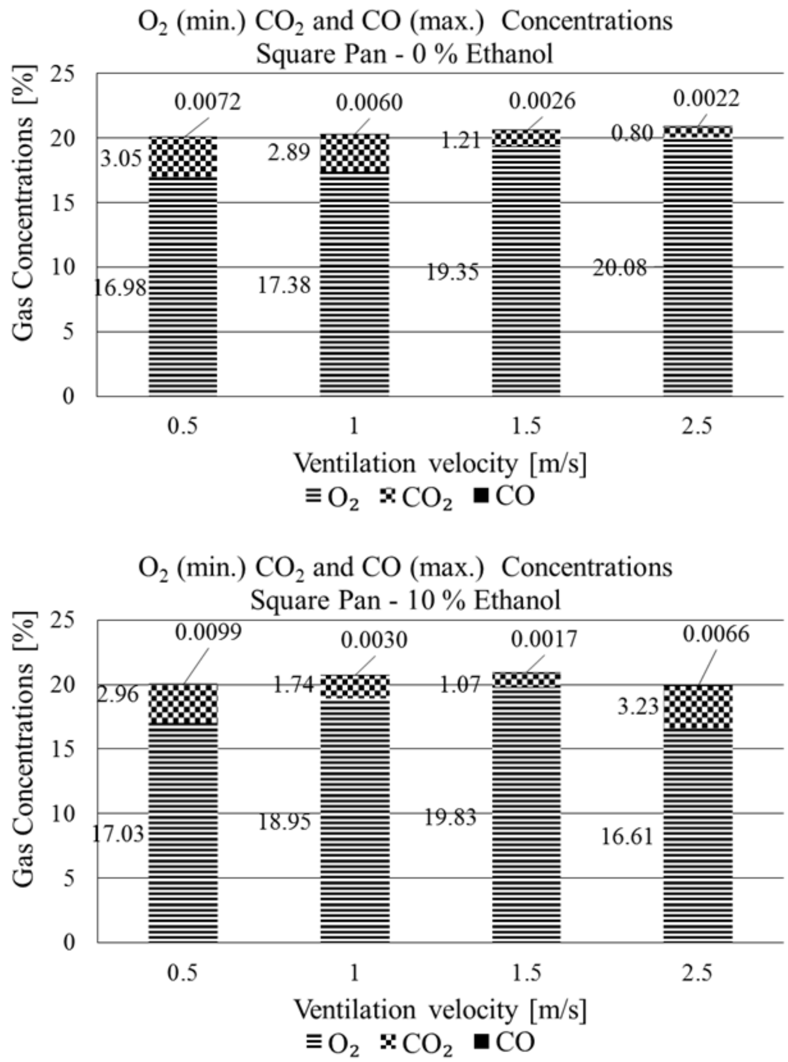

Figure 4.22 O_2, CO_2 and CO concentrations of 0 % and 10 % ethanol/heptane pool fires with square pan

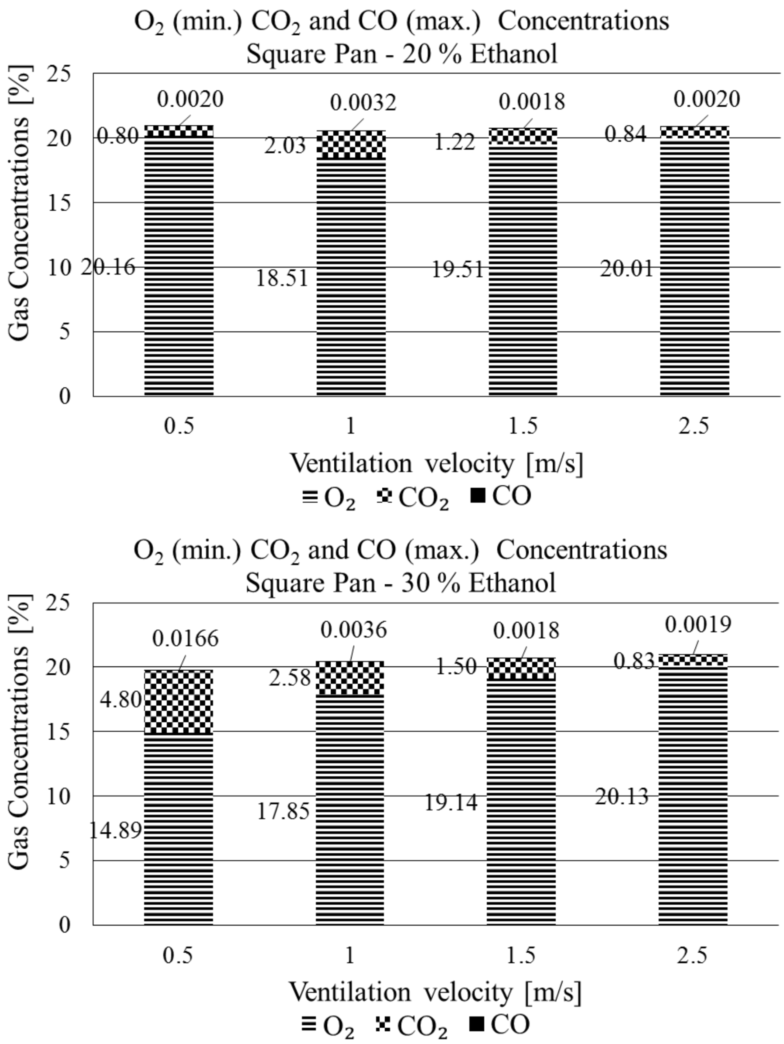

Figure 4.23 O_2, CO_2 and CO concentrations of 20 % and 30 % ethanol/heptane pool fires with square pan

In rectangular ethanol fire cases, the concentration of CO_2 and CO are comparatively high due to increasing interactions between air and fuel surface. An interesting point is the decreasing CO_2 and CO concentration for increasing ethanol fractions under 0.5 m/s ventilation condition. A reverse situation is observed for 1 m/s, 1.5 m/s and 2.5 m/s ventilation velocities. Therefore, it may be considered that the concentrations of CO_2 and CO increase with increasing ethanol fractions for rectangular pool fires with ventilation velocities higher than the critical ventilation velocity as shown in Figure 4.24 and Figure 4.25.

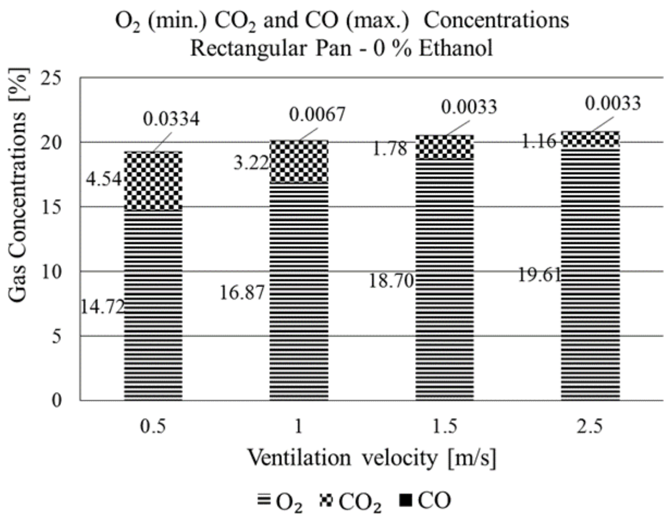

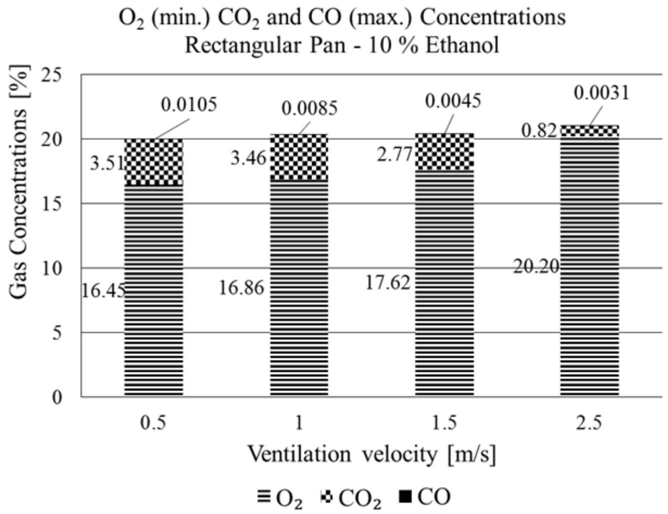

Figure 4.24 O_2, CO_2 and CO concentrations of 0 % and 10 % ethanol/heptane pool fires with rectangular pan

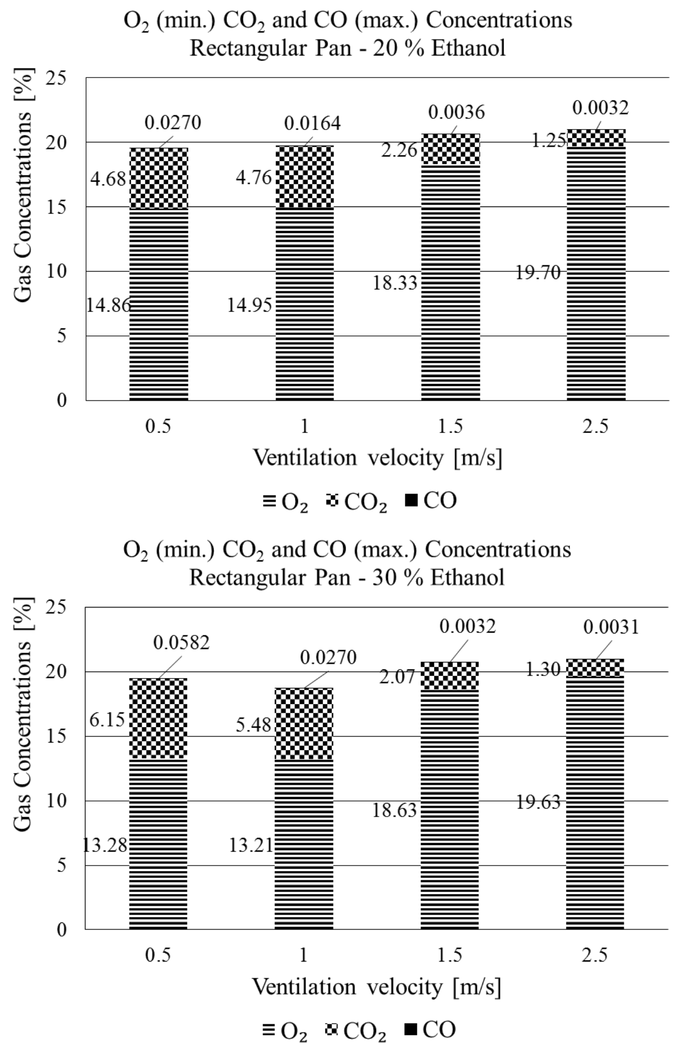

Figure 4.25 O_2, CO_2 and CO concentrations of 20 % and 30 % ethanol/heptane pool fires with rectangular pan

4.2.4 Effects of Ventilation Velocity, Pool Geometry and Ethanol Content on Burning Rate and Combustion Duration

The steady burning rate results tend to increase with ethanol ratio which is due to higher combustion temperatures associated with ethanol. Consistently, the burning rate of 30 % ethanol fires reached the maximum values compared to different volumetric fractions with same ventilation conditions in square pan cases. It should be noted that the combustion durations of 30 % ethanol square pool fires are also the lowest values under the same ventilation conditions (Figure 4.27).

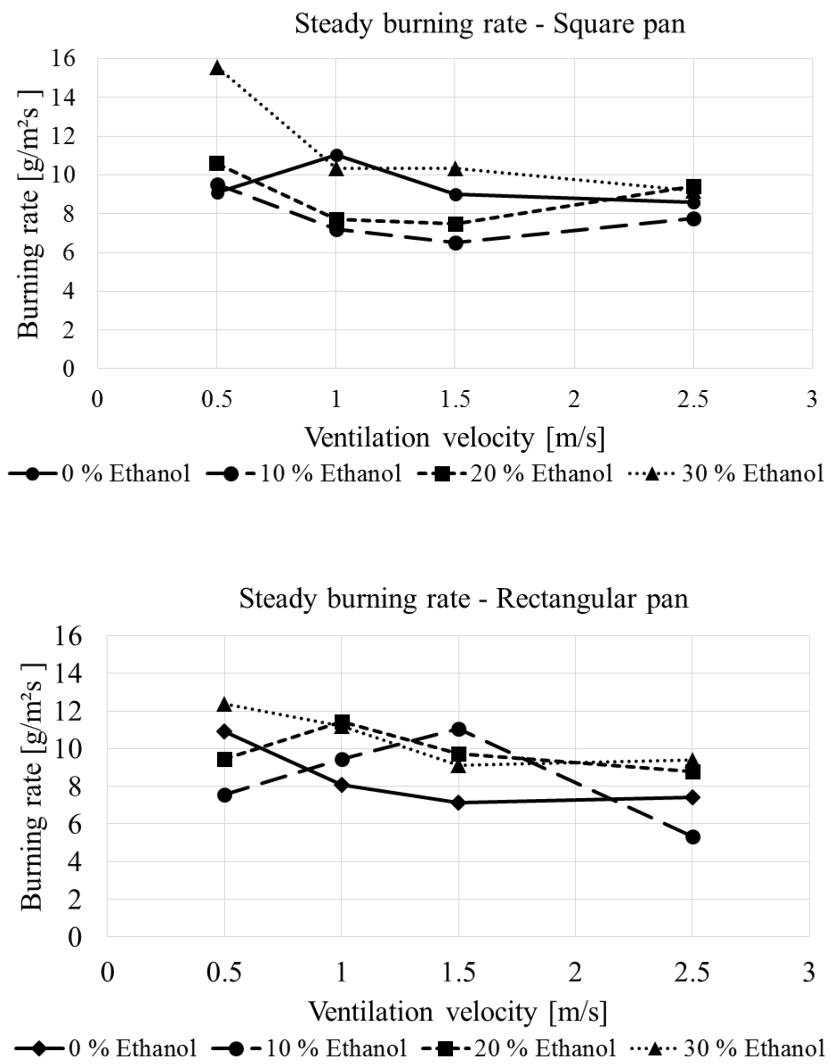

Figure 4.26 Effects of mixing ratio on burning rates of ethanol/heptane pool fires

The combustion durations of rectangular pool fires are relatively low under 1 m/s and 1.5 m/s ventilation conditions. Figure 4.27 shows that the steady burning rates of rectangular and square pool fires change between 6-8 g/m^2s and 6-10 g/m^2s, respectively. The maximum durations occur in square pool fire cases. As a general trend, it is seen that increasing the ethanol content in n-heptane/ethanol mixture pool fires results in decreasing of combustion duration, i.e. faster combustion which could be associated with increased oxygen content of the fuel mixture. It is also seen that the combustion duration of rectangle pool fires are less dependent on ventilation conditions than corresponding square pool fires where a strong dependency of mass loss rate is apparent on ethanol content in the mixture and ventilation conditions.

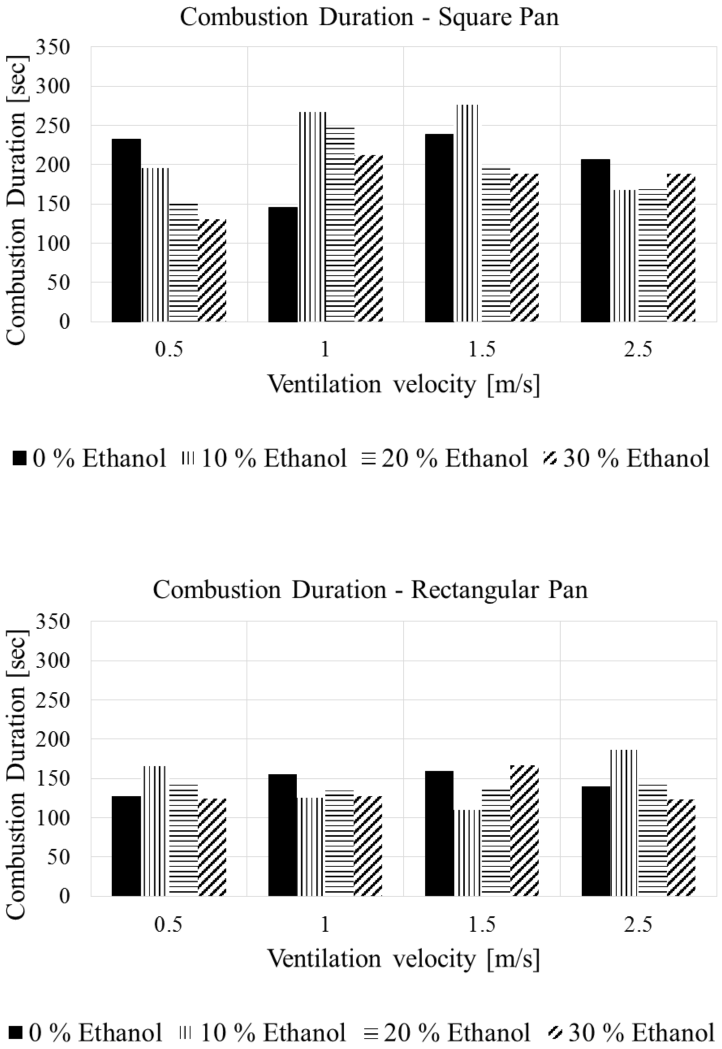

Figure 4.27 Combustion durations of ethanol/heptane pool fires

4.3 Results of Ethanol Pool Fire Experiments

A series of radiative heat flux measurements are obtained from 100 ml, 200 ml and 300 ml ethanol pool fires with square pan under 0.5 to 2.5 m/s ventilation conditions. The heat flux gauge shown in Figure 3.7 is placed 3 cm away from the upstream rim of the pan. The tunnel wall are surrounded with reflecting and absorbing materials to compare the back-radiation effects of surroundings. The gauge is mounted in two different positions to measure the radiation emitted from the fire, surrounding walls and hot product gas layer. First, the heat flux sensor is placed horizontally parallel to tunnel axis in order to measure the convective and radiative heat emitted directly from the fire. The gauge sight is obscured by an opaque object to measure the convective errors in individual tests. The HRR, burning rate and temperature distributions are also obtained simultaneously. A comprehensive list of experimental results are illustrated in appendices.

The high temperatures in combustion section are expected to contribute the radiative heat transfer mechanism inside the tunnel. At 0.5 m/s ventilation velocity, the temperatures of combustion section reach to 600˚C, 800˚C and 825˚C for 100 ml, 200 ml and 300 ml ethanol pool fires, respectively. The temperatures in all region are gradually decrease 100-200˚C with enhancing ventilation velocities as shown in Figure 4.28.

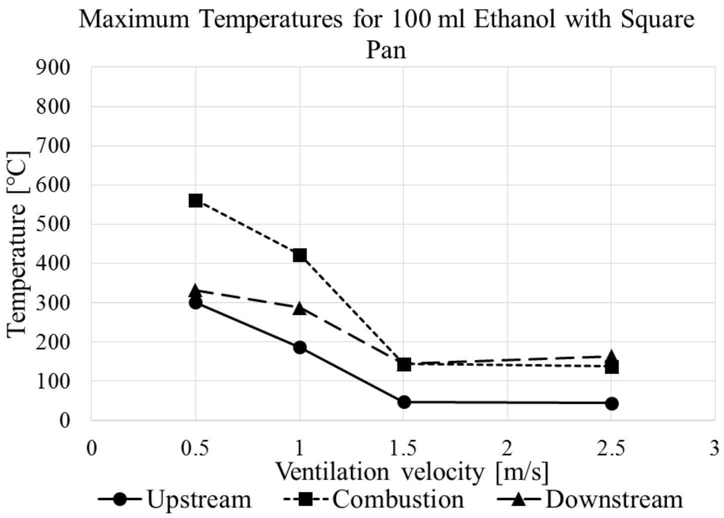

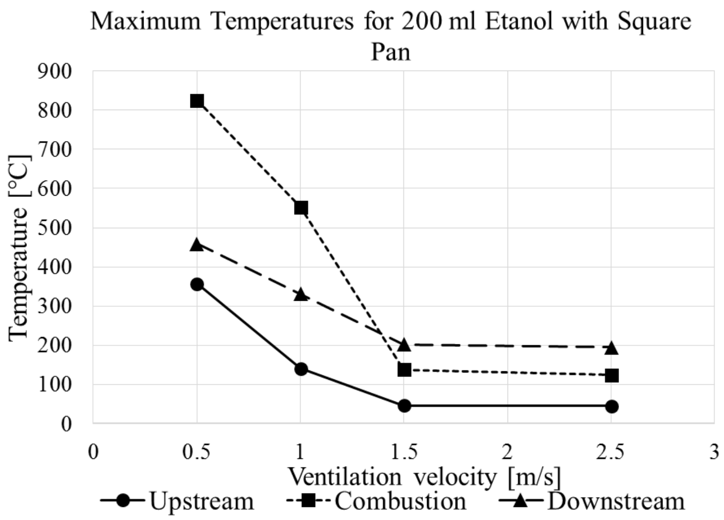

Figure 4.28 Maximum ceiling temperature of ethanol pool fires

The heat flux measurements show that 0.5 m/s and 1 m/s ventilation velocities don’t have significant effects on heat emissions of fire, however further increase in ventilation velocity causes convective and radiative heat flux to increase. A possible reason of this increment may be the parallel increasing HRR due to oxygen supply effect.

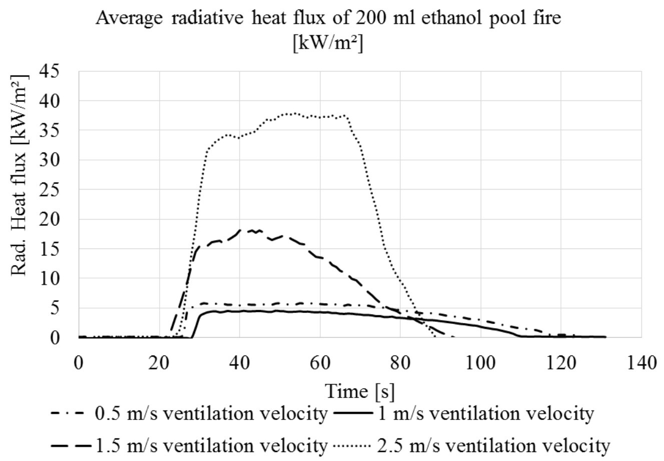

Figure 4.29 Radiative heat emissions of 200 ml ethanol pool fires

The maximum values of temperature, heat flux and HRR are shown in Table 4.1 and Table 4.2. The HRR, convective and radiative heat flux results show that the convective and radiative heat reaches up to 78 % of the HRR for 100 ml ethanol pool fire under 2.5 m/s ventilation condition. The increasing cooling effect of ventilation is also seen in Table 4.1.

Table 4.1 Maximum temperatures in combustion section and convective/radiative heat flux measurements under tunnel walls with high reflectivity

Exp. Code	***T_{smoke} [˚C]***	***$\dot{q}''_{sur}$ [kW/m²]***	***$\dot{q}''_{fire}$ [kW/m²]***	***Heat Flux Sensor Configuration***
ET02-Ref-05	825.2	-	5.9	Horizontal
ET01-Ref-10	422.0	-	4.1	Horizontal
ET02-Ref-10	552.3	-	4.4	Horizontal
ET01-Ref-15	143.7	0.7	-	Vertical
ET02-Ref-15	137.5	1.0	-	Vertical
ET02-Ref-15	273.3	-	22.9	Horizontal
ET01-Ref-25	94.1	0.6	-	Vertical
ET01-Ref-25	137.4	-	19.4	Horizontal
ET02-Ref-25	123.8	1.0	-	Vertical
ET02-Ref-25	175.1	-	39.7	Horizontal
ET03-Ref-25	123.9	1.1	-	Vertical

Table 4.2 HRR, THR and NTHR results of experiments under tunnel walls with high reflectivity

Exp. Code	***Quasi-steady HRR [kW]***	***THR [MJ]***	***NTHR [kJ/ml]***
ET02-Ref-05	32.1	4.9	24.7
ET01-Ref-10	43.8	4.4	44.3
ET02-Ref-10	49.6	6.5	32.5
ET01-Ref-15	13.5	1.9	18.6
ET02-Ref-15	14.4	6.1	30.4
ET02-Ref-15	55.6	6.3	31.5
ET01-Ref-25	16.6	3.0	29.7
ET01-Ref-25	25.0	2.7	27.4
ET02-Ref-25	23.6	6.1	30.3
ET02-Ref-25	59.4	6.2	31.1
ET03-Ref-25	33.6	9.6	32.0

The similar experiments are performed after the interior walls of tunnel model are covered with a black body material. The heat flux gauge is placed 3 cm away from the pan rim towards the upstream section. The reflection effect of radiation is investigated using materials with completely opposing radiative properties. The highly absorbing material is found to have significant contribution. The results are tabulated as in Table 4.3 and Table 4.4.

Table 4.3 Maximum temperatures in combustion section and convective/radiative heat flux measurements with black body covered tunnel walls

Exp. Code	T_{smoke} ***[°C]***	$\dot{q}''_{sur}$ ***[kW/m²]***	$\dot{q}''_{fire}$ ***[kW/m²]***	***Heat Flux Sensor Configuration***
ET02-Abs-05	498.7	-	15.6	Horizontal
ET01-Abs-10	280.0	-	15.4	Horizontal
ET01-Abs-10	392.9	-	5.5 (Obsc.)	Horizontal
ET01-Abs-15	101.1	0.59	-	Vertical
ET02-Abs-15	123.4	0.46	-	Vertical
ET02-Abs-15	203.4	-	26.7	Horizontal
ET01-Abs-25	79.4	0.43	-	Vertical
ET01-Abs-25	110.7	-	30.7	Horizontal
ET02-Abs-25	85.8	0.46	-	Vertical
ET02-Abs-25	112.9	-	6.39 (Obsc.)	Horizontal
ET02-Abs-25	102.9	-	31.2	Horizontal

The specific experiments are repeated after the visual angle of heat gauge is completely obscured by a nontransparent object. The radiative heat transmitted to the sensitive surface of heat flux sensor is minimized to observe the convective portion of heat energy. The sensor is kept cold via water-cooling setup and the conduction through surrounding materials are also reduced. It is found that the ratios of convective to radiative heat transferred to the gauge are 55 % and 25 % under 1 m/s and 2.5 m/s ventilation conditions.

Table 4.4 HRR, THR and NTHR results of experiments with black body covered tunnel walls

Exp. Code	***Quasi-steady HRR [kW]***	***THR [MJ]***	***NTHR [kJ/ml]***
ET02-Abs-05	35.2	5.7	28.4
ET01-Abs-10	36.5	4.6	46.4
ET01-Abs-10	48.7	4.8	48.4
ET01-Abs-15	16.7	3.1	31.3
ET02-Abs-15	32.6	6.6	33.2
ET02-Abs-15	55.8	7.4	36.8
ET01-Abs-25	25.3	3.2	31.7
ET01-Abs-25	38.0	3.0	30.3
ET02-Abs-25	33.6	7.1	35.6
ET02-Abs-25	68.3	7.6	37.9
ET02-Abs-25	57.8	7.2	35.9

The heat flux measurements of 100 ml and 200 ml ethanol pool fires are also taken from a measuring point 30 cm away from the fire in upstream direction. Exactly the same experimental procedure is performed. The CO, CO_2, O_2 concentrations, temperature data and fuel mass are simultaneously measured.

Table 4.5 The experimental results with heat flux sensor located 30 cm away from the fire

Exp. Code	***Quasi-steady HRR [kW]***	***THR [MJ]***	***NTHR [kJ/ml]***	T_{smoke} ***[°C]***	$\dot{q}''_{fire}$ ***[kW/m²]***
ET01-Abs-05	17.9	3.8	37.6	488.4	0.07 (Obsc.)
ET01-Abs-05	18.1	3.8	38.1	440.4	0.62
ET02-Abs-05	25.0	6.8	33.8	556.6	1.1
ET01-Abs-10	31.1	5.8	57.5	367.6	0.53
ET02-Abs-10	47.4	12.1	60.5	448.1	0.9
ET01-Abs-15	20.9	4.0	40.3	104.9	0.42
ET01-Abs-25	22.2	3.7	37.1	75.9	0.35

CHAPTER 5 CONCLUSIONS

The aim of the study is to investigate the effects of ventilation velocity, pool depth and pan geometry on n-heptane pool fires in tunnels. 100 ml, 200 ml and 300 ml heptane pool fires with square and rectangular pans are tested under ventilation velocities in range of 0.5-2.5 m/s with 0.5 m/s increment in a reduced scale tunnel model based on the Froude number scaling. 100 ml, 200 ml and 300 ml ethanol blended heptane fuels with 10 %, 20 % and 30 % volumetric fractions are also used with same conditions to observe the effect of ethanol additive. Two separate experimental matrices are prepared with one variable at a time approach. The fuel mass, temperature distribution, O_2, CO_2 and CO gas concentration are measured and are compared to observe the effect of changing parameters. To observe the role of radiation in pool fires, the interior wall surfaces of tunnel are cover with high reflecting material for particular ethanol pool fire experiments. The radiative heat flux of fire, the back radiation of walls and exhaust gases are respectively measured through a series of experiments. The overall results of conducted experiments can be highlighted as follows,

- The results of different ventilation conditions show that ventilation velocity has a significant role on HRR, burning rate and ceiling gas temperatures.
- The ceiling temperatures in upstream section start to decrease under 1 m/s ventilation condition. This shows that the critical ventilation velocity is achieved between 0.5 m/s and 1 m/s ventilation velocities. The formulations of Thomas (1968) and Wu and Bakar (2000) also verify that the critical ventilation should change between 0.96 m/s and 1.3 m/s for estimated temperatures and convective HRR values.
- From 1.5 m/s to 2.5 m/s ventilation condition, the temperatures of heptane pool fires with square pan cases change in the range of 180-310˚C, 300-480˚C and 480-500˚C for 0.92 mm, 1.84 mm and 2.76 mm pool depths respectively.
- The ceiling temperatures of rectangular heptane fires with 1.24 mm and 1.86 mm pool depths change between 400-500˚C and 500-700˚C however the variation is between 320-350˚C for 0.62 mm pool depth case.

- The downstream temperatures of 0.5 m/s ventilation condition are 800˚C for 30 % ethanol blended heptane pool fire and they barely decreased to 600˚C regardless of other ventilation conditions.
- Except for rectangle pan cases with 1.86 mm heptane pool depth, HRR and NTHR of heptane fires have peak values at 1 m/s after which point, they tend to decrease at 1.5 and 2.5 m/s ventilation velocities.
- The NTHR with 0.5 m/s ventilation condition has the lowest values as it happens in heptane pool fire scenarios. It can also be deduced that increasing ethanol fraction leads to lower NTHR.
- The quasi-steady HRR of ethanol pool fires increases with increasing ethanol content. The HRR of rectangular pool fires have peak values at 1 m/s critical ventilation condition for 20 % and 30 % ethanol fractions.
- The minimum O_2 concentrations are reached in underventilated (0.5 m/s) conditions.
- The CO_2 and CO concentrations of rectangular pan cases are higher than the square pool fires.
- The total of O_2, CO_2 and CO concentrations for 0.5 m/s ventilation case is always lower than the ones with 1 m/s, 1.5 m/s and 2.5 m/s ventilation conditions.
- The concentrations of CO_2 and CO increase with increasing ethanol fractions for rectangular pool fires with ventilation velocities higher than the critical ventilation velocity as shown in Figure 4.24 and Figure 4.25.
- 0 % and 30 % ethanol cases of square pool fires show that the product concentrations increase with increasing ethanol fractions.
- The burning rates of rectangular heptane fires are generally high. The steady burning rates of heptane pool fires has the highest values for 2.76 mm (for square pan fires) and 1.86 mm (for rectangular pool fires) pool depths as shown in Figure 4.12.
- The steady burning rate results tend to increase with ethanol ratio which is due to higher combustion temperatures associated with ethanol.
- The general trend of combustion duration can be interpreted as the decremented increase with increasing pool depths. The majority of

rectangular pool fire durations are lower than the square pan cases. The combustion durations are lower for 1.84 mm and 2.76 mm square pan pool fires at 1 m/s ventilation velocity. However the lowest HRR are obtained in 0.5 m/s ventilation condition due to low oxygen availability.

- The reflection effect of radiation is investigated using materials with completely opposing radiative properties. The highly absorbing material is found to have significant contribution.
- It is found that the ratios of convective to radiative heat transferred to the gauge are 55 % and 25 % under 1 m/s and 2.5 m/s ventilation conditions.

BIBLIOGRAPHY

Babrauskas, V. (1980). Flame Lengths Under Ceilings. *Fire and Materials, 4*, 119-126.

Brahim, K., Mourad, B., Afif, E. C., & Ali, B. (2011). Control of Smoke Flow in a Tunnel. *Journal of Applied Fluid Mechanics, 6*, 49-60.

Brohez, S., Delvosalle, C., Marlair G., & Tewarson, A. (1999). Soot Generation in Fires: An Important Parameter for Accurate Calculation of Heat Release. *International Symposium on Fire Safety Science* (pp. 265-276). Poitiers: International Association for Fire Safety Science.

Brohez, S., Delvosalle, C., Marlair, G., & Tewarson, A. (2000). The Measurement of Heat Release from Oxygen Consumption in Sooty Fires. *Journal of Fire Sciences, 18,* 327.

Capros, P., Mantzos, L., Papandreou, V., & Tasios, N. (2007). *European Energy and Transport Trends to 2030: Update 2007.* Bruxelles: European Commission Directorate General for Energy and Transport.

Celik, A. (2011). *Experimental and Numerical Study on Fire in Tunnels.* MSc Thesis, Middle East Technical University, Department of Mechanical Engineering, Ankara.

Chen, B., Lu, S.-X., Li, C.-H., Kang, Q.-S., & Lecoustre, V. (2011). Initial fuel temperature effects on burning rate of pool fire. *Journal od Hazardous Materials, 188*, 369-374.

Chevron. (2007). *Diesel fuels technical review*.

Danziger, N. H., & Kennedy, W. D. (1982). Longitudinal Ventilation Analysis for The Glenwood Canyon Tunnels. *Proceedings of the Fourth International Symposium Aerodynamics and Ventilation of Vehicle Tunnels*, (p. 169). York, England.

Drysdale, D. (1998). In *Introduction to Fire Dynamics* (2nd ed., pp. 109-110). Chichester: John Wiley and Sons.

European Commission. (2004). *Promoting Biofuels in Europe.* Bruxelles: European Commission, Directorate-General for Energy and Transport.

Hansen, R., & Ingason, H. (2012). Heat Release Rate of Multiple Objects at Varying Distances. *Fire Safety Journal, 52*, 1-10.

Hasemi, Y., & Takunaga, T. (1984). Some Experimental Aspects of Turbulent Diffusion Flames and Buoyant Plumes from Fire Sources Against a Wall and in a Corner of Walls. *Combustion Science and Technology, 40,* 1-17.

Hu, L. H., Huo, R., Wang, H. B., Li, Y. Z., & Yang, R. X. (2007). Experimental studies on fire-induced buoyant smoke temperature distribution along tunnel ceiling. *Building and Environment, 42*, 3905-3915.

Hu, L. H., Liu, S., Peng, W., & Huo, R. (2009). Experimental study on burning rates of square/rectangular gasoline and methanol pool fires under longitudinal air flow in a wind tunnel. *Journal of Hazardous Materials, 169*, 972-979.

Hu, L., Liu, S., & Li, D. (2011). A Wind Tunnel Experimental Study on Burning Rate Enhancement Behaviour of Gasoline Pool Fires by Cross Air Flow. *Combustion and Flame, 158*, 586-591.

Hu, L., Liu, S., & Wu, L. (2013). Flame radiation feedback to fuel surface in medium ethanol and heptane pool fires with cross air flow. *Combustion and Flame, 160*, 295-306.

Hu, L., Liu, S., Xu, Y., & Li, D. (2011). A Wind Tunnel Experimental Study on Burning Rate Enchancement Behaviour of Gasoline Pool Fires by Cross Air Flow. *Journal of Combustion and Flame, 158,* 586-591.

Ingason, H., & Lönnermark, A. (2005). Heat Release Rates from Heavy Goods Vehicle Trailer Fires in Tunnels. *Fire Safety Journal*, 646-668.

Karlsson, B., & Quintiere, J. G. (2000). *Enclosure Fire Dynamics.* Washington, D.C.: CRC Press LLC.

Kayili, S. (2009). *Effect of vehicles' blockage on heat release rate in case of tunnel fire.* PhD Thesis, Middle East Technical University, Mechanical Engineering Department, Ankara.

Kayili, S., Yozgatligil, A., & Eralp, C. (2011). An Experimental Study on the Effects of Blokage Ratio and Ventilation Velocity on the Heat Release Rate in Tunnel Fires. *Journal of Fire Sciences, 29*, 555-575.

Kayili, S., Yozgatligil, A., & Eralp, C. (2012). Effects of Ventilation and Geometrical Parameters of the Burning Object on the Heat Release Rate in Tunnel Fires. *Combustion Science and Technology, 184*, 1-13.

Kunsch, J. P. (2002). Simple Model for Control of Fire Gases in a Ventilated Tunnel. *Fire Safety Journal, 37*, 67-81.

Lawson, J. R. (2009). *A History of Fire Testing.* Gaithersburg: National Institute of Standard and Technology.

Li, L., Cheng, X., Wang, X., & Zhang, H. (2011). Temperature distribution of fire-induced flow along tunnels under natural ventilation. *Journal of Fire Sciences, 30*, 122-137.

Li, Y. Z., & Ingason, H. (2012). The maximum ceiling gas temperature in a large tunnel fire. *Fire Satefy Journal, 48,* 38-48.

Li, Y. Z., Lei, B., & Ingason, H. (2010). Study of Critical Velocity and Backlayering Length in Longitudinal Ventilated Tunnel Fires. *Fire Safety Journal, 45*, 361-370.

Li, Y. Z., Lei, B., & Ingason, H. (2011). The maximum temperature of buoyancy-driven smoke flow below the ceiling in tunnel fires. *Fire Safety Journal, 46*, 204-210.

McCaffrey, B. (1995). *SFPE Handbook of Fire Protection Engineering* (2nd ed.). Quincy, MA: National Fire Protection Association.

McClellan, J. E., & Dorn, H. (2006). *Science and Technology in World History: An Introduction.* Baltimore, Maryland: The Johns Hopkins University Press.

McGrattan, K. B., Baum, H. R., & Hamins, A. (2000). *Thermal radiation from large pool fires.* NIST, U.S. Department of Commerce. NIST.

Meijer, M. (2010). *Characterization of N-heptane as a Single Component Diesel Surrogate Fuel.* PhD Thesis, Technical University of Eindhoven Automotive Technology.

Miclea, P. C., Chow, W. K., Shen-Wen, C., Junmei, L., Kashef, A. H., & Kang, K. (2007). International Tunnel Fire-Safety Design Practices. *ASHRAE Journal*, 57.

NFPA. (2009). *NFPA 502 Standard for Roasd Tunnels, Bridges, and Other Limited Access Highways.* Quincy: National Fire Protection Association.

Oka, Y., & Atkinson, G. T. (1995). Control of Smoke Flow in Tunnel Fire. *Fire Safety Journal, 25*, 305-322.

Parker, W. J. (1977). *An Investigation of th Fire Environment in the ASTM E84 Tunnel Test.* Washington: National Bureau of Standards.

Parker, W. J. (1982). *Calculations of the Heat Release Rate by Oxygen Consumption for Various Applications.* National Bureau of Standards, U.S. Department of Commerce, Washington, DC.

Pretrel, H., Le Saux, W., & Audouin, L. (2013). *Experimental Determination of Fire Heat Release Rate with OC and CDG Calorimetry for Ventilated Compartments Fire Scenario.* doi:10.1002/fam.2193

Quintiere, J. G. (2006). *Fundamentals of Fire Phenomena.* Chichester, England: John Wiley and Sons, Ltd.

Roh, J. S., Ryou, H. S., Kim, D. H., Jung, W. S., & Jang, Y. J. (2007). Critical Velocity and Burning Rate in Pool Fire During Longitudinal Ventilation. *Tunneling and Underground Space Technology, 22*, 262-271.

Tang, F., Hu, L., Zhang, X., Zhang, X., & Dong, M. (2015). Burning Rate and Flame Tilt Characteristics of Radiation-controlled Rectangular Hydrocarbon Pool Fires with Cross Air Flows. *The Journal of Science and Technology of Fuel and Energy, 139*, 18-25.

Tewarson, A. (1995). Generation of Heat and Chemical Compounds in Fires. In *SFPE Handbook of Fire Protection Engineering* (pp. 3-53 to 3-124). Quincy, MA: The National Fire Protection Association Press.

Thomas, P. H. (1968). *The Movement of Smoke in Horizontal Passages Against an Air Flow.* Fire Research Station.

Thomas, P. H., Webster, C. T., & Raftery, M. M. (1960). *Some Experiments on Buoyant Diffusion Flames.* Boreham Wood: Department of Scientific and Industrial Research and Fire Offices' Commitee Joint Fire Research Organization.

Thornton, W. (1917). The Relation of Oxygen to the Heat of Combustion of Organic Compounds. *Philosophical Magazine and J. of Science, 33*, 196-203.

U.S Department of Housing and Urban Development. (2011). *Acceptable Separation Distance Guidebook.*

Vianello, C., Fabiano, B., Palazzi, E., & Maschio, G. (2012). Experimental Study on Thermal and Toxic Hazards Connected to Fire Scenerios in Road Tunnels. *Journal of Loss Prevention in the Process Industries*, 718-729.

Walton, W. D., & Thomas, P. H. (1995). In *SFPE Handbook of Fire Protection Engineering* (2nd ed., p. 172). Quincy: National Fire Protection Association.

Woods, J. A., Fleck, B. A., & Kostiuk, L. W. (2006). Effects of Transverse Air Flow on Burning Rates of Rectangular Methanol Pool Fires. *Combustion and Flame, 146*, 379-390.

Wu, Y., & Bakar, M. A. (2000). Control of Smoke Flow in Tunnel Fires Using Longitudinal Ventilation systems-a study od the critical velocity. *Fire Safety Journal, 35*, 363-390.

Zukoski, E. E. (1985). *Fluid Dynamic Aspects of Room Fires.* Pasadena: California Instute of Technology.

Zukoski, E. E., & Kubota, T. (1975). *An Experimental Investigation of Heat Transfer from a Buoyant Gas Plume to a Horizontal Ceiling, Part 2: Effects of a ceiling layer.* Washington D.C.: National Bureau of Standarts.

APPENDIX-A

Technical Specifications of Instruments

Testo 350-S flue gas analyzer

Parameter	Measuring range	Accuracy		Resolution	Response time 1)
O2	0...25 vol.%	±0.2 vol.%		0.01 vol.%	20 s (t95)
CO, H2-comp.	0...10000 ppm	±10 ppm ±5 % of reading ±10 % of reading	(0...99 ppm) (100...2,000 ppm) (2,001...10,000 ppm)	1 ppm	40 s (t90)
COlow, H2-comp.	0...500 ppm	±2 ppm ±5 % of reading	(0.0...39.9 ppm) (40.0...500.0 ppm)	0.1 ppm	40 s (t90)
CO2(IR)	0...50 vol.%	±0.3 vol.%+1 % of reading ±0.5 vol.%+1.5 % of reading	(0.00...25.00 vol.%) (25.1...50.0 vol.%)	0.01 vol.% 0.1 vol.%	10 s (t90)
Draught	-40...40 hPa	±0.03 hPa ±1.5 % of reading	(-2.99...2.99 hPa) (rest of range)	0.01 hPa	-
dP	-200...200 hPa	±0.5 hPa ±1,5 % of reading	(-49.9...49.9 hPa) (rest of range)	0.1 hPa	-
Temperature	-40...1,200°C	±0.5 °C ±0.5 % of reading	(-40.0...99.9 °C) (rest of range)	0.1 °C	depending on the probe
Efficiency	0...120 %	-		0.1 %	-
Flue gas loss	-20.0...99.9 %	-		0.1 %	-

Testo 350-S flue gas analyzer,
CO dilution (CO measuring range extension option)

Parameter	Measuring range	Accuracy
CO, H2-comp.	0...400,000 ppm (maximum)	+2 % of reading additional error
COlow, H2-comp.	0...20,000 ppm (maximum)	+2 % of reading additional error

Testo 350-S flue gas analyzer,
dilution overall (fresh air valve option)

Parameter	Measuring range	Accuracy	dP 1)
CO, H2-comp.	2500...50000ppm	±5 % of reading additional error	-150...0 hPa
COlow, H2-comp.	2500...50000ppm	±5 % of reading additional error	-100...0 hPa
NO2	2500...50000ppm	±5 % of reading additional error	-50...0 hPa
SO2	500...25000ppm	±5 % of reading additional error	-100...0 hPa
NOlow	300...1500ppm	±5 % of reading additional error	-150...0 hPa
NO	1500...15000ppm	±5 % of reading additional error	-100...0 hPa
H2S	200...1500ppm	±5 % of reading additional error	-100...0 hPa

1) Accuracies only valid in the range of the given pressure difference (pressure at the probe tip)

Figure A. 1 Measuring ranges and accuracies

CO_2 Recalibration

Zero point calibration must be performed before CO2(IR) is recalibrated. Gradient adjustment (2nd calibration point) can be carried out subsequently if necessary.

Zero point calibration requires a test gas of 0 % CO2 or a CO2 filter (absorption filter). If using a CO2 filter, please follow the corresponding instructions for use.

1 → **Sensors** → OK.

2 **Recal.** → OK.

3 If password protection is activated: Enter the password → End.

4 **CO2I** → OK.

5 Connect the CO2 filter or apply test gas (0 % CO) and confirm with OK.

- A rinse phase is started.

6 When the rinse phase is over start zero point calibration with Start.

- Once a stable actual value is reached, the zero point is automatically calibrated.

Repeat zero point calibration: **Zeropoint calibr.** → OK.
-or-
End the function: ESC
-or-
Perform gradient adjustment: **Gradient** → OK.

8 Enter the test gas concentration (nominal value) → Start.

9 Start gradient adjustment with Start.

- Once a stable actual value is reached, the gradient is automatically calibrated.

A test gas check can be carried out to check the recalibration:

10 End the function without carrying out a check: ESC
-or-
Carry out a check: OK.

11 Enter the test gas concentration (nominal value) (or a different concentration as in recalibration) → Start.

- Once a stable actual value is reached, the result of the test gas check is displayed.

12 Save the nominal value/actual value and date/time of the test without calibrating the sensor and end the function: Mem..

$CO/SO_2/NO_2/NO/O_2$ Recalibration

1 → **Sensors** → OK.

2 **Recal.** → OK.

3 If password protection is activated: Enter the password → End.

4 Select the sensor → OK.

5 Enter the test gas concentration (nominal value) → End.

6 Charge the sensor with test gas and wait until the actual value is stable.

7 Save the nominal value/actual value and date/time of the test without calibrating the sensor and end the function: Mem..
-or-
Calibrate the sensor: OK.

A test gas check can be carried out to check the recalibration:

8 End the function without carrying out a check: ESC
-or-
Carry out a check: OK.

9 Enter the test gas concentration (nominal value) (or a different concentration as in recalibration) → End.

10 Charge the sensor with test gas and wait until the actual value is stable.

11 Save the nominal value/actual value and date/time of the test without calibrating the sensor and end the function: Mem..

Characteristic	Values
Measuring system	
Operating temperature	-5...45 °C
Storage/transport temperature	-20...50 °C
Housing	ABS
Guarantee (according to Testo guarantee terms)	Measuring instrument: 24 months (excluding printing mechanism) Measuring cells: 12 months, O2 measuring cell: 18 months, CO2(IR) measuring cell: 24 months Flue gas probe: 24 months, thermocouple: 12 months Rechargeable battery: 12 months
testo 350-S control unit	
Power supply	4x mignon AA 1.5V
Battery service life	approx. 2 years
Dimensions (L x W x H)	252 x 115 x 58 mm
Weight	approx. 850 g
Testo 350-S flue gas analyzer	
Power supply	Rechargeable battery pack (8.4 V/4.5 Ah) Integrated mains unit (90-260 V, 47-63 Hz, 0.3 A/230 VAC, 0.5 A/110 VAC)
Rech. battery charge time	approx. 4-5 h
Dimensions (L x W x H)	395 x 275 x 95 mm
Weight	approx. 3,200 g
Memory	250,000 readings
Max. flue gas positive pressure	50 hPa
Max. vacuum	200 hPa
Pump volumetric flow rate	0.8 m/s, monitored
Diluting gas	Fresh air or nitrogen
Max. flue gas dust load	20 g/m^3
Max. humidity load	70 °Ctd at measuring inlet
Trigger input (optional)	Voltage: 5...12 V (falling or rising flank) Pulse width: >1 s Load: 5 V/max. 5 mA, 12 V/max.40 mA
Option Bluetooth®	Range < 100m

Figure A. 2 Other instrument data

USB2.0 Edge of Module

Terminal Block	Left Signal	Type	Port	Type	Right Signal	Terminal Block
	Analog Common				Digital Common	
	DAC0 (Note 1)			Digital	CH 0	
	DAC1 (Note 1)			Digital	CH 1	
	DAC2 (Note 1)		PORT A	Digital	CH 2	
	DAC3 (Note 1)			Digital	CH 3	
	Analog Common			Digital	CH 4	
TB1	Self Calibration			Digital	CH 5	TB6
	Signal Ground			Digital	CH 6	
	Digital Common			Digital	CH 7	
	TTL Trigger				Digital Common	
	DPCR (DAC Pacer Clock I/O)				Timer 0 (TMR0)	
	APCR (A/D Pacer Clock I/O)				Timer 1 (TMR 1)	
	Analog Common				Digital Common	
	CH 0 / CH 0 HI	Analog		Digital	CH 0	
	CH 8 / CH 0 LO	Analog		Digital	CH 1	
	Analog Common		PORT B	Digital	CH 2	
	CH 1 / CH 1 HI	Analog		Digital	CH 3	
	CH 9 / CH 1 LO	Analog		Digital	CH 4	
TB2	Analog Common			Digital	CH 5	TB5
	CH 2 / CH 2 HI	Analog		Digital	CH 6	
	CH 10 / CH 2 LO	Analog		Digital	CH 7	
	Analog Common				Digital Common	
	CH 3 / CH 3 HI	Analog			Counter 0 (CNT0)	
	CH 11 / CH 3 LO	Analog			Counter 1 (CNT1)	
	Analog Common				Digital Common	
	CH 4 / CH 4 HI	Analog		Digital	CH 0	
	CH 12 / CH 4 LO	Analog		Digital	CH 1	
	Analog Common		PORT C	Digital	CH 2	
	CH 5 / CH 5 HI	Analog		Digital	CH 3	
	CH 13 / CH 5 LO	Analog		Digital	CH 4	
TB3	Analog Common			Digital	CH 5	TB4
	CH 6 / CH 6 HI	Analog		Digital	CH 6	
	CH 14 / CH 6 LO	Analog		Digital	CH 7	
	Analog Common				Digital Common	
	CH 7 / CH 7 HI	Analog			Counter 2 (CNT2)	
	CH 15 / CH 7 LO	Analog			Counter 3 (CNT3)	

DSUB25 Edge of Module

Figure A. 3 Pinout for OMB-DAQ-3005 module

DSUB25 Edge of OMB-PDQ30 Module

TB1	Analog Common	Analog CH 63 / CH 31 LO	TB6
	CH 16 / CH 8 HI Analog	Analog CH 55 / CH 31 HI	
	CH 24 / CH 8 LO Analog	Analog Common	
	Analog Common	Analog CH 62 / CH 30 LO	
	CH 17 / CH 9 HI Analog	Analog CH 54 / CH 30 HI	
	CH 25 / CH 9 LO Analog	Analog Common	
	Analog Common	Analog CH 61 / CH 29 LO	
	CH 18 / CH 10 HI Analog	Analog CH 53 / CH 29 HI	
	CH 26 / CH 10 LO Analog	Analog Common	
	Analog Common	Analog CH 60 / CH 28 LO	
	CH 19 / CH 11 HI Analog	Analog CH 52 / CH 28 HI	
	CH 27 / CH 11 LO Analog	Analog Common	
TB2	Analog Common	Analog CH 59 / CH 27 LO	TB5
	CH 20 / CH 12 HI Analog	Analog CH 51 / CH 27 HI	
	CH 28 / CH 12 LO Analog	Analog Common	
	Analog Common	Analog CH 58 / CH 26 LO	
	CH 21 / CH 13 HI Analog	Analog CH 50 / CH 26 HI	
	CH 29 / CH 13 LO Analog	Analog Common	
	Analog Common	Analog CH 57 / CH 25 LO	
	CH 22 / CH 14 HI Analog	Analog CH 49 / CH 25 HI	
	CH 30 / CH 14 LO Analog	Analog Common	
	Analog Common	Analog CH 56 / CH 24 LO	
	CH 23 / CH 15 HI Analog	Analog CH 48 / CH 24 HI	
	CH 31 / CH 15 LO Analog	Analog Common	
TB3	Analog Common	Analog CH 47 / CH 23 LO	TB4
	CH 32 / CH 16 HI Analog	Analog CH 39 / CH 23 HI	
	CH 40 / CH 16 LO Analog	Analog Common	
	Analog Common	Analog CH 46 / CH 22 LO	
	CH 33 / CH 17 HI Analog	Analog CH 38 / CH 22 HI	
	CH 41 / CH 17 LO Analog	Analog Common	
	Analog Common	Analog CH 45 / CH 21 LO	
	CH 34 / CH 18 HI Analog	Analog CH 37 / CH 21 HI	
	CH 42 / CH 18 LO Analog	Analog Common	
	Analog Common	Analog CH 44 / CH 20 LO	
	CH 35 / CH 19 HI Analog	Analog CH 36 / CH 20 HI	
	CH 43 / CH 19 LO Analog	Analog Common	

Figure A. 4 Pinout for OMB-PDQ30 expansion module

Table A. 1 Convective related error estimates for SBG01 heat flux sensor

φ_{rad}	C_{tr}	R_{sen}	T_{air}	T_{sen}	φ_{conv}	CONVECTIVE ERROR	SENSITIVITY ERROR
kW/m^2	W/(m^{2}K)	W/(m^{2}K)	deg C	deg C	kW/m^2	%	%
10	50	2000	20	15	0.5	5%	3%
50	50	2000	20	35	0.5	1%	3%
100	50	2000	20	60	0.5	1%	3%
10	10	2000	20	15	0.1	1%	1%
50	10	2000	20	35	0.1	0%	1%
100	10	2000	20	60	0.1	0%	1%
10	50	1000	20	20	0.5	5%	5%
50	50	1000	20	60	0.5	1%	5%
100	50	1000	20	110	0.5	1%	5%
10	10	1000	20	20	0.1	1%	1%
50	10	1000	20	60	0.1	0%	1%
100	10	1000	20	110	0.1	0%	1%
10	50	2000	400	15	19.5	195%	3%
50	50	2000	400	35	19.5	39%	3%
100	50	2000	400	60	19.5	20%	3%
10	10	2000	400	15	3.9	39%	1%
50	10	2000	400	35	3.9	8%	1%
100	10	2000	400	60	3.9	4%	1%
10	50	1000	400	20	19.5	195%	5%
50	50	1000	400	60	19.5	39%	5%
100	50	1000	400	110	19.5	20%	5%
10	10	1000	400	20	3.9	39%	1%
50	10	1000	400	60	3.9	8%	1%
100	10	1000	400	110	3.9	4%	1%

APPENDIX-B

Complementary Results

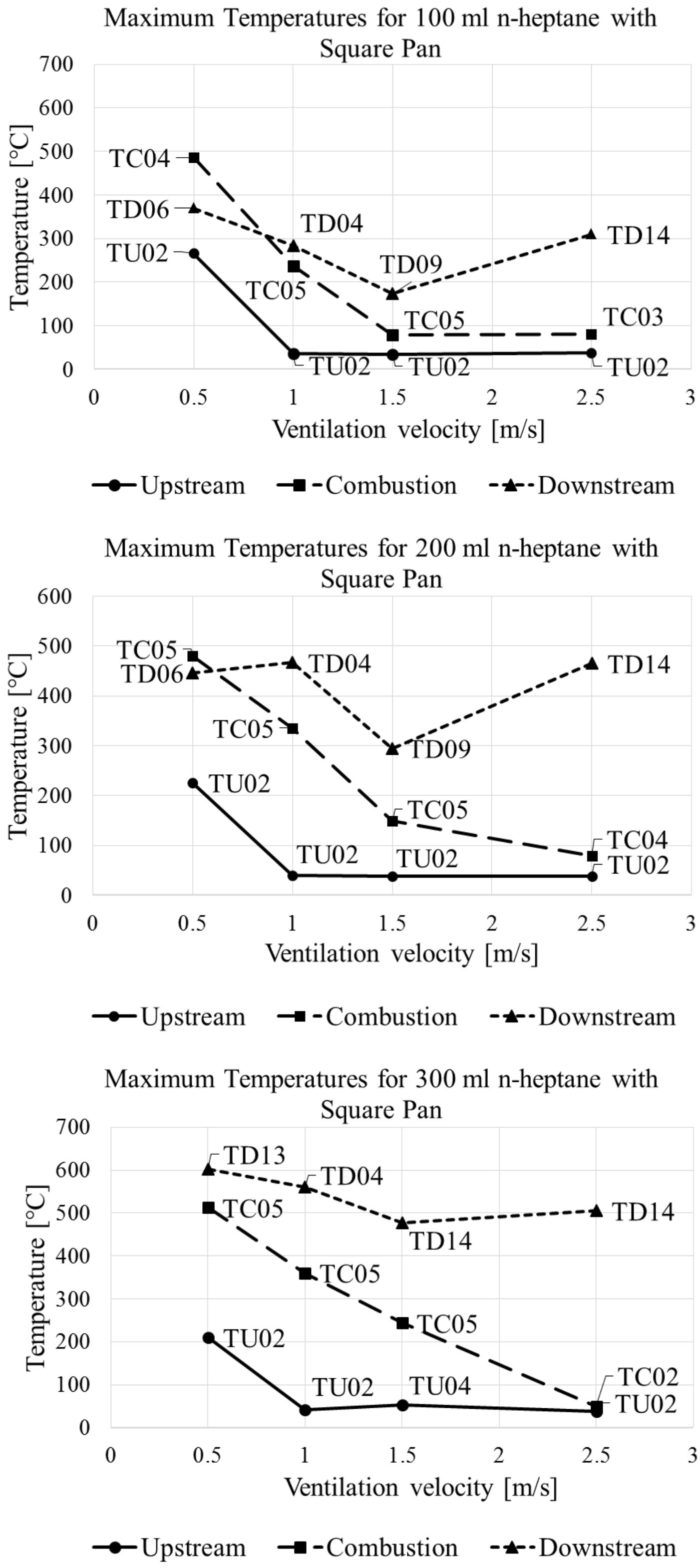

Figure B. 1 Temperature results of n-heptane pool fire experiments with square pan

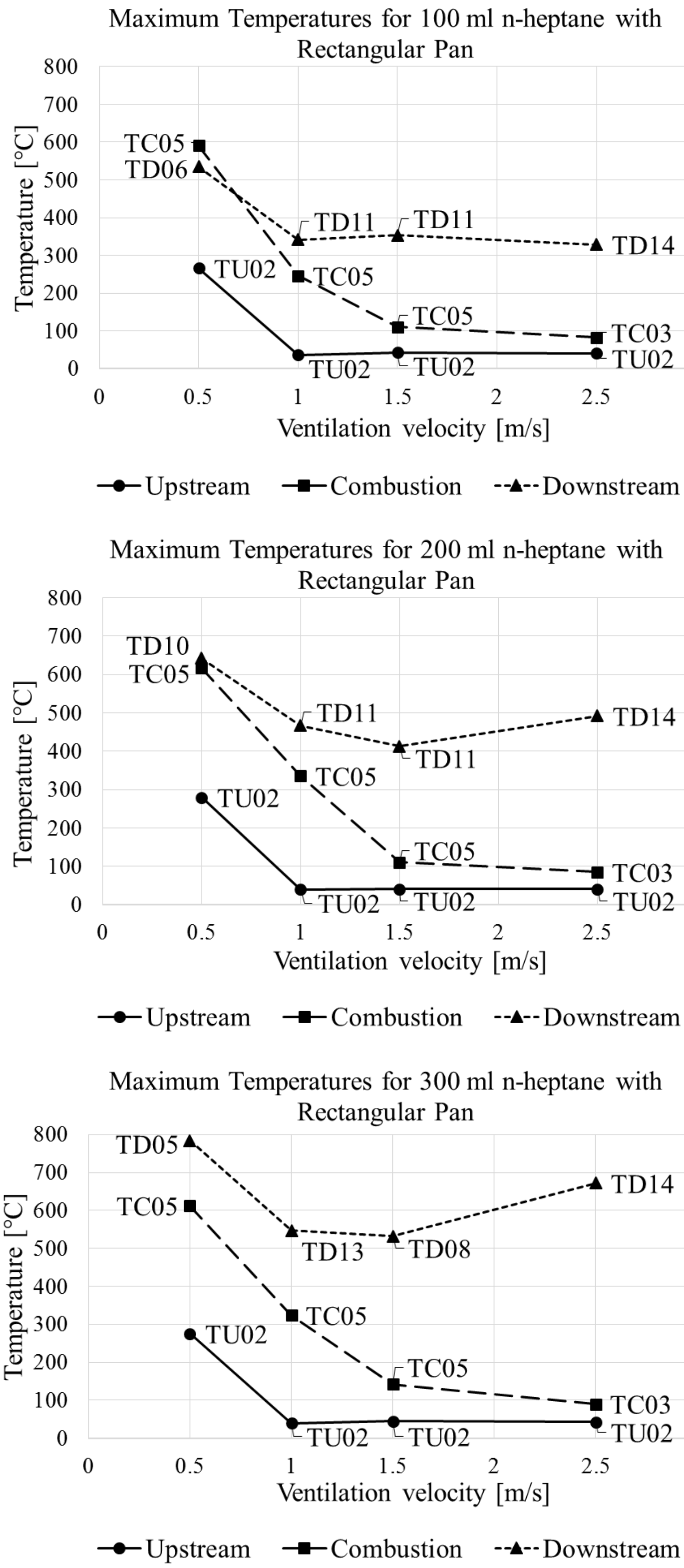

Figure B. 2 Temperature results of n-heptane pool fire experiments with rectangular pan

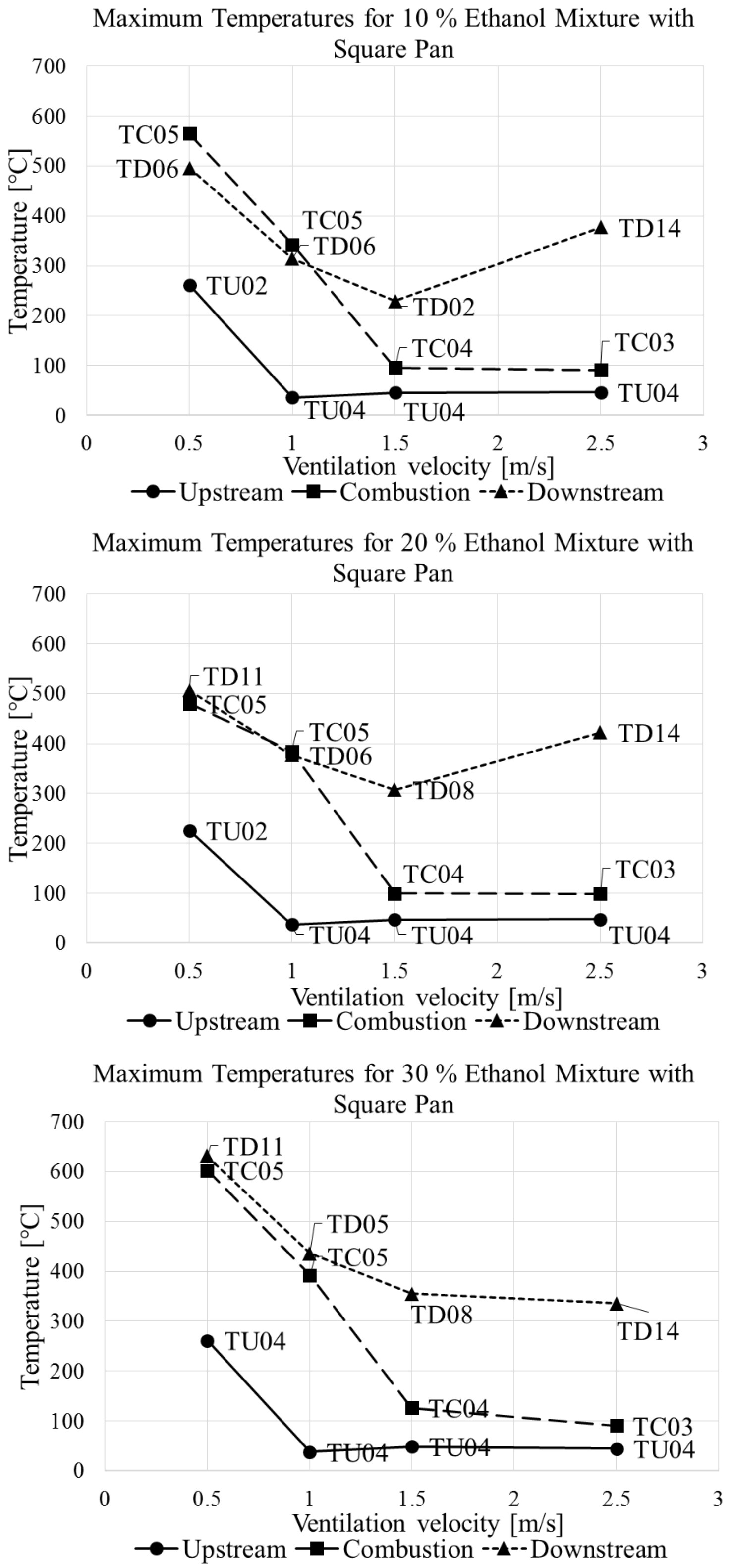

Figure B. 3 Temperature results of ethanol blended n-heptane pool fire experiments with square pan

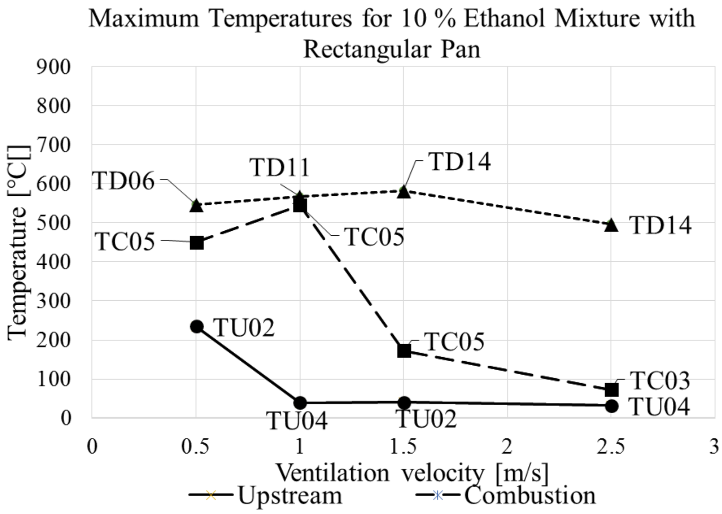

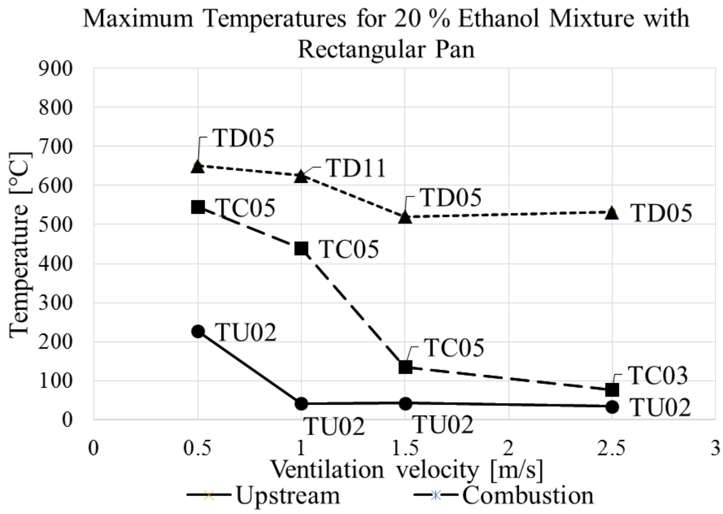

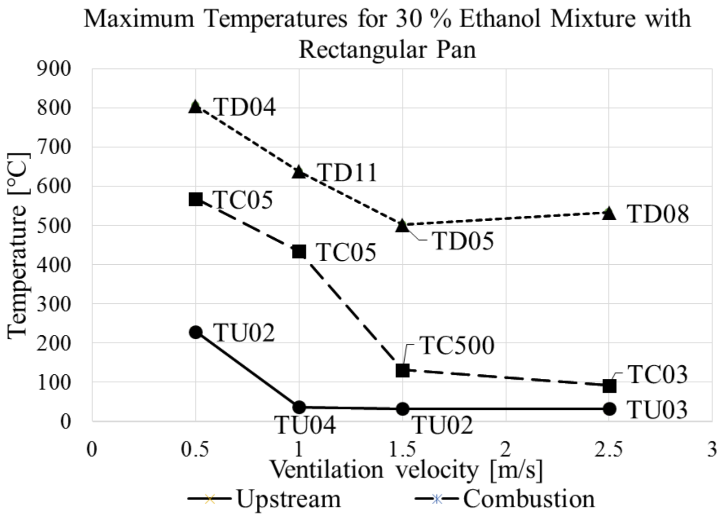

Figure B. 4 Temperature results of ethanol blended n-heptane pool fire experiments with rectangular pan

Table B. 1 List of ethanol pool fire results

Exp. Code	QHRR [kW]	THR [MJ]	NTHR [kJ/ml]	T_{smoke} [˚C]	$\dot{q}''_{sur}$ [kW/m²]	$\dot{q}''_{fire}$ [kW/m²]	Sensor Config	Dist. [cm]
ET02-Ref-05	32.1	4.9	24.7	825.2	-	5.9	Hrzntl.	3
ET01-Ref-10	43.8	4.4	44.3	422.0	-	4.1	Hrzntl.	3
ET02-Ref-10	49.6	6.5	32.5	552.3	-	4.4	Hrzntl.	3
ET01-Ref-15	13.5	1.9	18.6	143.7	0.7	-	Vrtcl.	3
ET02-Ref-15	14.4	6.1	30.4	137.5	1.0	-	Vrtcl.	3
ET02-Ref-15	55.6	6.3	31.5	273.3	-	22.9	Hrzntl.	3
ET01-Ref-25	16.6	3.0	29.7	94.1	0.6	-	Vrtcl.	3
ET01-Ref-25	25.0	2.7	27.4	137.4	-	19.4	Hrzntl.	3
ET02-Ref-25	23.6	6.1	30.3	123.8	1.0	-	Vrtcl.	3
ET02-Ref-25	59.4	6.2	31.1	175.1	-	39.7	Hrzntl.	3
ET03-Ref-25	33.6	9.6	32.0	123.9	1.1	-	Vrtcl.	3
ET01-Abs-05	17.9	3.8	37.6	488.4	-	0.07 (Obsc.)	Hrzntl.	30
ET01-Abs-05	18.1	3.8	38.1	440.4	-	0.62	Hrzntl.	30
ET02-Abs-05	25.0	6.8	33.8	556.6	-	1.1	Hrzntl.	30
ET02-Abs-05	35.2	5.7	28.4	498.7	-	15.6	Hrzntl.	3
ET01-Abs-10	36.5	4.6	46.4	280.0	-	15.4	Hrzntl.	3
ET01-Abs-10	48.7	4.8	48.4	392.9	-	5.55 (Obsc.)	Hrzntl.	3
ET01-Abs-10	31.1	5.8	57.5	367.6	-	0.53	Hrzntl.	30
ET02-Abs-10	47.4	12.1	60.5	448.1	-	0.9	Hrzntl.	30
ET01-Abs-15	16.7	3.1	31.3	101.1	0.59	-	Vrtcl.	3
ET01-Abs-15	20.9	4.0	40.3	104.9	-	0.42	Hrzntl.	30
ET02-Abs-15	32.6	6.6	33.2	123.4	0.46	-	Vrtcl.	3
ET02-Abs-15	55.8	7.4	36.8	203.4	-	26.7	Hrzntl.	3
ET01-Abs-25	25.3	3.2	31.7	79.4	0.43	-	Vrtcl.	3
ET01-Abs-25	38.0	3.0	30.3	110.7	-	30.7	Hrzntl.	3
ET01-Abs-25	22.2	3.7	37.1	75.9	-	0.35	Hrzntl.	30
ET02-Abs-25	33.6	7.1	35.6	85.8	0.46	-	Vrtcl.	3
ET02-Abs-25	68.3	7.6	37.9	112.9	-	6.39 (Obsc.)	Hrzntl.	3
ET02-Abs-25	57.8	7.2	35.9	102.9	-	31.2	Hrzntl.	3